UNDERSTANDING LIQUIDS PRODUCTION FROM SHALES

by

Palash Panja

A dissertation submitted to the faculty of
The University of Utah
in partial fulfillment of the requirements for the degree of

Doctor of Philosophy

Department of Chemical Engineering

The University of Utah

December 2014

The University of Utah Graduate School

STATEMENT OF DISSERTATION APPROVAL

The following faculty members served as the supervisory committee chair and members for the dissertation of Palalsh Panja.

Dates at right indicate the members' approval of the dissertation.

Milind Deo, Chair September 29, 2014
Date Approved

John McLennan, Member September 30, 2014
Date Approved

Jules Magda, Member September 30, 2014
Date Approved

Hong Sohn, Member September 30, 2014
Date Approved

Anil Virkar, Member September 30, 2014
Date Approved

The dissertation has also been approved by Milind Deo, Chair of the Department of Chemical Engineering and by David B. Kieda, Dean of The Graduate School.

ABSTRACT

The growth of production from liquid shale plays has been phenomenal. However, the recoveries are low of the order of 10% and more efficient methods of producing liquids are necessary. This research is aimed at understanding production performances involving complex interaction between phase behavior and flow in unconventional reservoirs like shales. A new rapid semianalytical forecast tool for transient state linear flow in ultralow permeability (100 nD to 5000 nD) fractured reservoir was developed. The tool is useful for well inflow performance, condensate drop out and material balance calculations of condensate production in unconventional reservoirs.

Effects of individual parameters such as reservoir properties (matrix permeability, heterogeneity, rock compressibility and reservoir pressure) on production oil were studied using reservoir simulations with an appropriate number of grid blocks. The matrix permeability, initial reservoir pressure, fracture spacing were the most influencing factors in recoveries from gas-condensate as well as from oil reservoirs. Operating the well at higher flowing bottom hole pressure (FBHP) is preferable for low permeability (100 nD) reservoir and low FBHP for higher permeability (1000 nD) reservoir to recover more liquid. Production data, including Gas Oil Ratios (GOR) are valuable in assessing reservoir performance. A single characteristic factor affecting the produced gas oil ratio was found to be $(1- R_{sw}/R_{sb})\ (1-P_{wf}/P_b)\ /(1-P_{wf}/P_i)$ that predicts deviation of gas oil ratio from its initial value.

Effect of the interaction of parameters on recovery was examined using experimental design and response surface methodology. This study resulted in surrogate reservoir models for a quick assessment of production performance from ultralow permeability black oil and condensate reservoirs. Risks of production performance and investment were quantified by preparing the probability density functions (PDF) of production outcomes and the hierarchy of the most significant input factors using the surrogate reservoir models for given input distributions. Average condensate recoveries from gas condensate reservoirs and oil recoveries from oil reservoirs were 16% and 13%, respectively, after 10 years of production. Abandonment time for well with 18 fractures in ultralow permeability oil reservoir was approximately 7 years.

To my family.

TABLE OF CONTENTS

APPENDICES

LIST OF FIGURES

LIST OF TABLES

NOMENCLATURE

Symbol

ψ	Co-efficient in diffusivity equation	$foot^2/sec$
γ	Euler's constant, 1.781	-
ϕ	Porosity	-
γ_g	Productivity Index of Gas	(RB/Day) (cp/psi)
$\Delta m(P)_g$	Pseudopressure for Gas	(SCF/RB)(psi/cp)
$\Delta m(P)_o$	Pseudopressure for Oil	(STB/RB)(psi/cp)
γ_o	Productivity Index of Condensate	(RB/Day) (cp/psi)
λ_{xz}	Aspect Ratio, XZ Plane	-
$\overline{Y}_{obs}$	Mean of Observed Values	Unit of Output
Δx_j	Size of 'jth' Grid	feet
μ	Viscosity	cp
μ_g	Gas Viscosity	cp
μ_o	Oil Viscosity	cp
μ_t	Total Viscosity	cp
A	Flow Area	$foot^2$
a_0	The intercept of the Surrogate Model	-
a_1	Unit Conversion Factor, $1/(2*\pi*141.2)$ for Field Unit, 1 for SI unit	-
a_2	Unit Conversion Factor, 0.0002672 for Field Unit, 1 for SI unit	-
a_{ij}	Coefficient of 2^{nd} Order Interaction of Inputs	-
a_k	Coefficient of independent input	-
B	Formation Volume Factor	RB/SCF or RB/STB
B_{gd}	Dry Gas Formation Volume Factor	RB/SCF
BHP	Bottom Hole Pressure	psi
B_o	Oil Formation Volume Factor	RB/STB
c	Constant	$1/foot^2$
C_f	Formation Compressibility	1/psi
c_g	Gas Compressibility	1/psi
CGR	Condensate to Gas Ratio	STB/MMSCF
c_o	Condensate Compressibility	1/psi
C_r	Rock Compressibility	1/psi

c_t	Total Compressibility	1/psi
c_w	Water Compressibility	1/psi
d_x, d_y, d_z	Reservoir Dimensions in X, Y and Z Directions, respectively	
$e_{k+1,k}$	Error in any Production Parameter Error between $(k+1)^{th}$ and k^{th} Grids	-
FBHP	Flowing Bottom Hole Pressure	psi
F_{CD}	Dimensionless Fracture Conductivity	-
f_g	Correction Factor in Transient State Productivity Index	-
f_p	Difference in Pressure Ratio Factor	-
GCR	Gas Condensate Ratio	SCF/STB
GOR	Gas Oil Ratio	SCF/STB
h	Formation Thickness	foot
ICIP	Initially Condensate In-Place	MSTB
IGIP	Initially Gas In-Place	MMSCF
IOIP	Initially Oil In-Place	MSTB
k	Absolute Permeability	mD
k_f	Fracture Permeability	mD
k_{fx}, k_{fy}, k_{fz}	Fracture Permeability in X,Y and Z direction respectively	mD
k_m	Reservoir Absolute Permeability	nD
K_{rg}	Gas Relative Permeability	-
K_{ro}	Oil Relative Permeability	-
k_{rog}	Oil Relative Permeability in Gas-Oil System	-
k_{row}	Oil Relative Permeability in Water-Oil System	-
k_{rw}	Water Relative Permeability	-
k_x	Reservoir Absolute Permeability in X-direction	nD
k_y	Matrix Permeability in Y-direction	nD
k_z	Matrix Permeability in Z-direction	nD
LGR	Liquid to Gas Ratio	STB/MMSCF
LGR_i	Initial Liquid to Gas Ratio	STB/MMSCF
LGR_p	Produced Liquid to Gas Ratio	STB/MMSCF
n	Total numbers of the independent inputs	-
n_g	Exponent of Relative Permeability Curve for Gas	-
n_h	Half Number of Grids in X-direction excluding fracture grid	-
n_o	Exponent of on Relative Permeability Curve for Oil	-
n_w	Exponent of on Relative Permeability Curve for Water	-
P	Pressure	psi
P_1	Region 1 Boundary Pressure	psi
P_b	Bubble Point Pressure	psi
P_{bp}	Bubble Point Pressure	psi

P_{dew}	Dew Point Pressure	psi
P_e	Pressure at Reservoir's Outer Boundary	psi
P_{frac}	Pressure at Fracture	psi
P_i	Initial Reservoir Pressure	psi
P_R	Average Reservoir Pressure	psi
P_{wf}	Flowing Bottom Hole pressure	psi
q_g	Gas Rate at Well	SCF/day
q_o	Oil or Condensate Rate at Well	STB/day
R^2	Coefficient of Determination	-
r_e	Distance of External Boundary of Reservoir	foot
R_{fg}	Gas Recovery	%
R_{fl}	Liquid Recovery	%
R_p	Produced Gas/Condensate Ratio	SCF/STB
R_{pc}	Cumulative Gas Oil ratio	SCF/STB
R_s	Solution Gas/Condensate Ratio or Gas Oil Ratio	SCF/STB
R_{sb}	Gas Oil Ratio at Bubble Point Pressure	SCF/STB
R_{si}	Initial Solution Gas/Condensate Ratio	SCF/STB
R_{sw}	Gas Oil ratio at Flowing Bottom Hole Pressure	SCF/STB
R_v	Volatilized Condensate/Gas Ratio	STB/MMSCF
R_{vf}	Flowing Volatilized Condensate/Gas Ratio	STB/MMSCF
R_{vi}	Initial Volatilized Condensate/Gas Ratio	STB/MMSCF
r_w	Wellbore Radius	foot
S^*	Effective Saturation	-
S_{cc}	Critical Condensate saturation	-
S_g	Gas Saturation	-
S_{gc}	Critical Gas Saturation	-
S_o	Condensate Saturation	-
S_{org}	Residual Oil Saturation in Gas-Oil System	-
S_{orw}	Residual Oil Saturation in Water-Oil System	-
SS_{res}	Residual Sum of Squares	Unit of Output
SS_{tot}	Total Sum of Squares	Unit of Output
S_w	Water Saturation	-
S_{wc}	Irreducible Water Saturation	-
S_{wc}	Connate Water Saturation	-
t	Time	hour
T	Reservoir Temperature	^oF
w	Fracture Width	foot
X	Reservoir Dimension in X-direction	foot
x_0	Minimum Size of Grid	foot
x_e	Distance of Boundary from Fracture	foot
x_e	Half-length of Reservoir in X-direction	foot
X_f	Fracture Spacing	foot

X_i	Scaled Independent Inputs	-
x_j	Distance of 'jth' Grid Boundary	foot
Y	Reservoir Dimension in Y-direction	foot
y_e	Half-length of Reservoir in y-direction	foot
$y_{k,i}$	Value of 'y', any Production Parameter at Time t_i for k^{th} Grid	-
$Y_{model,i}$	Modeled Value	Unit of Output
$Y_{obs,i}$	Observed Data	Unit of Output
$Y_{obs,max}$	The Maximum Value of Observed data	Unit of Output
$Y_{obs,min}$	The Minimum Value of Observed data	Unit of Output
Z	Reservoir Thickness	foot
z_e	Half-length of Reservoir in z-direction	foot

Subscripts

b	Bubble point
bp	Bubble point
cc	Critical condensate
CD	Conductivity
dew	Dew point
e	External
f	Formation, fracture
frac	Fracture
g	Gas
gd	Dry gas
i	Initial
j	Number count
m	Matrix
max	Maximum
min	Minimum
o	Oil
obs	Observed
r	Rock
R	Reservoir
t	Total
w	Water
x	X direction
y	Y direction
z	Z direction

Abbreviations

BHP	Bottom Hole Pressure
CGR	Condensate to Gas Ratio
CVD	Constant Volume Depletion

CVDMB	Constant Volume Depletion Material Balance
FBHP	Flowing Bottom Hole Pressure
GCI	Gas-Oil-Ratio Characteristic Index
GCR	Gas Condensate Ratio
GOR	Gas Oil Ratio
ICIP	Initially Condensate In-Place
IGIP	Initially Gas In-Place
IOIP	Initially Oil In-Place
LGR	Liquid to Gas Ratio
LGR_i	Initial Liquid to Gas Ratio
LGR_p	Produced Liquid to Gas Ratio
MB	Material Balance
MBO	Modified Black Oil
NRMSE	Normalized Root Mean Square Error
NTG	Net to Gross Ratio
PDF	Probability Density Function
PVT	Pressure Volume Temperature
RMSE	Root Mean Square Error

ACKNOWLEDGEMENTS

First of all, I am extremely grateful to my adviser, Professor Milind Deo, for his guidance, and encouragement throughout this research work and his support during some tough phases of my personal life. I thank him for allowing me to nurture my intellectual faculties to their utmost levels. I would like to thank the members of the supervising committee, Dr. John McLennan, Dr. Jules Magda, Dr. Hong Sohn, and Dr. Anil Virkar for their comments and suggestions. I am thankful to all the faculty and staff of the Chemical Engineering Department for their support in the graduate program. I am extremely grateful to the Chemical Engineering Department for awarding me the graduate fellowship award in my first year of graduate study and to the ConocoPhillips Corporation for providing me financial support for the following years. I thank my colleagues and classmates Tyler, Justin, Rob, Pankaj, John, Raul for making the workplace friendly and productive. Apratim will always be special, whom I regard as family at Salt Lake City. I have had the good fortune of making great friends during my stay at Salt Lake City. Dipanjan, Rambo, Aishwaryadev, Sayan, Prateep, Niladri, Payel, Anushka and Debolina have made my life a very enjoyable and unforgettable one here. I will always treasure our times together. Finally, I express my respect to my family members for their support, encouragement and motivation. I would like to thank my wife Sudipta, a perfect companion, for her patience and support during difficult times and her sister, Swagata, for helping me to cope with some tough moments in life.

CHAPTER 1

INTRODUCTION

Within the current decade, the United States is poised to become the largest oil producer. This is the unprecedented growth in oil production from unconventional reservoirs (IEA, 2012) such as the Bakken play or shales like the Eagle Ford.

1.1 Importance of Producing Liquids from Shales

The EIA (U.S. Energy Information Administration) published a report on "Review of Emerging Resources: U.S. Shale Gas and Shale Oil Plays" in July 2011. The report indicated that the US has shale oil resources of 24 billion barrels onshore in the Lower 48 States. The Monterey/Santos play in southern California is the largest formation of these containing 64% of the total US shale oil resources. The Bakken and Eagle Ford plays, comprising around 30% of all US shale oil, are the next largest plays. Figure 1.1 shows the locations of the shale plays in the Lower 48 States. Many uncertainties are associated with the calculation of technically recoverable shale gas and shale oil resources. Oil production from tight formations as shown in Figure 1.2 more than tripled in three years increasing from about 250 MSTB per day at the beginning of 2009 to nearly 900 MSTB per day by November 2011. Eighty four percent of total tight oil production in November 2011 came from two important plays, namely the Bakken plays in North Dakota and Montana, and the Eagle Ford shale in south Texas. Despite the higher cost for multilateral

horizontal wells with hydraulic fractures, the exploitation of oil production is considered profitable under the current oil prices.

1.2 Research Motivation

The growth of production from liquid bearing shale plays has been phenomenal. However, since the recoveries are low, of the order of 10%, a more efficient methods of producing liquids are necessary. This research is aimed at understanding factors that control production of near critical fluids from very low permeability formations. Condensates are a class of hydrocarbon fluids that produce liquids upon pressure reduction. It is important to understand whether there is significant dropout of these liquids in the reservoir impeding production. In this regard, it is also important to understand the basic changes in production behavior as we transition from condensate to volatile oils. Reservoir simulation has become a standard tool to study complex interaction between phase behavior and flow. However, the simulations need to be structured in a logical fashion to ascertain accurate results. Situations involving multiple, complex parameters need to be handled using specific methods that prioritize the parameter list. Assessment of uncertainty in the face of uncertain parameters is critical.

1.3 Objectives

In the view of important requirements, the following research objectives have been proposed.

- Develop a rapid forecasting tool to understand the behavior of condensates in tight formations.
- Quantify the effects of grid size on important simulation outcomes.

- Use converged grids to study the importance of petrophysical and other parameters on production and recovery from shales.
- Develop understanding the behavior of producing gas oil ratio and relationship with operating condition, reservoir parameters and initial gas oil ratio.
- Develop experimental design and combinatorial study techniques to assess the uncertainties in recoveries.
- Discern the effect of producing volatile oils and condensates near the critical point of the P-T phase diagram.

Figure 1.1: Map of U.S. shale gas and shale oil plays (as of May 9, 2011)

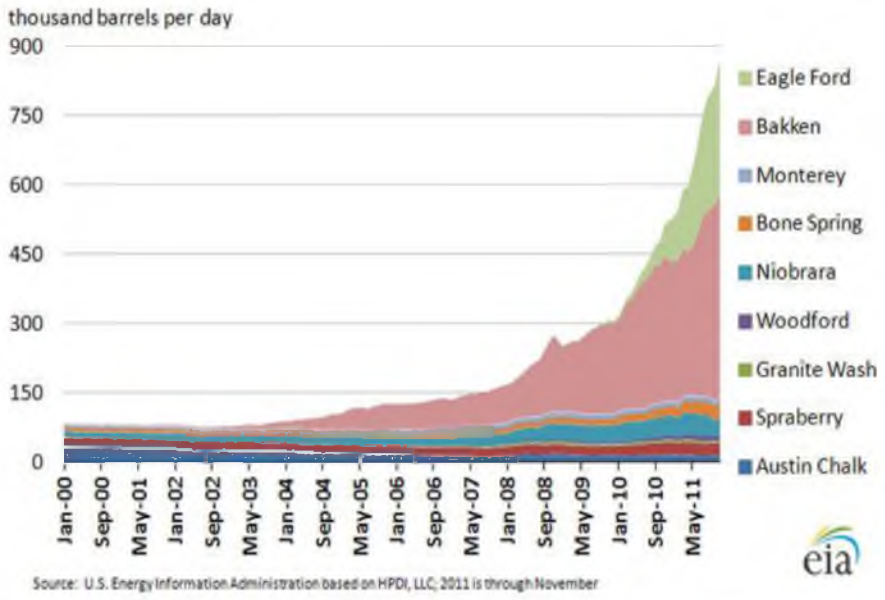

Figure 1.2: Tight oil production for selected plays

CHAPTER 2

FORECASTING OF GAS CONDENSATE DELIVERABILITY

Well deliverability impairment due to condensate blockage near fractures is a common problem in low permeable gas condensate reservoirs. Flowing bottom hole pressure (BHP) below dew point pressure causes condensate drop out near fracture inside reservoir. Sharp changes in block properties (mainly pressure and oil and gas saturations) are observed near the fracture in low permeable reservoirs. Different depletion stages with time are clearly explained in terms of pressure declines and the physical conditions. Rapid forecast tools are required for quick assessment of the reservoir performance to avoid detailed fine grid simulations.

A new rapid forecast tool for transient state flow in ultralow permeability fractured reservoir has been developed in MATLAB (MathWorks Inc.). The two-phase pseudopressure is modified for transient state linear flow system. The productivity index is deduced from single phase transient state linear flow equation using a semianalytical method. Produced gas oil ratio with time from simulation or field is required in this method. Production profiles such as gas flow rate, condensate flow rate and gas condensate ratio with time are established for various conditions and compared with fine grid simulations using Modified black oil PVT data. The method is also useful for quick sensitivity analysis of various reservoir, fluid and operating parameters. The model works

very well for the ultralow permeable reservoir (100 nD to 5000 nD).

2.1 Background

Due to the sharp decline in the reservoir pressure near fracture, condensate drops out inside the reservoir. The generation of condensate near fracture impairs the flow. Extent of blockage depends on PVT, absolute permeability of rock, relative permeability and well production conditions. A number of studies have been conducted on saturated conventional reservoirs in primary production. Evinger and Muskat (1942) introduced the concept of theoretical productivity factor using pseudopressure for solution gas drive reservoirs in steady state conditions. General expressions for Pseudopressure for gas – condensate with modified black oil (MBO) model are shown here:

$$m(P) = \int_{P_{ref}}^{P} \left(\frac{K_{ro}}{B_o \mu_o} R_s + \frac{K_{rg}}{B_{gd} \mu_g} \right) dP \tag{2.1}$$

The concept of pseudopressure is not new; it is normally used for gas flow performance, and normal pressure is replaced by pseudopressure for gas reservoir. It can easily be realized during solving flow equation that pseudopressure approach is advantageous to express all flow equations in terms of these pseudopressures. Equation 2.1 is used to calculate gas flow rate from gas-condensate reservoir as shown in Equation 2.2

$$q_g = \gamma \left[m(P_R) - m(P_{wf}) \right] = \gamma \int_{P_{wf}}^{P_R} \left(\frac{K_{ro}}{B_o \mu_o} R_s + \frac{K_{rg}}{B_{gd} \mu_g} \right) dP \tag{2.2}$$

The productivity indices (γ) are varied for type of flow and the choice of upper limit of integration. Reservoir average pressure (p_R) and external boundary pressure (p_e) are the two most commonly used pressure for upper limit in pseudo steady flow while initial reservoir pressure is considered as the upper limit for transient state flow.

The first numerical simulations were conducted for radial gas condensate well deliverability by Kniazeff and Navilee (1965) and Eilerts et. al. (1965). Gondouin et el. (1967) modified the numerical program developed by Kniazeff and Naville (1965) and compared field with field measurements. Fussel (1973) developed a compositional simulator for 1-D radial flow in gas condensate reservoirs. Fussel (1973) proved that the steady state predictions were incorrect especially when the reservoir average pressure is below saturation pressure. Jones and Raghavan (1988) used pseudopressure integrals to capture the effect of multiphase flow and changes in fluid composition during production. They also developed numerical models to determine flow capacity and skin factor from well test data in gas condensate reservoirs. The constant volume depletion material balance method (CVDMB) was subsequently developed using reservoir pseudopressures (Evinger and Muskat 1942) for peudosteady state condition. Average pressure is used to characterize reservoir performance which is quite similar to the Material balance method in Constant Volume Depletion Material Balance Method (CVDMB). In this method, whole reservoir is considered as homogeneous at any time and reservoir is characterized by its average pressure.

Average pressure was used in this method to characterize the reservoir. O'Dell and Miller (1967) introduced a pseudopressure function to calculate gas rate in gas condensate reservoirs when the reservoir pressure is above the dew point pressure.

Fevang and Whitson (1996) modified the CVDMB and divided the reservoir into three regions.

Fevang and Whitson (1996) split the pseudopressure equation (Equation 2.1) into three parts corresponding to the three flow regions. They modified the CVDMB method and divide the reservoir into three regions as described earlier. Gas and condensate both flow in the first region near a hydraulic fracture. Gas and condensate both exist in a second zone (somewhat away from the fracture) but only gas flows.

$$\Delta m(P) = \underbrace{\int_{P_{wf}}^{P_1} \left(\frac{K_{ro}}{B_o \mu_o} R_s + \frac{K_{rg}}{B_{gd} \mu_g}\right) dP}_{\text{Region 1}} + \underbrace{\int_{P_1}^{P_{dew}} \frac{K_{rg}}{B_{gd} \mu_g} dP}_{\text{Region 2}} + \underbrace{K_{rg}(S_{wc}) \int_{P_{dew}}^{P_R} \frac{1}{B_{gd} \mu_g} dP}_{\text{Region 3}} \quad (2.3)$$

In the third zone, only gas exists and flows. The method was applicable to pseudosteady state flow to vertical well and to horizontal wells and vertically fractured reservoirs. The flowing CGR (Condensate to Gas Ratio) is the key factor for this calculation method. Fevang and Whitson (1996) assumed that the produced GOR is equal to the flowing GOR in the deep reservoir. Guehria (2000) followed the same method except that the GOR is calculated using Muskat (1945) material balance method, modified for a gas condensate system. Using a material balance, Mott (2002) modified Fevang's method and introduced the flowing GOR based on the volume of the first region. Many combinations of existing methods have been developed to obtain better results. Existing methods can also be converted to iterative procedures. Xiao and Al-Muraikhi (2004) adopted Mott's method (2002) with the modification of material balance method to calculate the growth of first region. Gerami et al. (2010) introduced

an iterative method coupled with material balance calculation. Their technique avoids the need for production data as required in the original method (Fevang and Whitson 1996). However, this iterative method converges with difficulty and is very sensitive to PVT data. Bonyadi et al. (2012) developed an iterative method which combined Mott's (2002) and Xiao and Al-Muraikhi's (2004) methods. The material balance used in existing methods is only applicable for depleted reservoirs where the average reservoir pressure is characteristics feature.

Modified black oil model (MBO) is used for all deliverability calculation. Low gravity liquids like volatile oils and gas condensates can exist as a gas phase in a vaporized form. This vaporized liquid in the gas phase is first conceptualized by Cook et al. (1974) for a gas injection scenarios.

All the methods were used in the conventional reservoirs in pseudosteady state condition with reasonably high reservoir permeabilities. Transient state conditions persist for a long time in unconventional reservoirs with ultralow reservoir permeability. A rapid forecast tool is developed using MATLAB (MathWorks Inc.) for quick and simpler engineering calculation to evaluate the production performance from ultralow permeability fractured reservoirs with transient state linear flow. The results from model are validated with fine grid reservoir simulation. This proposed method is also utilized for sensitivity analysis of various parameters such as initial gas condensate ratio, flowing bottom hole pressure, initial reservoir pressure, formation porosity etc.

2.2 Proposed Method

All existing methods are developed for steady state and pseudosteady state flows. Average reservoir pressure or external boundary pressure was used to calculate productivity index for the methods. Production performances (produced GOR) from conventional and unconventional reservoirs are compared for different permeability in Appendix A. It can be concluded that average reservoir pressure is not the characteristics property for low permeability reservoirs. An average pressure calculation accounting only the affected regions should be formulated. We consider transient state condition for the performance prediction because unconventional reservoirs (ultralow permeability reservoirs) show transient condition with moving boundary for long time of production. Initial reservoir pressure and flowing bottom hole pressure are used in this method.

2.2.1 Reservoir Model

A simple tank type model with one horizontal well and one vertical fracture parallel to YZ axis in the middle of the reservoir is chosen for this study. The fracture is extended fully with YZ plane of reservoir. All simulations were conducted using Eclipse 100, a Schlumberger black oil simulator with modified black oil PVT. The minimum number of grid blocks is assigned in the reservoir model to assure that the converged results are free of grid effects. The reservoir properties, initial conditions and operational parameters are given in Table 2.1.

2.2.2 Productivity Index for Transient State

Productivity index for constant bottom hole pressure solution for radial transient flow with vertical well is calculated by Earlougher (1977). Guo and Schechter (1999)

presented a productivity index for vertically fractured reservoir with linear flow in pseudosteady state condition. Productivity index for vertically fractured reservoir with linear flow in transient state condition is conceptualized from Miller's solution (1962) for infinite acting reservoir operated at constant pressure. He provided a pressure distribution solution for infinite aquifer, constant flowing bottom hole pressure as shown in Equation 2.4:

$$\frac{P - P_{wf}}{P_i - P_{wf}} = \text{erf}\left(\frac{x}{2\sqrt{\psi t}}\right) \tag{2.4}$$

where, $\psi = \frac{k}{\phi \mu c}$

The flow rate is calculated using Darcy's law of flow through porous medium as given by Equation 2.5:

$$q = \frac{Ak}{\mu B} \frac{P_i - P_{wf}}{\sqrt{\frac{\pi kt}{\phi \mu c}}} \tag{2.5}$$

$$A = flow\ area = 2y_e h$$

Equations 2.4 and 2.5 are applicable for single phase linear flow in fractured reservoirs. Analytical solutions for multiphase linear flow are complicated. A simple form of multiphase flow solution is proposed through the pseudopressure method. Considering the development of pseudopressure concept for multiphase flow in pseudosteady state and steady state conditions from the analogy of their analytical solutions, we have approximated the pseudopressure for multiphase flow in transient state

using equation 2.5. The gas flow rate in multiphase flow system is presented in Equation 2.6.

$$q_g = \frac{2\pi a_1 khf_g}{\sqrt{\frac{\pi a_2 kt}{\phi \mu_{gi} c_{ti} y_e^2}}} \int_{P_{wf}}^{P_i} \left(\frac{K_{ro}}{B_o \mu_o} R_s + \frac{K_{rg}}{B_{gd} \mu_g} \right) dP \qquad (2.6)$$

We have proposed the productivity index for transient state linear flow for constant bottom hole pressure. It is noticed that the productivity index for transient state is function of time whereas it is constant for steady state and pseudosteady state condition. Therefore, productivity index is calculated in each step of depletion along with the pseudopressure calculations. Fevang and Whitson's (1996) method is adopted here to calculate the condensate rate using the regional division of the pseudopressure. The produced gas/condensate ratio (GCR) with time is required for the calculations and in this study; these data are taken from simulations. These data can also be supplied from field production log. Fluid viscosity and total compressibility in productivity index are calculated at initial reservoir conditions. Formation porosity, formation compressibility and water compressibility are held as constant. The unit of time in productivity index of transient flow is hour. The same PVT data are used both in simulations and proposed model. Condensate rate and gas rate are calculated using very fine pressure step to obtain better results and the linear interpolation is applied to the PVT data. Initial reservoir pressure is above the dew point pressure. The reservoir is initially filled with gas and connate water.

The total compressibility is also function of fluid saturations and the variation of fluid saturations with pressure is also considered in this calculation.

$$c_{ti} = c_f + c_{oi}S_{oi} + c_wS_{wc} + c_{gi}(1 - S_{oi} - S_{wc}) \quad (2.7)$$

Productivity indices are summarized in the Table 2.2.

where,

$$c = \frac{k}{x_e x_f k_f}$$

$$f_g = 1.5 + 1.7\left(\frac{R_{vi}R_{si}}{1 - R_{vi}R_{si}}\right)\left(\frac{P_{dew} - P_{wf}}{P_i - P_{dew}}\right)^{0.4\left(\frac{P_{wf}}{P_i}\right)}$$

The porosity, permeability and temperature are constant during the calculations. The reservoir temperature is greater than critical temperature but less than the cricondentherm temperature. Capillary effect and gravity segregation are not considered in this study.

2.2.3 Flow Regions

In course of production, single phase or multiple phases may exist in the reservoir. If the flowing bottom hole pressure is below dew point pressure, a saturated two-phase region near the fracture always exists. The reservoir is divided into four regions unlike three regions by Fevang et al. (1996) depending on the saturation of condensate and the flow of gas and condensate. The calculation method of pseudopressures in various regions is described in Appendix B. The pressure profile inside the reservoirs and the different regions is shown in Figure 2.1 through a schematic diagram.

The characteristics of each region are discussed here. A reservoir may have one or more coexisting regions depending on the depletion stage as discussed in Appendix C.

2.2.3.1 Region1 (R1). In this region, gas and condensate both flow. This is a saturated region near the fracture. The condensate saturation exceeds the critical condensate saturation in the region. The pressure where the condensate saturation

exceeds its critical saturation and starts flowing is designated as 'P_1'. The pressure on the inner boundary is considered as same as the pressure at the fracture (P_{frac}) or flowing bottom hole pressure (P_{wf}) and pressure on the outer boundary is 'P_1'.

2.2.3.2 Region2 (R2). Gas and condensate both exist in this region but only gas flows. This is also a saturated region but the condensate saturation does not exceed the critical saturation, i.e., amount of condensate is not sufficient to flow. The pressure in this region varies from P_1 to the dew point pressure (P_{dew}). In the regions 1 and 2, the gas contains less volatilized condensate as some of the condensates drop out as liquid phase.

2.2.3.3 Region3 (R3). Only gas exists and flows in this region. The pressure is above dew point pressure in this region. This is an undersaturated region and thus no condensates are generated in this region. The pressure ranges from dew point pressure (P_{dew}) to the outer boundary pressure (P_e) of the reservoir in this region, i.e., initial reservoir pressure (P_i) for transient state flow.

2.2.3.4 Region4 (R4). This region is totally unproductive and holds the initial reservoir conditions. The boundary of this zone starts when initial reservoir pressure is first detected from fracture side towards outer boundary of reservoir. The portion of reservoir is commonly exists in transient state conditions when all parts of the reservoir are not exploited.

2.3 Results and Discussion

A well is operated at constant bottom hole pressure condition. Gas flow rates for reservoirs of different permeabilities, initial reservoir pressures, dew point pressure, porosity and flowing bottom hole pressures are discussed here. The results from proposed models are compared with simulations by plotting them in the same figures.

2.3.1 Different Bottom Hole Pressure (P_{wf})

Various bottom hole pressures are considered in this study to assess the acceptability of the proposed model. The gas flow rates from proposed model for reservoir permeability of 100nD, 1000nD and 5000nD are compared with simulation results for two different bottom hole pressures of 1000 psi and 3000 psi as shown in Figure 2.2 a and b. The initial reservoir pressure is 6450 psi and dew point pressure is 5200 psi.

The predicted gas flow rates closely match with the simulation for the bottom hole pressures, 100 psi and 3000 psi, and also for the range of reservoir permeabilities considered in the study.

There are no significant differences in the flow rates from proposed model and simulation for low (1000 psi) to high (5000 psi) bottom hole pressure and for reservoir permeabilities of 10nD to 5000 nD. The low permeability reservoirs (100nD and 1000nD) show better fit than high permeability reservoir (5000 nD) in this case.

2.3.2 Different Initial Reservoir Pressures (P_i)

Similar results are displayed in Figure 2.3a and b with initial reservoir pressure of 5800 psi. Figure 2.2 a and Figure 2.3 a show the gas flow rates with the same bottom hole pressure of 1000 psi, dew point pressure of 5200 psi and porosity of 5% with two different initial reservoir pressures of 6450 psi and 5800 psi, respectively. Figure 2.2 b and Figure 2.3 b represent similar plots except that the bottom hole pressure is 3000 psi. It is observed that models with high bottom hole pressure and low reservoir permeability predict better than low bottom hole pressure and high reservoir permeability. These results can be attributed to the formation of condensate inside the reservoir. The bottom hole pressures keep the reservoir fluid in gas phase and condensate blockage near the

well bore or fracture is avoided.

2.3.3 Different Dew Point Pressures (P_{dew})

Robustness of the proposed model is also checked with the fluid models having different dew point pressures. Gas flow rates for dew point pressure of 4200 psi are shown in Figure 2.4 a and b.

Figure 2.4 a is compared with the Figure 2.3 a where initial reservoir pressure (5800 psi), bottom hole pressure(1000 psi) and reservoir porosity are the same for both cases but the dew point pressures are 4200 psi and 5200 psi, respectively. Flow rates from higher dew point pressure fluid match better than the flow rates from lower dew point pressure fluid. Lower dew point pressure with lower bottom hole pressure and lower initial reservoir pressure causes early condensate dropout in the reservoir hence two phase flow starts flowing. At higher reservoir pressure and higher bottom hole pressure, the effect of dew point pressure is not significantly noticed as compared in Figure 2.4 b and Figure 2.2 b where the initial reservoir pressure is 6450 psi and bottom hole pressure is 3000 psi.

2.3.4 Different Reservoir Porosities (ϕ)

Two different porosities of 5% and 10 % are verified in the proposed model. The gas flow rates from low permeability reservoirs with different porosity are shown in Figure 2.5 a and b. The porosity is not the significant parameter to affect the proposed model as clearly seen in the Figure. 2.5. Gas flow rates are almost perfectly predicted for both the porosities (5% and 10%).

The predicted rates closely follow the gas rates from simulations. Proposed models

predict rate more correctly for low permeability reservoirs than higher permeability reservoirs. The overall fit of the models with simulations are satisfactory for all cases with a wide range of initial reservoir pressure, bottom hole pressure, dew point pressure, reservoir porosity and reservoir permeability.

2.4 Key Findings

All existing deliverability methods presume only pseudosteady state and steady state conditions. A new method has been developed here to study transient using existing deliverability method after necessary modifications. The results from proposed models are verified with commercial simulator using very fine grid simulations. The concept of division of pseudopressure and productivity index according to fluid phase is developed. Three different matrix permeabilities and flowing bottom hole pressure are studied to check the robustness of the method. Gas flow rates for transient linear flow match closely with simulation. Gas rate is very sensitive to gas compressibility used in the calculation of total compressibility in the productivity index. The main features of the method include:

- It is applicable for unconventional fractured reservoirs.
- Only produced GOR versus time data is needed.
- Reservoir dimension is not needed, only fracture height and width are needed.
- Average reservoir pressure is not needed.
- The method works for wide range of formation permeability and bottom hole pressure.
- It is very fast and accurate.

The calculations are very sensitive to PVT data. Methods can be developed using a combination of transient and pseudosteady state conditions. This method is useful for well inflow performance and material balance method in unconventional reservoirs.

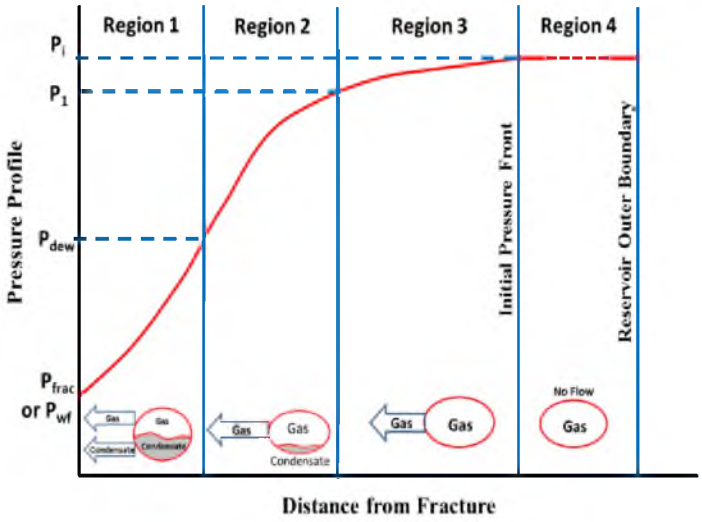

Figure 2.1: Physical conditions and flow ability of three regions.

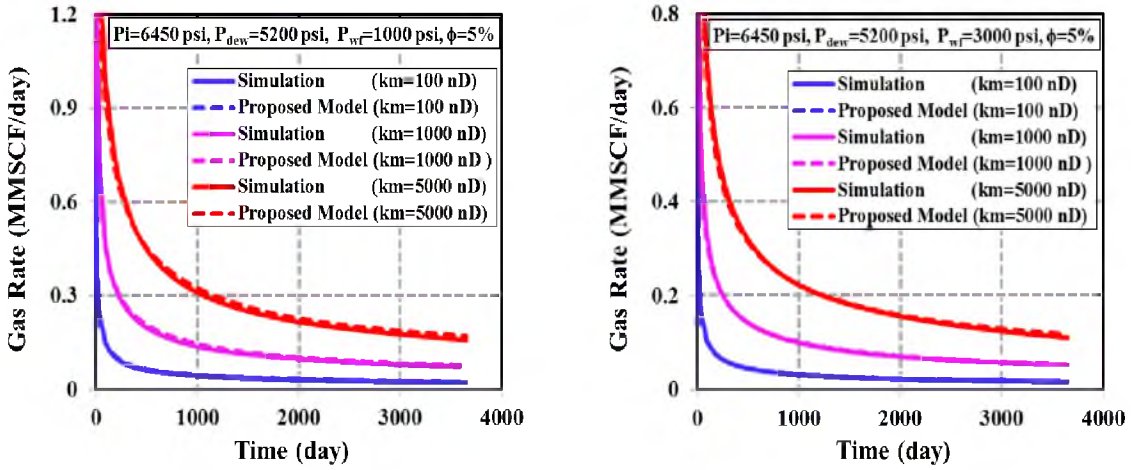

(a) (b)

Figure 2.2: Comparison of gas rate for initial reservoir pressure of 6450 psi and bottom hole pressure (a) 1000 psi (b) 3000 psi

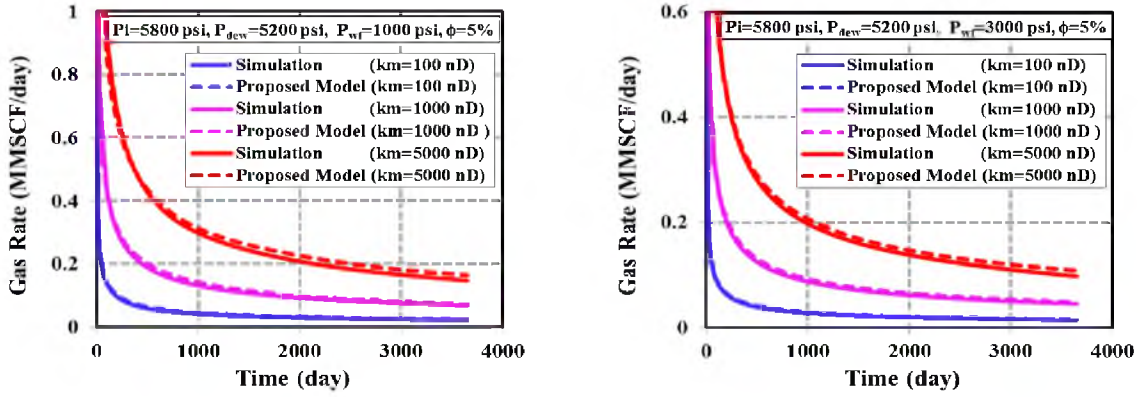

(a) (b)

Figure 2.3: Comparison of gas rate for initial reservoir pressure of 5800 psi and bottom hole pressure (a) 1000 psi (b) 3000 psi

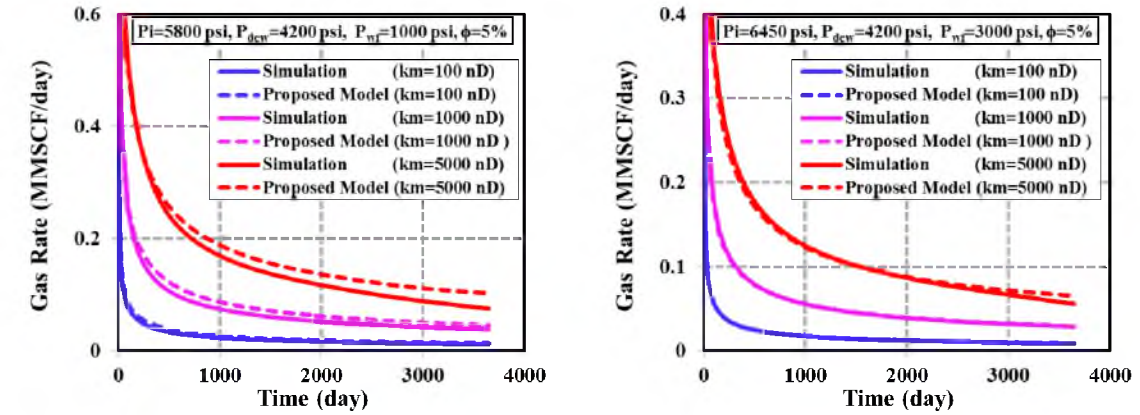

(a) (b)

Figure 2.4: Comparison of gas rate for dew point pressure of 4200 psi and bottom hole pressure (a) 1000 psi (b) 3000 psi

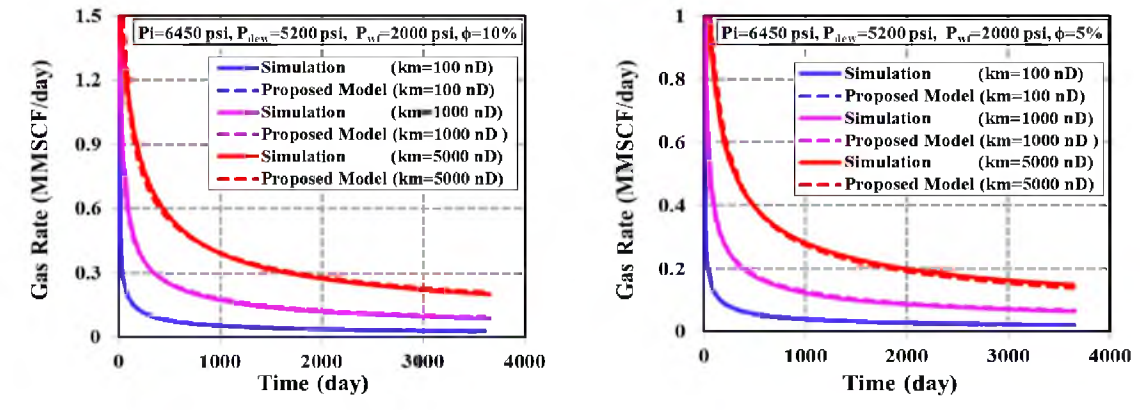

(a) (b)

Figure 2.5: Comparison of gas rate for initial reservoir pressure of 6450 psi, bottom hole pressure of 2000 psi and reservoir porosity (a) 10% (b) 5%

Table 2.1. Reservoir and operational parameters for simulations

Properties/Parameters	Value
Reservoir Top (ft):	12800
Reservoir Dimensions(ft)	dx=2000, dy=750, dz=200
Matrix Permeability, k_x (nD):	100,1000,5000
Fracture Permeability (mD):	$k_{fx} = k_{fy} = k_{fz} = 300$
Fracture Width (ft):	0.05
Initial Reservoir Pressure (psi):	6450,5800
Dew Point Pressure (psi):	5200
Initial HC Saturation (%):	84 (Single phase gas)
Reservoir Porosity (%):	5,10
Constant flowing BHP (psi):	1000, 2000, 3000

Table 2.2. Productivity index of condensate flow rate for various types of flow

Geometry	Pseudosteady state	Transient
Radial Flow: Vertical Well, constant bottom hole pressure	$\frac{2\pi a_1 kh}{ln\left({}^{r_e}/_{r_w}\right) - 0.75}$	$\frac{2\pi a_1 kh}{\ln\sqrt{\left(\frac{4a_2 kt}{\gamma \phi \mu_o c_t r_w^2}\right)}}$
Linear Flow: Vertical fracture, constant bottom hole pressure	$\frac{2\pi a_1 kh}{1.3889\, x_e\sqrt{c}\left(\frac{1}{1-\exp\left(-y_e\sqrt{c}\right)} - \frac{1}{2y_e\sqrt{c}}\right)}$	$\frac{2\pi a_1 khf_g}{\sqrt{\frac{\pi a_2 kt}{\phi \mu_{gi} c_{ti} y_e^2}}}$

CHAPTER 3

GRID SENSITIVITY STUDIES IN LOW PERMEABILITY RESERVOIRS

The accuracy and hence the validity of reservoir simulation results largely depend on the grid system used in the simulation. It is observed that when there is a large difference in permeability between two adjacent geologic layers, conventional grid systems do not accurately predict production behavior. Grid refinement is used near the well bore and fractures to better resolve the fluid flow between grid blocks. Logarithmically refined grids are commonly applied near the well bore region as there are large changes in pressure and saturation in this zone. Grid refinement must be applied even more carefully when dealing with the production of condensates. Effects of grid refinement on simulation results such as cumulative gas, cumulative oil, condensate gas ratio (CGR) or gas oil ratio (GOR), planar pressure distribution were studied using a generic reservoir model with one horizontal well and one vertical planar fracture for wet gas, gas-condensate and black oil fluids. These results were generated using a full feature compositional simulator. The results from these studies were used to develop empirical relationships between the dimensionless fracture conductivity and the grid size necessary for convergence.

3.1 Background

The United States is poised to become the largest oil producer in the current decade due to the unprecedented growth in oil production from unconventional reservoirs (IEA, 2012). The shale formations from which the fluids are being produced are low permeability resources. Multistage hydraulic fracturing is used to create the surface area required to realize the production. Low permeability in the matrix creates a large drawdown. When predicting rates and recovery, or for history matching, the appropriate type of grid system must be used.

Many researchers have studied the sensitivity of production prediction to grid and time step sizes. Reservoir simulation models were significantly improved by developing the formulations for irregular and nested grid systems and applying them to actual reservoirs with complex geometries (Graham and Smart 1980; Heinemann, Gerken et al. 1983; Quandalle 1983; Quandalle and Besset 1985). Local mesh refinement near the well was extensively studied for a repeated five-spot geometry in a homogeneous reservoir (Rosenberg 1982). In the finite difference method, reservoir simulations using block centered, nonuniform grids yielded large numerical errors (Settari and Aziz 1972). A hybrid grid system implementing an orthogonal curvilinear grid in the well regions and a rectangular grid elsewhere in the reservoir showed an exact match with the relevant analytical solution (Pedrosa Jr. and Aziz 1986). The main challenge in the early development of grid refinement was to implement the modified grid into existing code. Wasserman (1987) developed and implemented a static local grid refinement technique into a three-dimensional, three-phase reservoir simulator. A general theoretical formulation on grid refinement using composite grids with variable coefficients was

developed and could be incorporated into existing codes without disrupting the basic solution process (Ewing and Lazarov 1988). An adaptive static and dynamic local grid refinement technique was developed for multidimensional, multiphase reservoirs (Biterge and Ertekin 1992). Single/multiwell, multiphase black oil flow problems were solved using static and composite grids to illustrate the effectiveness of the local grid refinement technique (Ewing, Boyett et al. 1989). A truncation error analysis for an irregular system using six different kinds of gridding showed that 'distributed' methods yielded more accurate results than 'centered' methods (Nacul and Aziz 1991). Satisfactory results, requiring less computational time, can be obtained using nonuniform grids and explicit modeling with uniform grid refinement (Wan, Penmatcha et al. 1998). Recently, it has become common practice to use local grid refinement for various numerical reservoir simulations. The displacement fronts in heterogeneous three-dimensional reservoirs with two-phase immiscible flow were more accurately tracked using adaptive local grid refinement (Ding and Lemonnier 1993). In steamflood reservoir models, the recoveries and pore volume injected (PVI) were less sensitive to time step size than to grid size (Abou-Kassem and Aziz 1984). Similar studies show that inaccurate oil recovery and productivity index (PI) were obtained by using coarse grids in homogeneous and heterogeneous waterflood simulations (Haajizadeh and Begg 1993). Local grid refinement in highly faulted reservoirs (Kilic and Ertekin 1999), slanted, undulating horizontal, multilateral wells (Goktas and Ertekin 1999) are studied. Flow behavior around cavity completions was captured using static local grid refinement technique (Goktas and Ertekin 1999). Log distributed grids around a wellbore (Aqeel and Cunha 2006; Al-Mohannadi, Ozkan et al. 2007) and linearly distributed grids near vertical

fractures have been used commonly. It has been found that there is a threshold of grid refinement beyond which the results do not improve (Aqeel and Cunha 2006; Al-Mohannadi, Ozkan et al. 2007).

The unconventional fluid systems are characterized by their ultralow permeabilities. It is important that simulation grids that provide accurate results be constructed in order to understand production of fluids and to design optimum production strategies. In a play like the Eagle Ford, multiple fluid systems are seen. As one traverses from the northwest to southeast across the Edwards Reef in the Eagle Ford play we see transition from black oil to volatile oil to condensate and finally to gas. The grid systems required to simulate production of these different, complex fluid systems will be different and one of the objectives of this paper is to establish guidelines for constructing the grids for given fluid systems.

3.2 Model Description

3.2.1 Reservoir Model

All simulations were conducted using GEM, a Computer Modeling Group compositional simulator. The reservoir dimensions were 2000 ft in the x-direction, 750 ft in the y-direction, and 200 ft in the z-direction; with a top depth of 12000 ft (shown in Figure 3.1). The construction of the reservoir model is performed using the properties found in Table 3.1. These dimensions were not varied from simulation to simulation; however, the matrix permeabilities and the reservoir temperature were varied in the range given in Table 3.1. The horizontal well was drilled through the middle of the reservoirs' YZ plane in the direction of X-axis. The well was open only at the fracture which is located vertically in the middle of the X-domain. The radius of the well was 0.375 feet.

The initial reservoir pressure, fracture width and orientation, fracture permeability, initial hydrocarbon saturation, and reservoir porosity were also held constant in the various simulations.

Implementing the aforementioned properties allowed for the study of the effects of grid refinement under various conditions. The grid resolution was expected to vary depending on the dimensionless fracture conductivity. Fracture conductivity (F_{CD}) is defined as:

$$F_{CD} = \frac{k_f w}{k_m x_f} \tag{3.1}$$

$$k_f = fracture\ permeability$$

$$k_m = matrix\ permeability$$

$$x_f = fracture\ half\ length$$

$$w = fracture\ fracture\ width$$

1. Model reservoir was brick shaped with an aspect ratio of $\lambda_{xy}=x_e/y_e=2.67$ *and* $\lambda_{xy}=x_e/z_e=10.0$
2. The fracture penetrated the whole YZ plane at the middle of the reservoir.
3. The fracture had conductivity (F_{CD}) ranges from $4 \leq F_{CD} \leq 20{,}000$
4. No flow boundary conditions were used in the simulations.
5. For each case, the permeabilities were equal in the x and y directions ($k_x = k_y$); however, k_z is chosen to be a tenth of k_x ($k_z = 0.1*k_x$).
6. The rock-fluid properties used in this study are shown in Figure 3.2. Fracture conductivities used in the simulations are shown in Table 3.2.

The relative permeability curves used in the simulations are shown in Figure 3.2.

3.2.2 Fluid Description

The effects of grid refinement on simulation results are studied for three distinct fluids: wet-gas, gas-condensate and black oil. Figure 3.3 shows the pressure-temperature plots of the three fluids obtained using Winprop from Computer Modeling Group. The compositional data used to create the fluids were obtained from various resources (Wet gas data – McCain (1990); Gas condensate data - Personal Communications (2012); and Black oil data - M. Ghuraiba (2000)).

3.2.3 The Grid Systems

To study the grid sensitivity of the simulation results, 10 types of grid refinement were used. The reservoir was divided into four sections from fracture to the outer no flow boundary. The pressure profile within an unconventional reservoir is complex. For the purposes of refinement, it was assumed that within each of the subblocks, the grid may be refined linearly. The section nearest to the fracture was the most highly refined. Coarse refinement was used in the outer sections. The following formula is used to create the linear grid refinement with the logic that the pressure gradient over any given distance is constant.

$$x_j = x_0 + \frac{j}{n}(x_e - x_0) \text{for } j = 1 \text{ to } n \tag{3.2}$$

Grid block size is calculated as:

$$\Delta x_j = x_j - x_{j-1} = \frac{x_e - x_0}{n} \quad \text{for } j = 1 \text{ to } n \tag{3.3}$$

Various grid distributions in x-directions were prepared for simulation as shown in Appendix D. Table 3.3 shows the different grid systems (one side of fracture) used in all of the simulations.

3.3 Results and Discussion

3.3.1 Error Analysis

The final converged results were assured by comparing the results of simulations from successive grids. Errors associated with successive grids were analyzed by a standard error analysis method. Relative errors were calculated using a modified root mean square method using following formula:

$$e_{k+1,k} = \sqrt{\frac{\sum_{i=1}^{n}\left(\frac{y_{k+1,i} - y_{k,i}}{y_{k,i}}\right)^2}{n}} \qquad (3.4)$$

where, $e_{k+1,k}$ = error between $(k+1)^{th}$ and k^{th} grids

$y_{k,i}$ = value of 'y' at time t_i for k^{th} grid

$y_{k+1,i}$ = value of 'y' at time t_i for $(k+1)^{th}$ grid

n= total number of time points at which a given outcome (either recovery or gas oil ratio) are calculated.

The errors calculated from Equation 3.4 for two successive grids were plotted to obtain the converged value. Only relevant properties such as cumulative oil or condensate and cumulative gas were used to calculate the errors. The Error Count is the RMS Error shown in equation 3.4. Figures 3.4, 3.5 and 3.6 show that the convergence was achieved as the grid is progressively refined.

In these figures, the "error count" on the x-axis was defined as the numerical count as the grid is progressively refined. For example, error count 1 refers to the calculation of error according to equation 3.4 when the grid is refined from 1 to 2. The flow performances with the different fluid systems in the reservoir with respect of oil and gas rates, and consequently of condensate to gas ratios for the condensate reservoirs and gas oil ratios for black oils are distinct. The pressure profiles in the XZ plane located in the middle of the reservoir for the various fluids were also studied to examine variability due to the use of different grid systems.

Matrix properties, barring matrix permeability, were held constant in every simulation; thus for each fixed matrix permeability case, the changes in the production behaviors and the pressure profiles were due solely to the effects of the grid refinement. The matrix permeability was varied between 1, 50, 100, 400, and 5000 nanoDarcy (nD).

3.3.2 Reservoir Fluid: Gas Condensate

Reservoirs in which the pressure and temperature were in the gas-condensate window will show the greatest sensitivity to grid effects in a low permeability scenario.

In the case where the matrix permeability was held at 1 nD, the number of grids in the x-direction was varied between 9 and 191 blocks. Figure 3.7 shows that when 9 and 13 grid blocks were used in an ultralow permeability scenario, the simulator was unable to converge on a solution, failing after 146 days and 816 days, respectively.

This effect is due to the large changes in the calculated block properties, such as saturation and pressure, and illustrates that there is a minimum number of grid blocks necessary to achieve basic convergence. This minimum refinement value depends on the matrix permeability and in the 1 nD case, it was 29 blocks. However, though the

simulation will run to completion with 29 blocks, it would yield inaccurate results when predicting the cumulative CGR of the system. Grids 1 through 8 all predict CGR values that were too high, whereas when appropriate refinement was implemented, namely Grids 9 and 10, the predicted CGR values converge. The number of grid blocks necessary for achieving convergence must be employed for ensuring accurate prediction of condensate to gas ratios. The manner in which the grid refinement was implemented is not unique.

The grid systems do provide guidelines for performing simulations of condensate fluids in ultralow permeability reservoirs. The results from the CGR study indicate that in an ultralow permeability reservoir, the grid used in the simulation should be more highly refined so as to prevent an overestimation in the CGR. As the reservoir permeability increased, the effects of grid refinement are diminished.

3.3.3 Reservoir Fluid: Black Oil

Reservoirs in which the pressure and temperature are in the black oil window also showed a notable sensitivity to grid system used. These effects are shown in Figure 3.8, which shows the cumulative GOR results for reservoirs where black oil is present. Figure 3.8 shows the cumulative GOR at various grid refinements and matrix permeabilities. These results illustrated that at ultralow permeabilities the chosen grid refinement can have serious effects on the predicted cumulative GOR of the reservoir. If the grid is refined poorly the simulator will be unable to converge on a solution, and indeed this is the case when Grids 1 and 2 are implemented.

Due to the large changes in block properties (mainly pressure and oil and gas saturations), the simulations fail after 774 days and 591 days, respectively. The lower

grid refinements caused the GOR predictions to fall below those which the well refined simulations predict. After Grid 6, the simulation results for the 1 nD case are not improved by any additional grid refinement. As permeability increased, the effects of grid refinement on the reservoir are diminished, though they were not negligible until 5000 nD.

3.3.4 Reservoir Fluid: Wet Gas

Reservoirs in which the pressure and temperature are in the wet-gas window showed a pronounced sensitivity to grid effects. This relationship is presented in Figure 3.9, which shows the results for the cumulative gas production. Figure 3.9 shows the effects of grid refinement on the cumulative gas production when the matrix permeability is varied between simulations.

These results indicate that with ultralow permeability cases, there is a minimum grid refinement that must be implemented or the simulator will not converge on a solution. Again, this is due to the large step changes in block properties which the simulator is unable to handle. The effects of this can be seen in the 1 nD reservoir permeability plot for cumulative gas production.

In the case where 9 grid blocks were used, the simulation failed after 384 days; similarly, when 13 grid blocks were used, it failed after 600 days. The cumulative condensate to gas ratio (CGR) ratio decreased with grid refinement for condensate systems. The condensate ratios for wet gas reservoirs do not change – hence, cumulative gas production values were tracked. Higher cumulative gas production was predicted with coarser grids. In the ultralow permeability case, this trend continued until Grids 6 and 7, which predict the same cumulative gas production. Again, as the permeability of

the matrix was increased, the grid refinement effects are diminished, though are not negligible until 5000 nD.

3.3.5 Grid Number Correlation

The number of grids required to obtain converged results depend on the type of fluid in the reservoir and on the matrix permeability employed. Results obtained from the simulations are summarized below.

It is evident that the grid system has the least effect on a single phase and highly permeable reservoir and a coarse grid is often satisfactory. Gas condensate reservoirs should be refined to a greater degree than wet gas or black oil reservoirs. The grid numbers obtained from converged results are summarized in Table 3.4. In this study, for the given relative permeability curves and fluid descriptions, a relationship was developed between dimensionless fracture conductivity and number of grids, as seen in Figure 3.10.

It can be seen that as we consider more complex condensate type fluids, a higher level of grid refinement is necessary. The relationships between total of number of grids required (for the given geometry and half reservoir) to reach convergence (n_h) and the fracture conductivity are shown below.

$$For\ Wet\ Gas: \qquad n_h = 8.0 \log(C_{FD}) \tag{3.5}$$

$$For\ Black\ Oil: \qquad n_h = 14.0 \log(C_{FD}) \tag{3.6}$$

$$For\ Gas\ Condensate: \qquad n_h = 20.5\ log(C_{FD}) \tag{3.7}$$

This relationship for the three different fluids indicates that the number of grids required for simulations is linearly proportional to the logarithms of dimensionless fracture conductivity. Additionally, the number of grids required for simulation of various fluids is also dependent on factors such as relative permeability curves, and fluid flow properties like viscosity.

Significant variations in these properties will have to be factored into constructing appropriate correlations. The relation shows that when reservoir permeability is very low (in nanoDarcy range), proper grid refinement is very important to get accurate results. This refinement is particularly important in gas condensate reservoirs. The proportionality constant (slope of lines in Figure 3.10) varies with type of fluids and depends on the aformentioned factors.

The study covers three different types of fluids and it has been shown that as the fluids become near critical, more grid blocks are required. This study can easily be extended to other geometries. An example of one such extension is shown below.

It can be shown that the number of grids required to reach convergence for a given dimensionless fracture conductivity and for black oil have log linear relationship with the overall size (in this case, length) of the domain. The relationship is shown in Figure 3.11.

The relationship is given by equation 3.8.

$$n_h = 18.171 \log(x_e) - 14.728 \tag{3.8}$$

3.4 Key Findings

We provide a quantitative analysis of the effect of grid refinement on important simulator outcomes in liquid rich unconventional reservoirs. After noting that grid

refinement is essential in such systems, it is shown that the number of grids required for a given geometry and for given set of fluid and fluid-rock properties depends on fluid type and reservoir matrix permeability. Near critical fluids (like condensates) and ultralow permeability systems require the highest level of grid refinement. A set of correlations that relate the number of grids to dimensionless fracture conductivities has been developed. These correlations are specific to the given geometry, fluid, and operational characteristics.

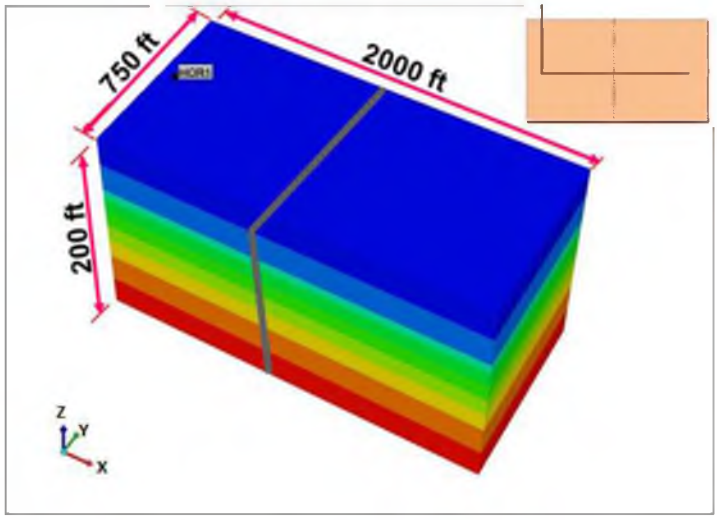

Figure 3.1: Dimensions of the reservoir model with schematic vertical cross sectional view on the right corner.

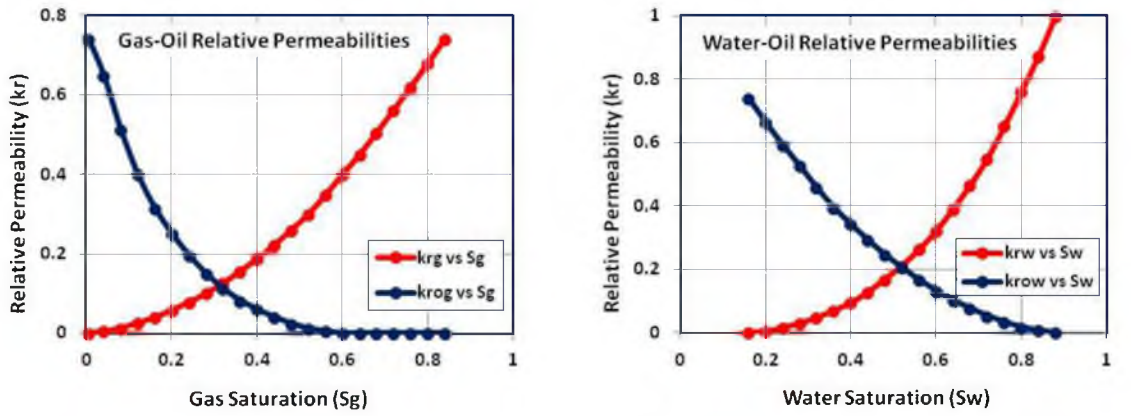

(a) (b)

Figure 3.2: Relative permeability curves (a) Gas-Oil System (b) Water-Oil System.

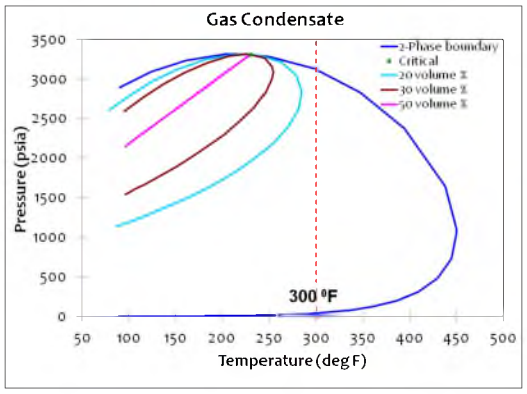

(a)

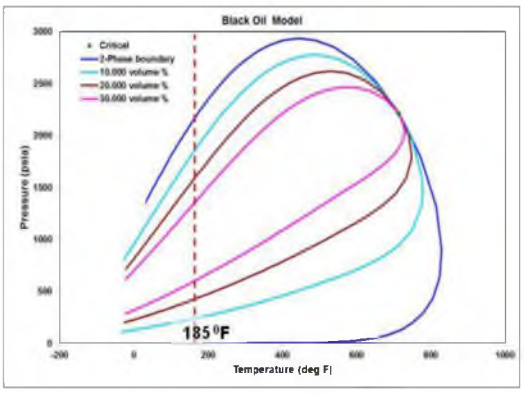

(b)

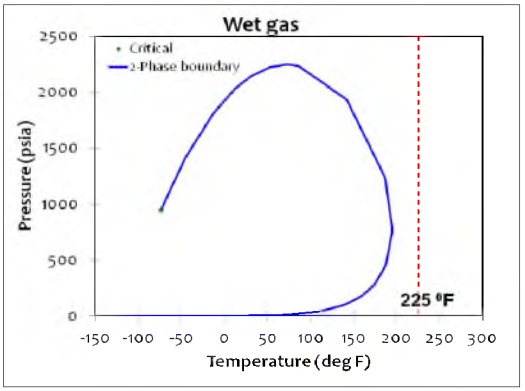

(c)

Figure 3.3: The pressure-temperature diagrams for (a) Gas condensate (b) Black oil (c) Wet gas.

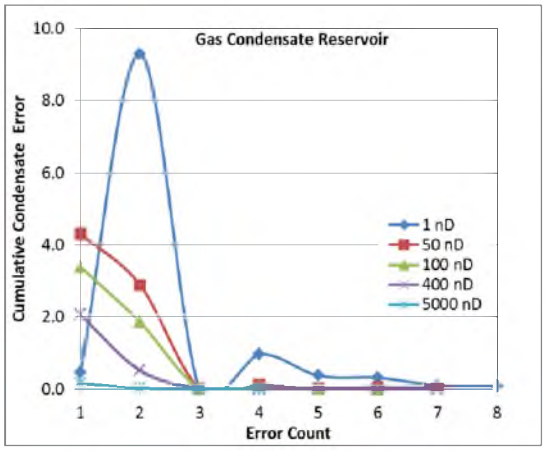

(a)

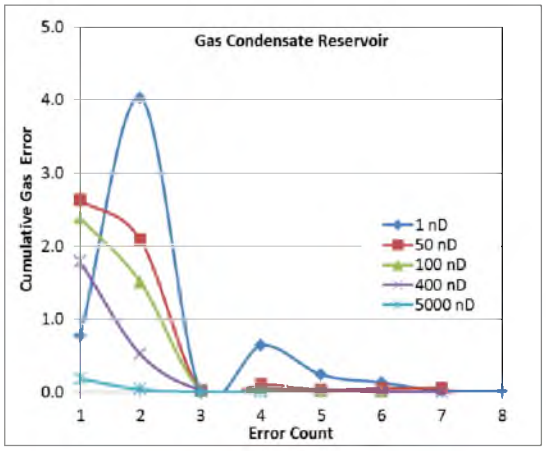

(b)

Figure 3.4: Modified RMS error for gas condensate reservoir (a) Error in cumulative condensate (b) Error in cumulative gas.

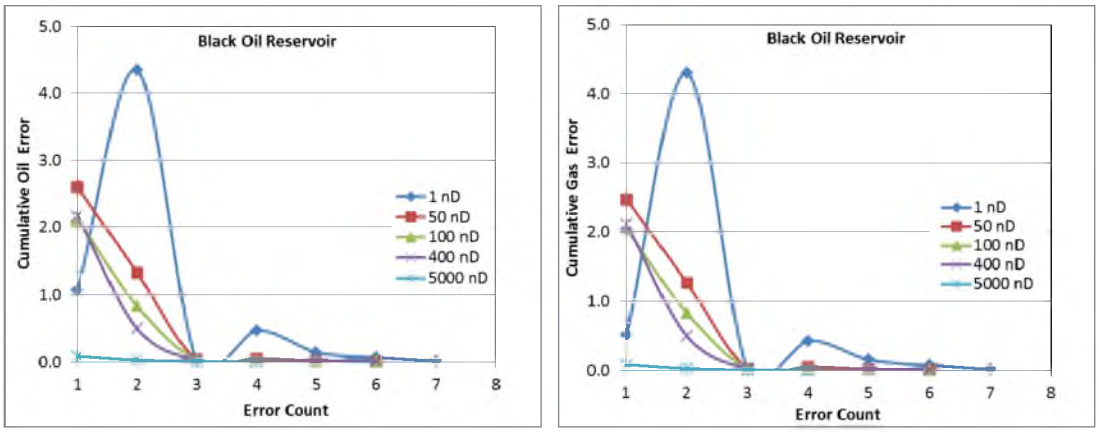

(a) (b)

Figure 3.5. Modified RMS error for black oil reservoir (a) Error in cumulative oil (b) Error in cumulative gas.

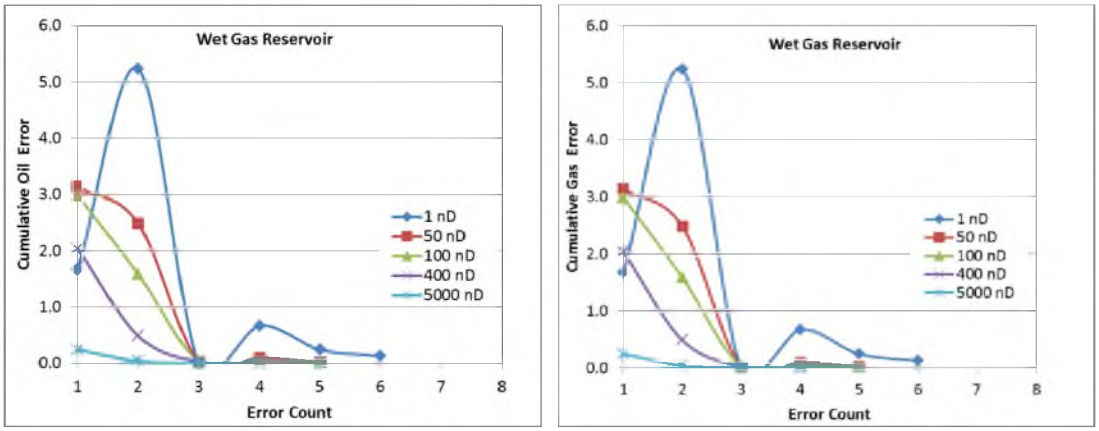

(a) (b)

Figure 3.6: Modified RMS error for wet gas reservoir (a) Error in cumulative oil (b) Error in cumulative gas.

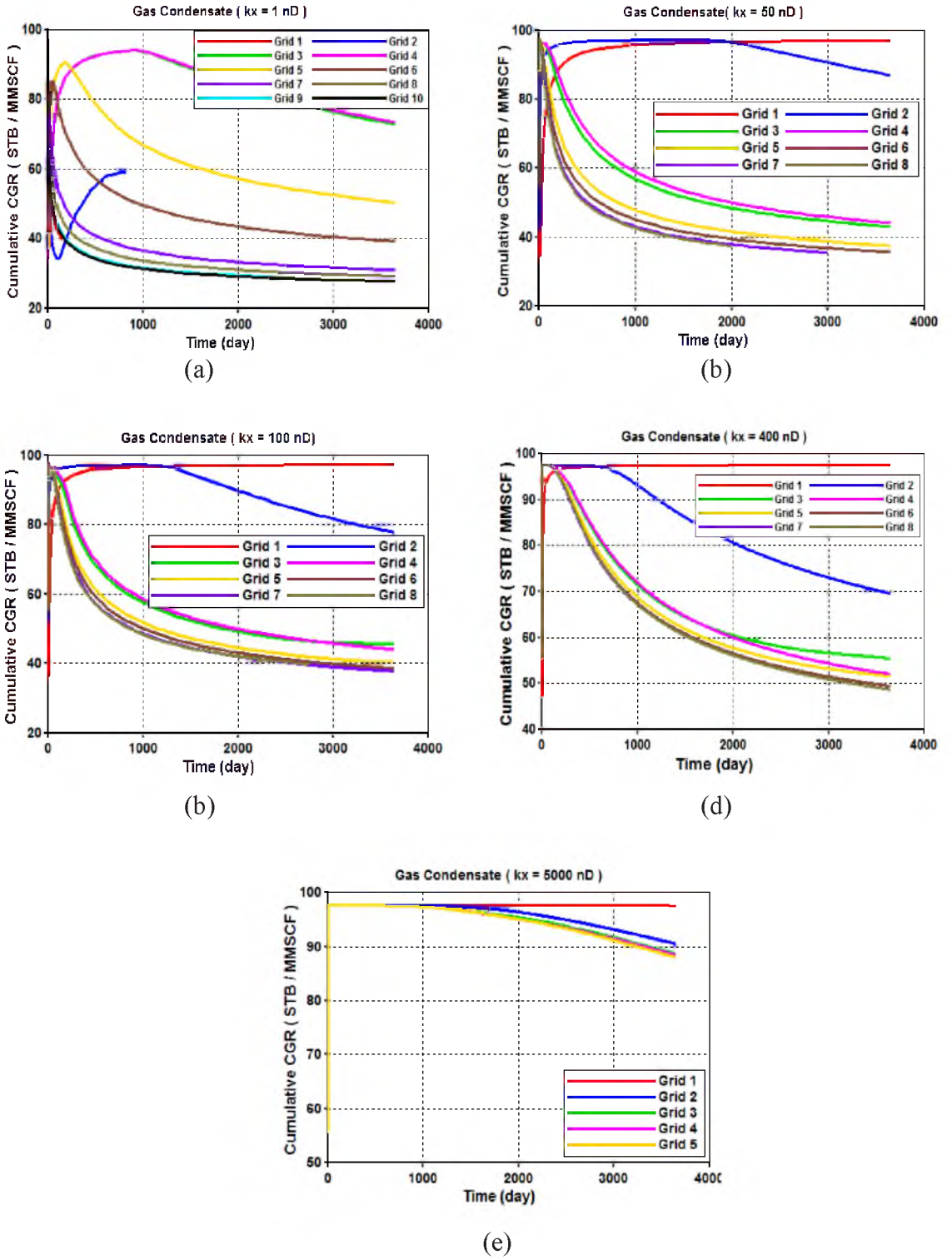

Figure 3.7: Cumulative CGR for gas-condensate reservoir with matrix permeability (a) 1nD (b) 50 nD (c) 100 nD (d) 400 nD (e) 5000 nD.

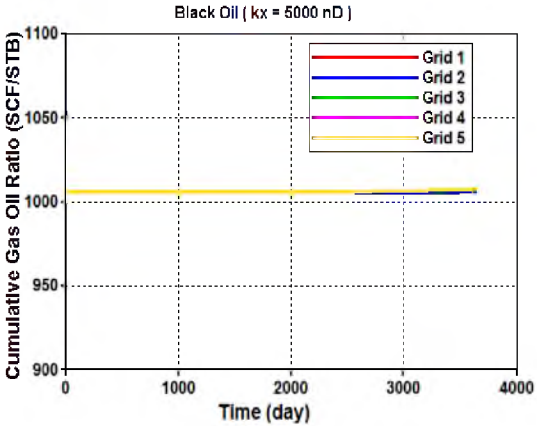

(e)

Figure 3.8: Cumulative GOR for black oil reservoir with matrix permeability (a) 1nD (b) 50 nD (c) 100 nD (d) 400 nD (e) 5000 nD.

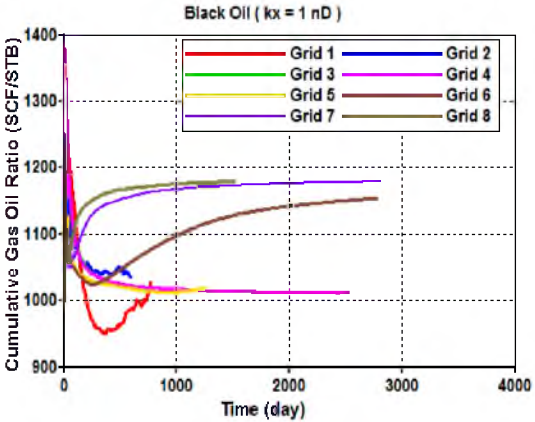
Black Oil (kx = 1 nD)
Cumulative Gas Oil Ratio (SCF/STB)
Time (day)
Grid 1
Grid 2
Grid 3
Grid 4
Grid 5
Grid 6
Grid 7
Grid 8

(a)

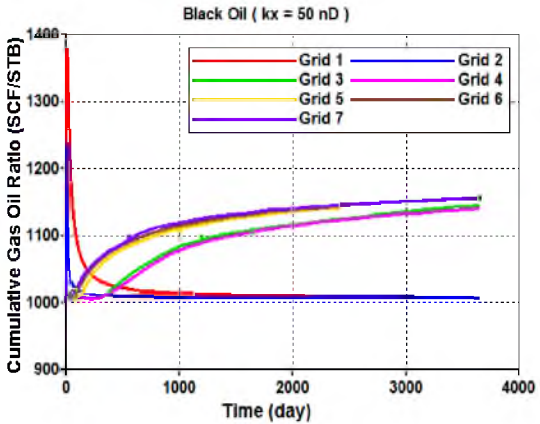
Black Oil (kx = 50 nD)
Cumulative Gas Oil Ratio (SCF/STB)
Time (day)
Grid 1
Grid 2
Grid 3
Grid 4
Grid 5
Grid 6
Grid 7

(b)

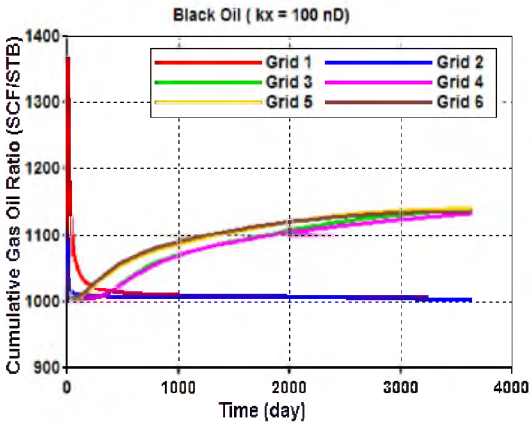
Black Oil (kx = 100 nD)
Cumulative Gas Oil Ratio (SCF/STB)
Time (day)
Grid 1
Grid 2
Grid 3
Grid 4
Grid 5
Grid 6

(b)

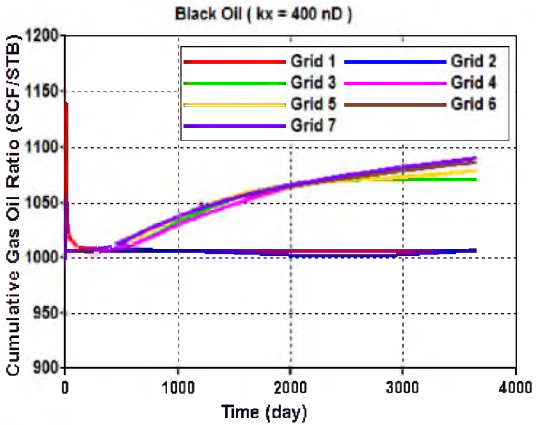
Black Oil (kx = 400 nD)
Cumulative Gas Oil Ratio (SCF/STB)
Time (day)
Grid 1
Grid 2
Grid 3
Grid 4
Grid 5
Grid 6
Grid 7

(d)

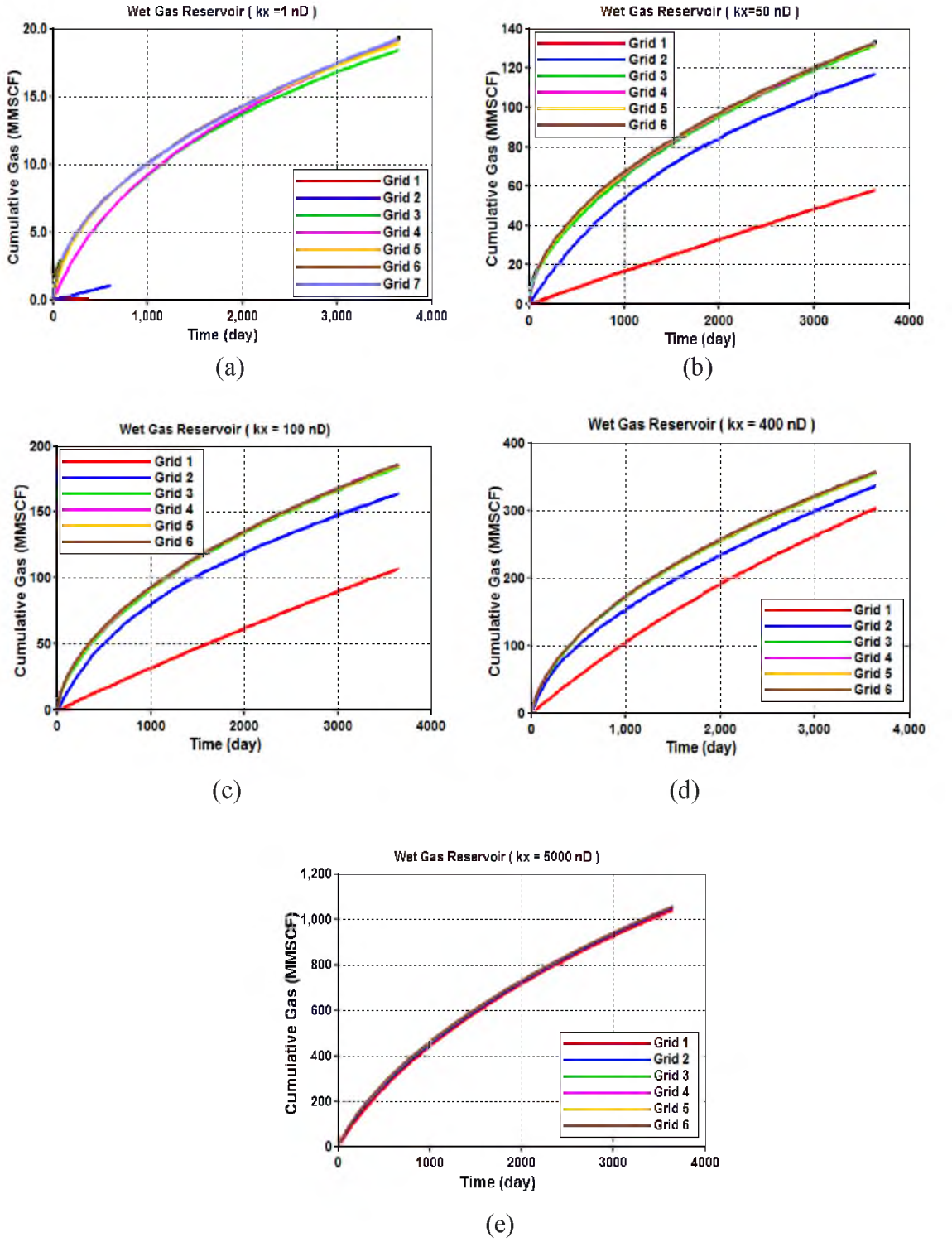

Figure 3.9: Cumulative gas production for wet gas reservoir with matrix permeability (a) 1 nD (b) 50 nD (c) 100 nD (d) 400 nD (e) 5000 nD.

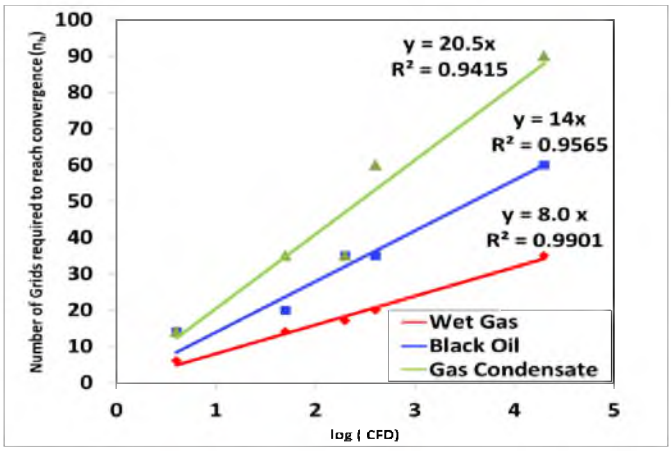

Figure 3.10: Relationship between dimensionless fracture conductivity and number of grids required to reach convergence.

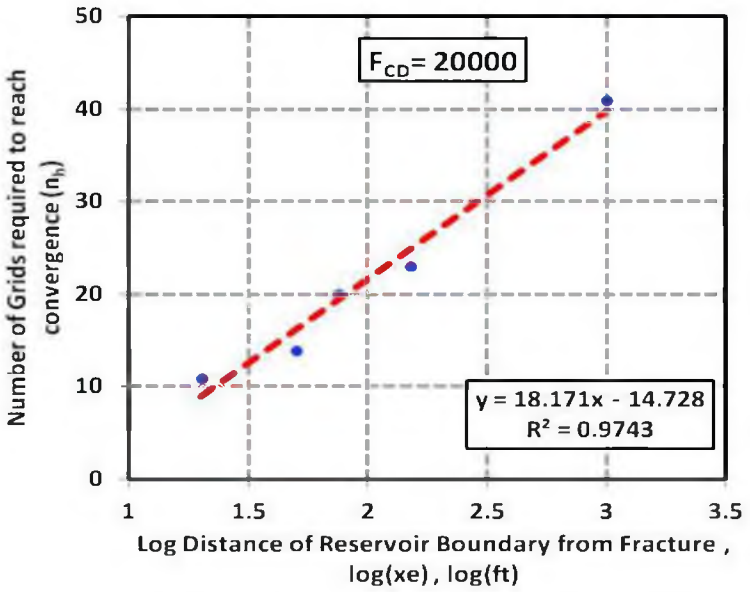

Figure 3.11: Number of grids required for black oil simulation for a given fracture conductivity (lowest matrix permeability of 1 nD) as the domain size is increased.

Table 3.1. Reservoir and operational parameters used in all of the simulations

Reservoir Top (ft):	12000
Matrix Permeability, kx (nD):	1,50,100,400,5000,
Fracture Permeability (mD):	kx = ky = 150; kz= 300
Fracture Width (ft):	0.05
Fracture Orientation	Parallel to YZ plane
Initial Reservoir Pressure (psi):	5300
Initial HC Saturation:	80% (Single phase)
Reservoir temperature (OF):	185 (Black Oil) 300 (Condensate) 225 (Wet gas)
Reservoir Porosity:	5%
Constant BHP (psi):	1500
Simulation time	10 years

Table 3.2**.** Fracture properties and conductivities used in the simulations.

w (ft)	x_f (ft)	k_{mx} (nD)	k_{fx} (mD)	C_{fD}
0.05	375	5000	150	4
0.05	375	400	150	50
0.05	375	100	150	200
0.05	375	50	150	400
0.05	375	1	150	20000

Table 3.3. Grid size distribution in X-direction.

Grid System	Grid number*Grid size(ft.) in the left side of fracture					Fracture Width, (ft.)	Total Grid in X-direction
1	-	-	-	3*250	1*249.975	0.05	9
2	-	-	-	5*190	1*49.975	0.05	13
3	5*100	4*100	3*30	1*5	1*4.975	0.05	29
4	5*100	4*90	5*25	2*5	1*4.975	.05	35
5	5*100	5*80	5*18	4*2	1*1.975	0.05	41
6	5*100	10*40	10*9	9*1	1*0.975	0.05	71
7	5*100	10*40	20*4.5	24*0.4	1*0.397	0.05	121
8	5*100	10*40	25*3.6	34*0.2857	1*0.2612	0.05	151
9	5*100	10*40	30*3.0	49*0.2	1*0.175	0.05	181
10	5*100	10*40	20*4.5	24*0.4	1*0.397	0.05	191

Table 3.4. Summarized results for grid refinement effect.

k_{mx} (nD)	C_{fd}	log (C_{fd})	One side excluding fracture (n_h)		
			Wet Gas	Black Oil	Gas Condensate
1	20000	4.30	35	60	90
50	400	2.60	20	35	60
100	200	2.30	17	35	35
400	50	1.70	14	20	35
5000	4	0.60	6	14	14

CHAPTER 4

MECHANISTIC STUDIES IN LOW PERMEABILITY OIL RESERVOIRS

Important factors governing recovery are not adequately studied due to the rapid development of unconventional reservoirs like shales. Fundamentals of fluid flow in ultralow permeability reservoirs need to be divulged to understand the production behaviors. In this paper, we perform sensitivity studies on generic reservoir models to understand the effects of important geological, petrophysical, completion and operational parameters on production of liquids from shales. We looked at the sensitivity of reservoir properties (matrix permeability, heterogeneity, rock compressibility and reservoir pressure), fluid properties (bubble point pressure and initial dissolved gas oil ratio), rock fluid properties (relative permeabilities), completion parameters (fracture spacing) and operating parameters (bottom hole pressure) on production performances. Matrix permeability, rock compressibility, fluid properties and fracture spacing have major impact on oil recovery and gas oil ratio.

4.1 Background

Flow behaviors of ultralow permeability reservoirs are different from conventional reservoirs. Performances of these types of reservoirs are not clearly understood. A number of studies have been published on primary production from undersaturated

conventional reservoirs. Evinger and Muskat (1942) introduced the concept of theoretical productivity factor for solution gas drive reservoirs. Production rates for a given drawdown decreased as the solution gas oil ratio of the oil increased. Levine and Prats (1961) provided detailed calculations of performance of solution gas drive reservoirs. They used numerical simulators and showed the dependence of rate on permeability and recovery. They were also able to generalize rate versus drawdown for their set of parameters. These and other solutions are presented in the chapter on solution gas drive reservoirs in the Petroleum Engineering Handbook (Steffensen 1987). For various cases presented here, the gas oil ratio goes through a maximum after starting out at the initial gas oil ratio. Sensitivities to such parameters as oil viscosity, permeability ratio, solution gas oil ratio, etc. were investigated. Vogel (1968) used simulation data to establish an empirical relationship between flow rate and reservoir pressure for solution gas drive reservoirs.

Many factors affect the production performance from low permeablity fractured reservoir. Laboratory experiments have shown that 30 to 100 % errors on oil in place calculations were introduced for undersaturated conventional reservoirs (Hall 1953) if the rock compressibility was neglected. The reservoir performance is very sensitive to the viscosity of reservoir fluids (Hernandez, Vesovic et al. 2002). Fracture spacing simply affects gas-oil gravity drainage when the ratio of fracture spacing and fracture height is larger than 0.3 (Clemens and Wit 2001). Oil production increases with increasing fracture permeability up to 10 Darcy and with an increase in the fracture – matrix surface contact area (Orangi, Nagarajan et al. 2011).

The impacts of fluid and rock properties such as permeability, rock compressibility,

viscosity, specific gravity, and oil Formation Volume Factor (FVF) have been investigated and Ling et al. (2011) studied the impact of these parameters on the OOIP and OGIP, recoverable oil and gas, and recovery factors. Similar studies were conducted for oil production from unconventional reservoirs such as the Eagle Ford (Chaudhary, Ehlig-Economides et al. 2011). Chaudhary et al. (2011) considered the impact of matrix permeability, flowing bottom hole pressure and fracture spacing on oil production from tight reservoirs. They didn't consider many other important properties like relative permeability, fluid PVT properties and rock compressibility in their study. In addition, their simulation results were not compared to field data. A wide range of various factors are selected to study the impacts on oil production from ultralow permeability reservoirs.

4.2 Reservoir Model

A reservoir is fractured vertically in the middle with one horizontal well in the middle of the reservoir in the X-direction. The fracture is extended up to the reservoir boundaries in Y-direction and Z- direction, i.e., height and fracture width are same as the reservoir height and width, respectively. A schematic diagram of a reservoir model is in Figure 4.1.

The reservoir width is 750 feet in the Y-direction and the reservoir height (Z-direction) is 200 feet. Width and height are considered constant for all simulations but the boundary in the X-direction is altered depending on the fracture spacing used in the particular simulation. The fracture spacing is considered the X-dimension of the model. The reservoir dimensions and other model properties are shown in Table 4.1.

Fracture width, fracture orientation, matrix porosity and initial hydrocarbon saturation remain constant. The reservoir dimension in the X-direction is varied in various studies; however, the fracture permeability, matrix porosity and the reservoir temperature are kept

constant. The reservoir properties and operational parameters used in various sensitivity studies are shown in Table 4.2.

Initial reservoir pressure, flowing bottom hole pressure, and fracture spacing vary in different studies. A wide range of matrix permeability (50 nD to 5000 nD) is also considered in various studies.

4.3 Sensitivity Studies

All simulations were conducted using IMEX, a Computer Modeling Group Black Oil simulator. Prior to conducting the sensitivity studies, we performed grid resolution studies (Panja, Conner et al. 2013) to ensure that grid resolution did not have an effect on the results. Once we ensured that convergent results were obtained by using the correct grid configurations, the following thematic studies were conducted: matrix permeability, PVT, Relative permeability, formation compressibility, overpressure, drawdown, fractured spacing and layered heterogeneity. In the following sections, we have discussed the effects of each parameter on production performance in terms of oil rate, cumulative oil or oil recovery and produced gas oil ratio.

4.3.1 Effect of Matrix Permeability

Matrix permeability is one of the most significant parameters in the production of liquids from shales. Before assessing the production data, pressure characteristics in the reservoir are analyzed. Average pressures as a function of time and pressure profile for black oil reservoirs are shown in Figure 4.2. The reservoir remains in a transient state for a long time of production until fractures are interfering. In the transient state, most of the portions in the reservoir are in initial condition as shown in Figure 4.2 b. For low

permeability reservoirs (1 nD to about 100 nD) there is little change in the average reservoir pressure from initial pressure, even though there is significant drawdown in the near fracture area. This underscores the fact that one needs to be careful when considering average properties using average pressure. The oil rate from simulation for permeabilities ranging from 1 nD to 5000 nD and the oil rate are shown in Figure 4.3 for three different initial gas oil ratios. Similar trends were reported by Chaudhary et al. (2011). The oil rate for a 400 nD reservoir (single fracture) is expected to be between 40 stb/day to about 10 stb/day in the first year. This depends on the drawdown, formation compressibility and a number of other factors.

It is evident from the figures that the oil rate does not depend on the initial gas oil ratio for matrix permeability of 1 nD to 5000 nD.

The GORs increase as the reservoir permeability decreases. The change is more significant at higher initial gas oil ratio whereas the change is negligible for lower initial gas oil ratio. This is a surprising result after having noted the slow average pressure decline in low permeability systems compared to the high permeability reservoirs. The reason for this may be the steep drawdown near the wellbore. We will discuss this as we look at pressure profiles in the near fracture region. When there is interference from other fractures, this trend is impacted as well.

It is seen that the pressure front does not move significantly outward even after about 10 years of production as shown in Figure 4.2 b. For the 400 nD case, the pressure front has propagated about 500 feet on each side of the fracture. The pressure does decrease below the bubble point (2750 psi) in the near fracture region. Only at the highest permeability (5000 nD), the pressure front reaches the boundary (1000 feet away) after 7

years and the pressure decreases below the initial reservoir pressure over the entire reservoir. It is the steep drawdown near the fracture that dominates the two-phase production behavior. Steeper decline typically leads to higher GOR at lower permeabilities. Free gas is formed in the reservoir below the bubble point. The region of the existence of free gas is very small in the case of low permeabilities. However, the GORs are higher. This shows that the initial fluid enters the "the flash chamber" near the wellbore and the steep pressure decline in that region determine the producing GOR.

4.3.2 Effect of Relative Permeability

The relative permeability is a prime factor in fluid flow through low porosity medium like shales. The relative mobility of gas and oil depends on the curvatures of relative permeability curves. Various relative permeability curves are prepared for this study by varying exponent of Corey models. The Corey models for gas-oil system are given in Equations 4.1 to 4.3.

$$S^* = \frac{(S_g - S_{gc})}{(1 - S_{org} - S_{gc})} \tag{4.1}$$

$$k_{rg} = k_{rw}(S_{gc})\ (S^*)^{n_g} \tag{4.2}$$

$$k_{rog} = k_{rg}(S_{org})(1 - S^*)^{n_o} \tag{4.3}$$

Relative permeability curves for water-oil systems are given in Equations 4.4 to 4.6.

$$S^* = \frac{(S_w - S_{wc})}{(1 - S_{orw} - S_{wc})} \tag{4.4}$$

$$k_{rw} = k_{rw}(S_{orw})\ (S^*)^{n_w} \tag{4.5}$$

$$k_{row} = k_{ro}(S_{wc})(1 - S^*)^{n_o} \tag{4.6}$$

The end point relative permeabilities were held constant during this study (S_{gc} = 0.1 and S_{org} = 0.25) . The five different cases studied are shown in Table 4.3 and the curves employed are shown in Figure 4.4. The curvature varies linear to cubic for both gas and oil relative permeability curves. The complete miscibility of gas and oil, i.e., the straight line curves (n_o=1, n_g=1) in Figure 4.5 are considered as the base case for the relative permeability study. When the effect of gas relative permeability is studied, the gas exponent (n_g) is varied and the oil exponent (n_o) is held constant (n_o=1). On the other hand, the case is vice versa for studying the effect of oil relative permeability.

We have plotted the effects of relative permeability and compared the results with base case. The results from lower oil mobility and the base case are compared for all matrix permeabilities in Figure 4.5. It is clear from this plot that the effect of oil relative permeability at higher matrix permeabilities is still noticeable compared to lower matrix permeabilities as seen in Figure 4.5a. Differences in oil production are not very significant for various oil permeabilities. The gas relative permeability is kept higher (n_g=1) than oil relative permeability in the study of effect of oil relative permeability.

Gas dominates the multiphase flow in the reservoir suppressing oil flow because of the higher gas relative permeability compared to oil relative permeability.

Oil relative permeability (in range of n_o =1 to 3) does not affect oil production for low matrix permeability (50 nD to 500 nD) if the gas relative permeability is higher.

Gas relative permeabilities on the other hand have a pronounced impact on oil

production as observed in Figure 4.5b. Lower gas mobilities can lead to 1.5 times as much oil production over 10 years at higher matrix permeabilities. The difference is smaller at lower permeabilities, yet considerable. The pronounced effect on GORs of gas relative permeabilities is also observed. The initial dissolved gas oil ratio in these simulations was 500 scf/stb. The observed differences also underscore the difficulty in interpreting production data since gas-oil relative permeabilities are not well known for shales. It is seen that at "favorable" gas relative permeabilities, the cumulative GORs can be several times the GORs at low gas mobilities.

During the study the effect of gas relative permeability, the oil relative permeability is considered as linear (n_o=1) which is higher than gas relative permeability. This fact enhances the flow of oil competing gas, more curvature in gas relative permeability curves, and better cumulative production of oil.

4.3.3 Effect of Rock Compressibility

It is hypothesized that for low permeability systems, rock compressibilities have a large effect. This hypothesis was validated when we looked at production from reservoirs with different rock compressibilities, everything else being the same. The effect of rock compressibility in very low porosity (around 5%) reservoirs like shales is very prominent because a little compression of rock assures pressure maintenance in the reservoirs. The effects can be significant as seen in Figure 4.6.

Gas oil ratios are also much lower with higher rock compressibilities as shown in Figure 4.6a. The oil production is about double in 10 years when the rock compressibility is 25 times higher as shown in Figure 4.6b.

These trends were also observed by Orangi et al. (2011). Lower compressibility rocks

do not permit the structure to deform; on the other hand, higher compressible rock sustains the pressure of reservoir by squeezing the rock and reducing the pore space for overburden pressure when the pressure in the pore is reduced in course of production. Holding pressure in reservoir helps gas to stay in oil phase as dissolved form, and thus, more oil with less GOR is produced on surface.

4.3.4 Effect of Fluid Properties

Fluid properties play the greatest role to achieve higher oil recovery. Heavy oil with little or no dissolved gas is hard to produce; on the other hand, light oil is produced with relative ease but in the cost of higher gas oil ratio. The effect of fluid properties namely bubble point pressure and initial gas oil ratio were studied. In this purpose, five different fluids with pressure-volume-temperature (PVT) properties were chosen as shown in Table 4.4. The gas oil ratio ranges from 700 SCF/STB to around 1600 SCF/STB and bubble point pressure from 1000 psi to 3700 psi. PVT 2, 3 and 4 have same *initial gas oil ratio* (R_{si}) but different bubble point pressures. PVT2 and 5 have same *bubble point pressure* (P_{bp}) but different initial gas oil ratios. PVT1, 3 and 5 have the same slope for solution gas versus pressure $\left(\frac{dR_s}{dP}\right)$ but have different bubble point pressures.

The effects of bubble point pressure for same initial gas oil ratio are shown in Figure 4.7 for matrix permeability of 50 nD. The initial gas oil ratios are kept constant at 700 SCF/STB while the bubble point pressures are changed by varying the slope of gas oil ratio with pressure in PVT. As the bubble point pressure is reduced, the oil production decreases and similar trends are observed for higher permeabilities (up to 5000 nD) too. For the economic rate of oil, the well is normally operated below bubble point pressure. A certain amount of gas remains in the oil phase as dissolved form. This gas billows out

of oil phase when reservoir pressure drops below bubble point pressure. A small segment of reservoir near to fracture becomes saturated quickly for flowing bottom hole pressure below bubble point pressure. The reservoir is transformed into a saturated condition much quicker in the case of higher bubble point pressure. Gas phase dominates flow in the saturated zone suppressing oil phase, and thus yields more produced GOR on surface. Quicker transition to saturated condition also helps to sustain pressure which, in turn, is effective to produce more oil. Reservoir with lower bubble point pressure remains in single oil phase except near fracture zone for a longer time and produces gas oil ratio close to initial GOR. In this case, less oil is produced due to higher pressure drop in reservoir for absence of free gas phase.

The effect of initial dissolved gas on production is shown in Figure 4.8. The higher amount of oil is recovered from higher initial dissolved gas as shown in Figure 4.8a, albeit the higher produced gas oil ratio (Figure 4.8 b). Produced gas oil ratio increases with time as pressure drops in the reservoir. The higher initial dissolved gas provides higher energy for oil production. The higher initial gas oil ratios indicate higher bubble point pressure for PVT with fixed slope of gas oil ratio with pressure. Transition from undersaturated to saturated condition occurs quicker for higher bubble point pressure as discussed in the previous section. Higher amount of gas dissolved in reservoir also makes oil lighter and improves mobility of oil.

4.3.5 Effect of Fracture Spacing

Optimum fracture spacing which will yield maximum recovery of oil is the primary concern of this study. Intuitively, minimum fractures spacing allowed by the economic constraint from the fracturing cost leads to maximum recovery of oil. Increasing the

number of fractures increases the cost. Depending on the payoff time and economic limit, optimization of fracture spacing is necessary. The effects of fracture spacing for different reservoir permeablities (1 nD to 5000 nD) are studied here. The basic parameters of the spacing study are shown in Table 4.2 and the schematic of the spacing away from the fracture is shown in Figure 4.1. The idea was that the no flow boundary would be an actual reservoir boundary or boundary of another fracture for a given spacing. Here recoveries were calculated at the "abandonment" rate of 1 stb/day. Oil recoveries for different spacing and at different matrix permeabilities are shown in Figures 4.9 a and b. Oil recovery decreases rapidly as fracture spacing increases for 1 nD to 500 nD as shown in Figure 4.9 a. Recovery stays constant with fracture spacing for 5000 nD permeability reservoir and decent recoveries are obtained at spacing between 50 and 150 feet. For more clarification on the effect of spacing on different reservoir permeability, oil recovery is plotted against reservoir permeability with different fracture spacing as shown in Figure 4.9 b.

Oil recovery increases sharply with fracture spacing for permeability upto 500 nD. Beyond this permeability, recoveries change 1 to 4 % with reducing fracture spacing from 150 feet to 20 feet as illustrated in Figure 4.9 b.

For ultralow permeability reservoirs (50 nD to 500 nD), a sharp decline in pressure is noticed near the fracture and transient state exists even for entire life of the reservoir, i.e., a significant part of reservoir remains in initial conditions. Oil rate reaches economic production value without exploiting the majority of the reservoir. Hence, less oil is recovered leaving most of the oil inside pores. Thus spacing affects oil recoveries significantly for reservoir permeabilities of 1 nD to 500 nD. On the other hand, initial

pressure front reaches reservoir boundary or interferes other fractures rapidly for relatively higher permeability reservoirs like 1000 nD to 5000 nD. Oil is produced from the entire fracture space and the reservoir is depleted well into saturated conditions. In this case, fracture spacing does not help a lot to improve recovery. It should be noted that we have not considered the effect of geomechanics when considering fracture spacing. It is acknowledged that this consideration may change our results.

4.3.6 Effect of Drawdown and Overpressure

We looked at the effect of drawdown on oil and gas recoveries at two different initial reservoir pressures. The bubble point is kept constant at 2800 psi for both cases. Oil recoveries were determined at the "abandonment" rate of 1 stb/day since only one fracture was modeled. Geomechanical effects of fracture closure with drawdown are not considered in these simulations. Oil and gas recoveries are compared for two different initial pressures (4500 psi and 5500 psi) in Figures 4.10 a and b.

Oil recoveries from 100 nD reservoir are higher than the 50 nD reservoir as expected but appear to be optimum with respect to drawdown at lower permeabilities of 50 and 100 nD, while the gas recoveries increase monotonically as drawdown increases. For the same drawdown, more oil is recovered from the reservoir with less initial pressure (4500 psi). The well is operated at higher flowing bottom hole pressure for higher initial pressure (5500 psi) to maintain same drawdown and less oil is recovered as a result, although higher optimum recovery is achieved from higher initial pressure reservoir because of a long time supply of energy to continue production before reaching the economic rate. The optimum value shifts towards higher drawdowns for higher initial reservoir pressures and for higher permeability (100 nD).

4.3.7 Effect of Impermeable Layer

Impermeable bentonite layers are found between two shale layers. Layered heterogeneity was studied by inserting impermeable layers (say bentonite) between two permeable layers. The thickness of the bentonite layer was 1 foot and permeability was kept at a hundred times less than the formation permeability. Bentonite layer permeability for open fracture (at bentonite layer) is kept same as fracture permeability, and in the case of closed fracture, bentonite layer permeability was used at the fracture. Cumulative oil and GOR for various cases of fracture opening and closing at bentonite layers are analyzed in Figure 4.11. Fracture acts as high conductive conduit in reservoirs, when impermeable layers are deposited between two layers; it hinders the vertical cross flow. Oil production is almost the same for reservoir (fractured) without any bentonite layers and reservoir with opened fracture at bentonite layers. This result confirms that there is no vertical cross flow between layers and linear flow is established. Gas and oil flow horizontally towards the fracture and then are connected through fracture into wells. It is observed that when bentonite layers heal and close at the fracture and assume the permeability of the layer, then the production is reduced significantly. This suggests that fracture closure at the bentonite layer isolates the fluid coming to the fracture from adjacent layer, and thus, fluid is produced only from the layer adjacent to well. For this case of isolated layer without fracture opening at bentonite layers, drawdown is solely applied to the layer adjacent to the well and higher pressure drop in this layer promotes higher gas oil ratio.

4.4 Comparison with Field data

Comparisons of field data (Eagle Ford, Niobrara and Bakken) with simulation results are shown in Figures 4.12, 4.13 and 4.14. It should be noted that the rates are for noninterfering single fracture, and net to gross ratio (NTG) is considered as 0.4 for Eagle Ford and 0.6 for Niobrara and Bakken. If there are five clusters per stage in a 16-stage well, with about 80 possible fractures, the rate for a 400 nD reservoir is expected to be between 500 stb/month to about 150 stb/month in the first year. This depends on the initial dissolved GOR, drawdown, formation compressibility and a number of other factors.

Analysis of the Eagle Ford oil rate indicates that the reservoirs fall within the 50 to 100 nD permeability range. The field oil rates are tightly clustered in 50-100 nD permeability range and then dipping below the 50 nD simulation results after about a year or so. The GOR values for Eagle Ford are much more variable.

The simulation results indicate that for initial gas oil ratios of 500 scf/stb and 1000 scf/stb, the cumulative GORs do not vary much for different permeabilities. At the highest value of the gas oil ratio, the lowest permeability yields highest cumulative GOR. Variations in field values span the entire range of initial gas oil ratios used in the simulation. These variations appear to be related more to the initial composition of the fluid than to permeability variations. The Niobrara production rates show a wider variation. This is because the producing compositions and reservoir quality are different for the different formations chosen – Silo, Hereford and Wattenberg. The cumulative gas oil ratios however are remarkably consistent. The average cumulative GOR values for Silo and Hereford lie between the initial GOR of 500 to 1000 scf/stb. The Wattenberg

GORs are higher – most likely due to the initial dissolved GOR being higher. The Bakken oil rates appear to correspond to higher reservoir permeabilities. These wells are some of the best in the Bakken – Parshall field. The permeabilities to which the field production correspond to appear to be over 400 nD, but less than 5000 nD.

This finding is consistent with the "conventional wisdom" that the Bakken permeabilities – for good wells – are in micro Darcies.

4.5 Key Findings

Impacts of important geological, fluid properties, operational and completion parameters on oil production from ultralow permeability reservoirs are investigated and the important findings are summarized here.

— As the permeabilities decrease, oil production increases with increase in reservoir permeability but produced gas oil ratio also increases.

— Gas relative permeabilities have more significant impact than oil relative permeabilities.

— The oil production is higher with more compressible rock. Produced gas oil ratio is also reduced for higher compressible rock.

— Higher reservoir energy in the form of higher initial dissolved gas is better for oil production. Higher initial dissolved gas oil ratio results in higher oil production at higher GORs.

— Quicker transition to bubble point leads to higher GORs but does not hurt oil production.

— Reduced spacing, generally speaking, results in higher recovery. Spacing has the greatest influence up to 500 nD permeability.

— Overpressure is one of the key variables. Less oil and gas are recovered from a reservoir with higher initial pressure for same drawdown.

— Optimum oil recoveries are obtained with drawdown for low permeability reservoir (50 nD and 100 nD) although gas recoveries increase monotonically

— Higher drawdown generally results in higher recovery – with production at higher GORs. Higher drawdown may also result in fracture closures, even though this geomechanical effect was not considered in the simulations.

— Impermeable layers like bentonite layers between produced layers reduce recovery when the hydraulic fractures heal and close.

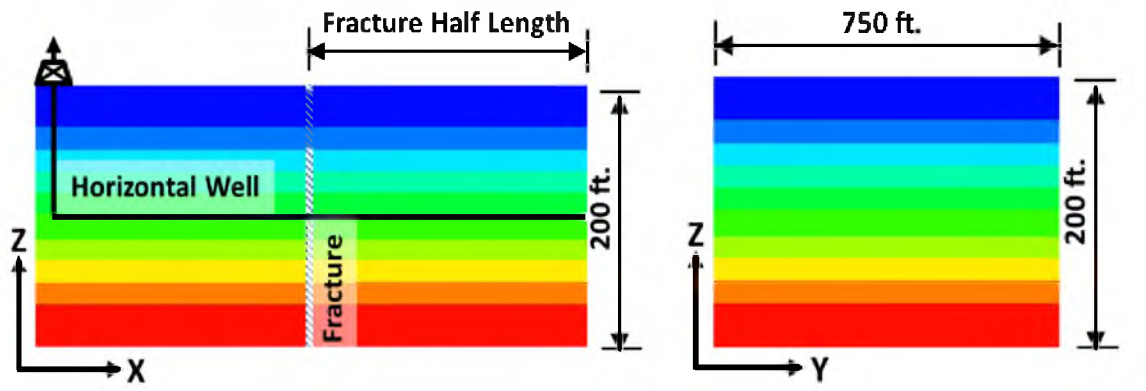

Figure 4.1: The geometry and dimensions of the reservoir model

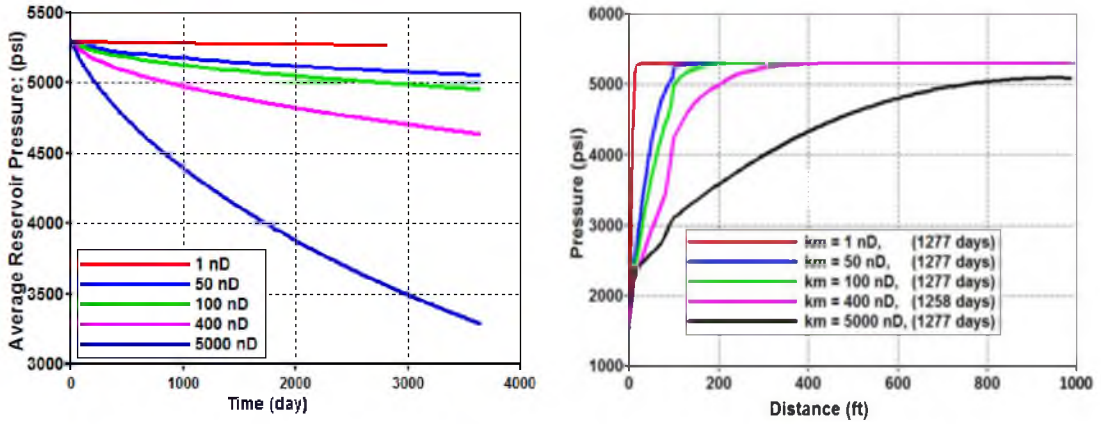

(a) (b)

Figure 4.2: Pressure characteristics for different permeabilities (a) Average reservoir pressures with time (b) Pressure profiles inside reservoir.

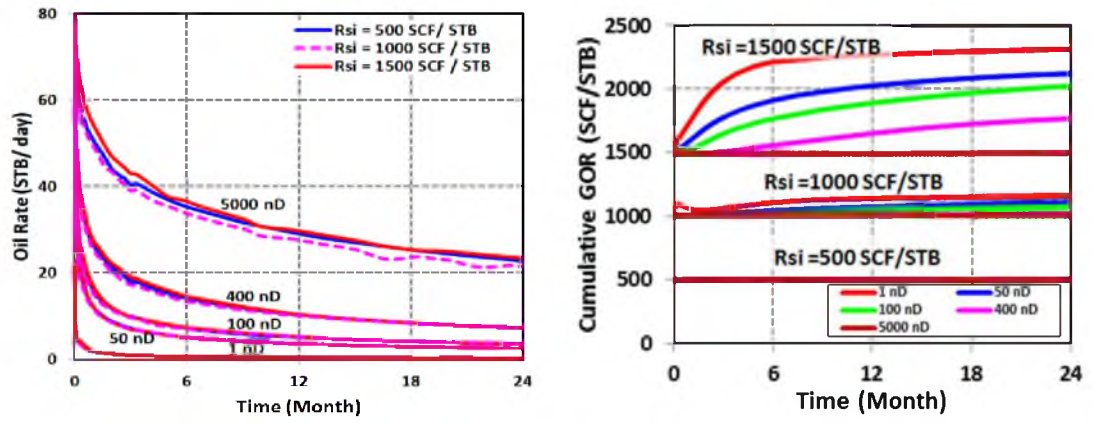

(a) (b)

Figure 4.3: Production from different matrix permeabilities a) Oil rate (b) Cumulative GOR.

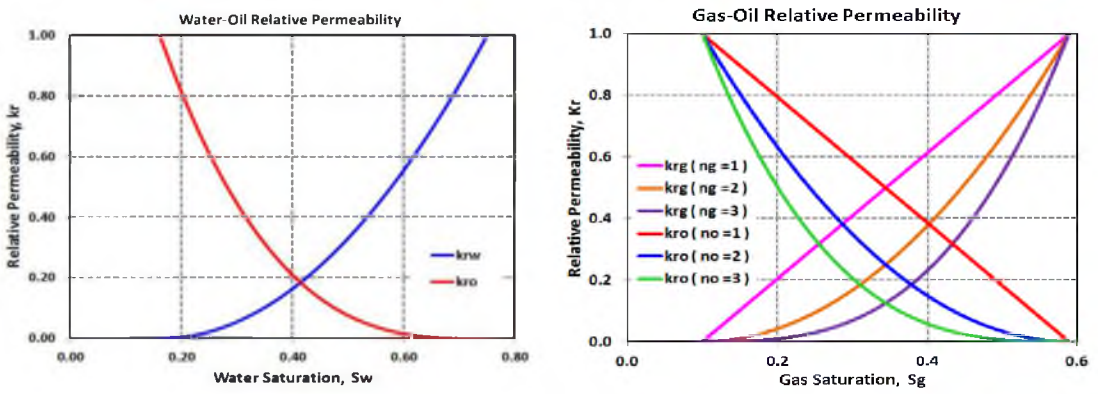

(a) (b)

Figure 4.4: Relative permeability curves for (a) Water-Oil two-phase system (b) Gas-Oil two-phase system.

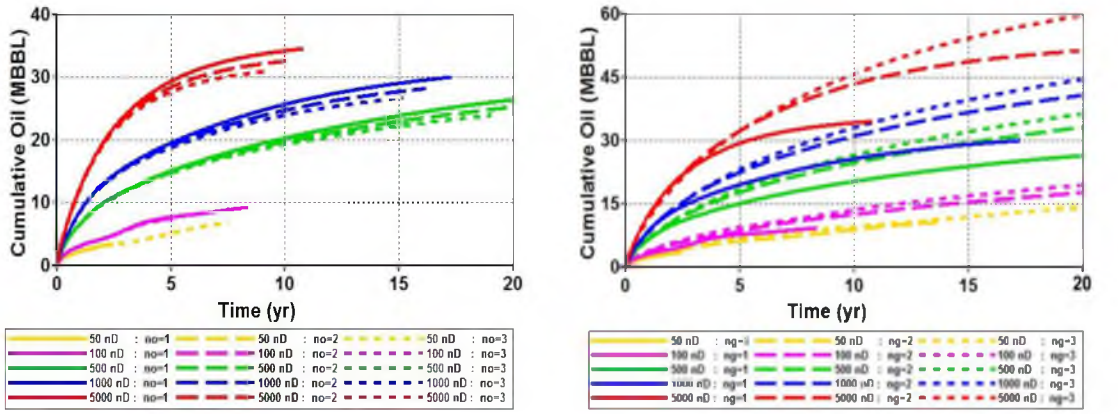

(a) (b)

Figure 4.5: Cumulative oil for three different exponents of (a) Oil relative permeabilities (b) Gas relative permeabilities.

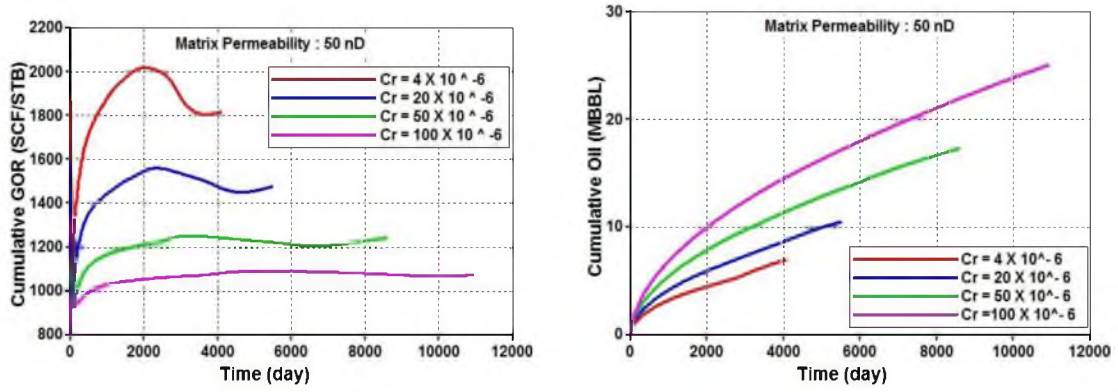

(a) (b)

Figure 4.6: Impact of compressibilities for matrix permeabilities of 50 nD on (a) Cumulative gas oil ratio (b) Cumulative oil production.

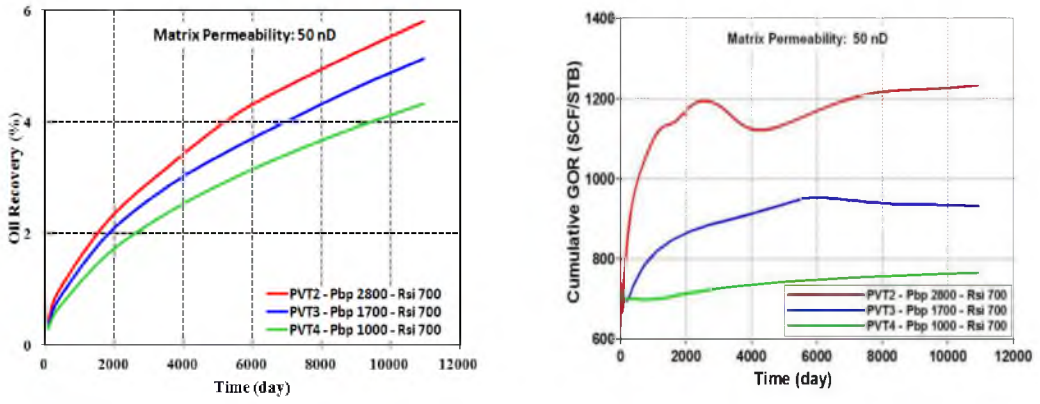

(a) (b)

Figure 4.7: Effect of bubble point pressure with fixed initial gas oil ratio on (a) Oil recovery (b) Cumulative gas oil ratio.

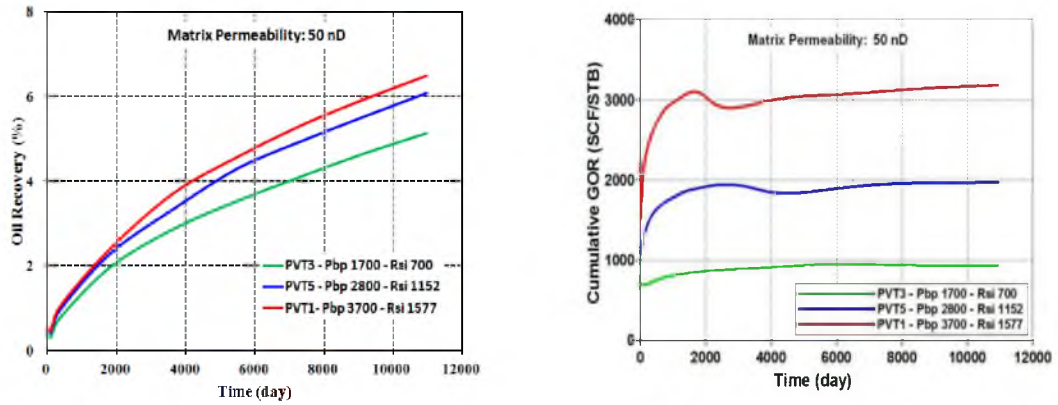

(a) (b)

Figure 4.8: Effect of gas oil ratio with fixed slope dRs/dp for matrix permeabilities of 50 nD on (a) Oil recovery (b) Cumulative gas oil ratio.

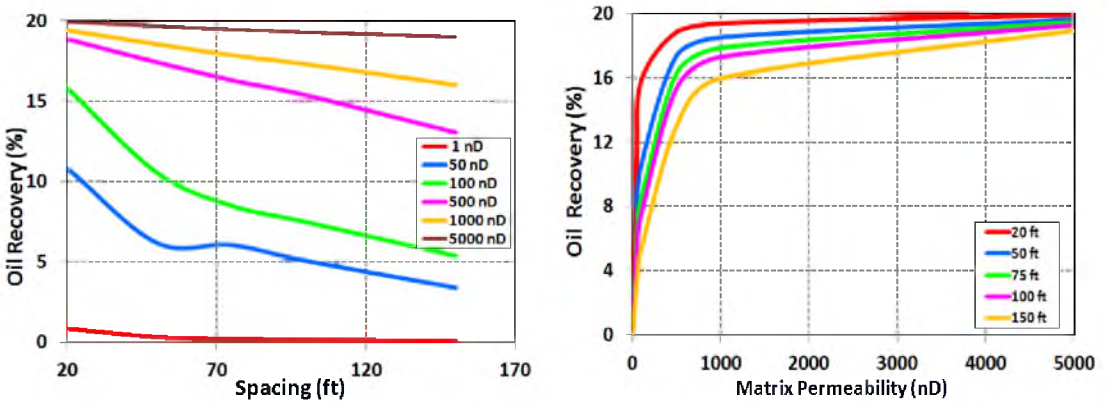

(a) (b)

Figure 4.9: The effect on oil recovery of (a) Fracture spacing (b) Permeability for different spacing.

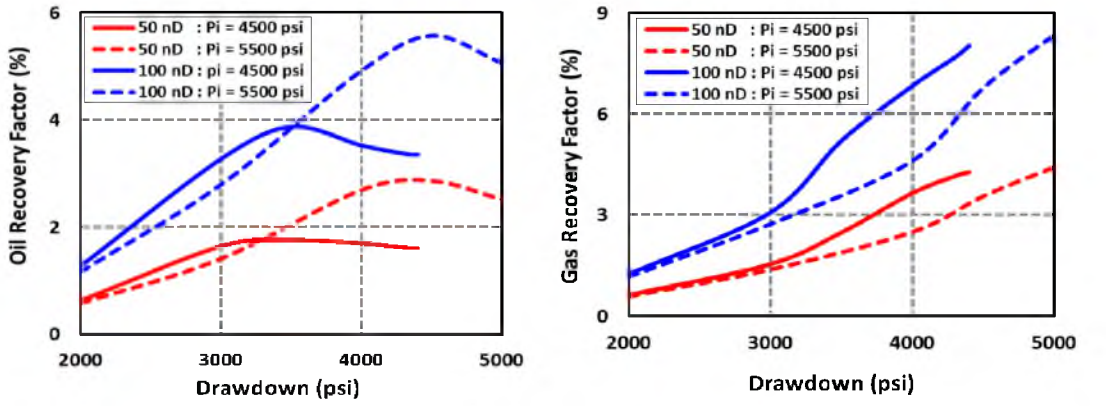

(a) (b)

Figure 4.10: Effect of drawdown and initial reservoir pressures on (a) Oil recoveries (b) Gas recoveries.

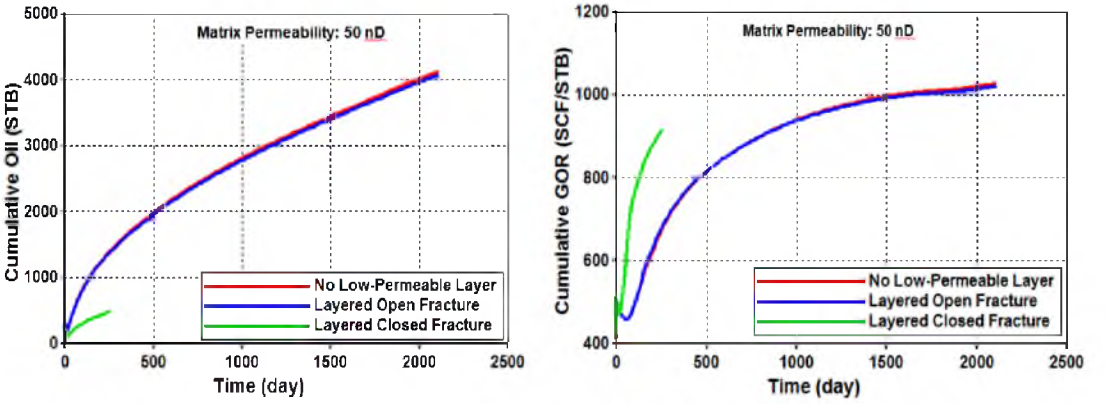

(a) (b)

Figure 4.11: Comparison of performances from open and closed fractures (a) Cumulative oil (b) Cumulative gas oil ratio.

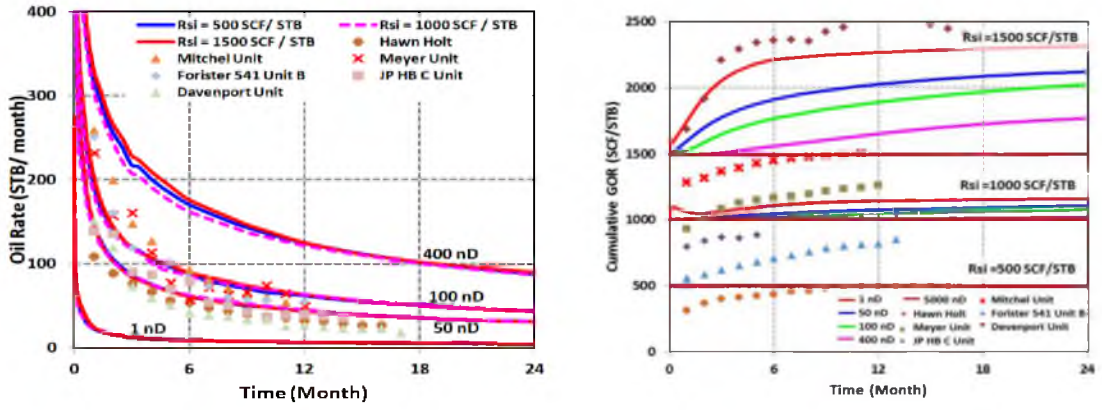

(a) (b)

Figure 4.12: Comparison of Eagle Ford field data with simulation for (a) Oil rate (b) Cumulative gas oil ratio.

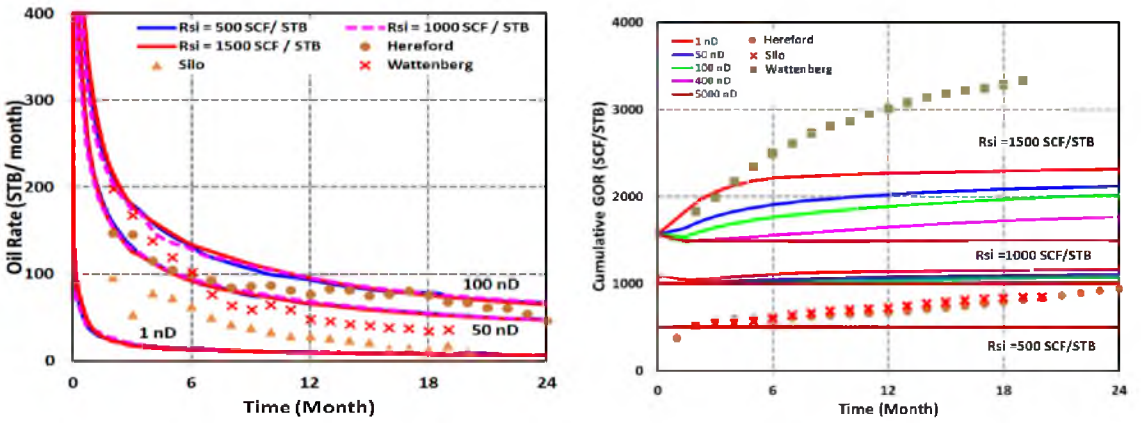

(a) (b)

Figure 4.13: Comparison of Niobrara field data with simulation for (a) Oil rate (b) Cumulative gas oil ratio

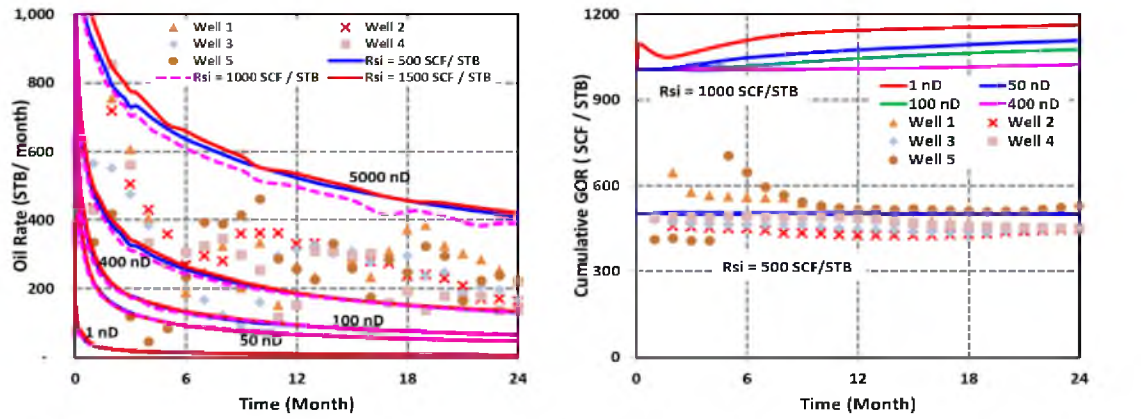

(a) (b)

Figure 4.14: Comparison of Bakken field data with simulation for (a) Oil rate (b) Cumulative gas oil ratio.

Table 4.1. Reservoir and fracture parameters used in all studies.

Reservoir Height (ft)	200
Y-dimension of Reservoir (ft)	750
Fracture Permeability (mD)	$k_{fx} = k_{fy} = 150$; $k_{fz} = 300$
Fracture Width (ft)	0.05
Fracture Height (ft)	Reservoir Height
Fracture Orientation	Parallel to YZ plane
Reservoir Porosity:	5%

Table 4.2. Reservoir and operational parameters used in different studies

Name of Study	Initial Pressure (psi)	BHP (psi)	Fracture Half Length (ft)
Matrix Permeability	5300	1500	1000
Relative Permeability	4500	500	150
Rock compressibility	5000	500	150
Fluid PVT	4500	500	150
Fracture spacing	5300	500	20,50,750, 100,150
Drawdown/ Overpressure	4500/5500	100, 200, 500, 1000,1500, 2500	150
Layered Heterogeneity	4500	500	150

Table 4.3. The relative permeability parameters used in the study

Case	Water – Oil System				Gas - Oil System			
	n_w	n_o	k_{rw} (S_{orw})	k_{ro} (S_{wc})	n_g	n_o	k_{rw} (S_{gc})	k_{rg} (S_{org})
1	3	3	0.6	1	1	1	1	1
2	3	3	0.6	1	1	2	1	1
3	3	3	0.6	1	1	3	1	1
4	3	3	0.6	1	2	1	1	1
5	3	3	0.6	1	3	1	1	1

Table 4.4. Bubble points and solution gas oil ratios used in the study

PVT	Slope dRs/dp ((SCF/STB)/psi)	Bubble Point Pressure (psi)	Rsi (SCF/STB)
1	0.415	3700	1577
2	0.247	2800	700
3	0.415	1700	700
4	0.710	1000	700
5	0.415	2800	1152

CHAPTER 5

EXPERIMENTAL DESIGN AND RESPONSE SURFACE METHODS: GAS CONDENSATE

Rapid development of shales for the production of oils and condensates may not be permitting adequate analysis of the important factors governing recovery. Understanding the performance of shales or tight oil reservoirs producing condensates requires numerically extensive compositional simulations. The purpose of this paper is to identify important factors that control production of condensates from low permeability plays and to develop analytical "surrogate" models suitable for Monte Carlo analysis. In this study, the surrogate reservoir models were second-order response surfaces functionally dependent on the nine main factors that most affect condensate recovery in ultralow permeability reservoirs. The models were developed by regressing the results of experimentally designed compositional simulations. The Box-Behnken technique, a partial factorial method, was used for design of these experiments or simulations. The main factors that controlled condensate recovery from ultralow permeability reservoirs were reservoir permeability, rock compressibility, initial condensate to gas ratio (CGR), initial reservoir pressure, and fracture spacing. Another main outcome of this paper was the generation of probability density functions, and P10, P50 and P90 of condensate recovery based on the uncertainty in input parameters. The condensate recovery P50 for rate based outcome of 5 barrels per day per fracture was found to be less than 10%.

5.1 Background

Current production of liquids – oils and condensates from Eagle Ford is over a million barrels per day, of which about 20% accounts for condensates. The increase in production is due primarily to the large number of wells being drilled. Because of the rapid pace of activity, it has not been possible to understand the important factors affecting production and get the most out of each well. In fact, the total production of condensates declined for the first time in the short history of Eagle Ford despite increased drilling activity (see Figure 5.1).

The first main objective of this paper is aimed at identifying important factors that affect production of condensates from ultralow permeability reservoirs. This identification provides an early screening tool to benchmark recovery expectations of condensates being produced from shales.

Prediction of condensate production from reservoirs requires compositional simulation. Simulation of hydraulically fractured wells with low permeability matrix necessitates high resolution simulation with a large number of grid blocks.

Generation of validated response surfaces that accurately represent the results of compositional simulations would be useful in performing uncertainty and subsequently risk analysis and generate P10, P50 and P90 numbers for important outcomes of condensate production in shales. Early analysis will provide realistic estimates of what is feasible in these exciting, but challenging plays. The second main objective of the paper was to generate validated response surface or surrogate models for condensate production in shales.

Response surface methodology has been used in reservoir engineering frequently.

The quest for optimal production and the associated uncertainty started in the early 1990s with the use of response surface methods (RSM) (Damsleth, Hage et al. 1992; Egeland, Holden et al. 1992; Aanonsen, Eide et al. 1995). Since then, the RSM method has been exploited for various purposes from uncertainty in initial hydrocarbon reserves (Peng and Gupta 2003), optimum well placements (Guyaguler and Horne 2001; Manceau, Mezghani et al. 2001; Manceau, Roggero et al. 2002; Landa and Güyagüler 2003; Carreras, Turner et al. 2006), and uncertainty in production performance and recovery (Dejean and Blanc 1999; Chewaroungroaj, Varela et al. 2000; Corre, Thore et al. 2000; Venkataraman 2000; Manceau, Mezghani et al. 2001; Mohaghegh 2006). Field development plans for gas condensate reservoirs were assessed by performing uncertainty analysis of reserves and production performance (Quinones, Lanchimba et al. 2010; Descubes 2012; Quinones and Lanchimba 2012). Yeten et al. (2005) compared various design of experiment and response surface methods to show the effectiveness of the technique. They determined that the response surface method can be used as an efficient and fast proxy model for reservoirs to forecast the production performance and to analyze uncertainty (Amorim and Schiozer 2012) if the appropriate design of experiment has been selected. Response surface consisting of four parameters and uncertainty analysis in oil recovery and pressure drop were studied in an Iranian fractured reservoir (Khosravi, Fatemi et al. 2011). Three of the most significant parameters were identified: aquifer strength, matrix block size, and fracture permeability. Artificial Intelligence (AI) based proxy model (Dahaghi, Esmaili et al. 2012) and pore network model (Xie, Lee et al. 2013) using fundamental equations with the uncertainty in pore length, pore size, pore number are also generated for production performance (gas rate and cumulative gas) from

shale gas reservoirs. Simple models comprising range of parameters to evaluate the performance and uncertainty of condensate production from ultralow permeability (10 nD to 5000 nD) fractured reservoirs were used.

A limited number of studies on response surfaces and uncertainty evaluation for gas condensates have also been reported. Simulations were run to examine important parameters in a modified pseudosteady state (Diamond, Pressney et al. 1996) analytical model with gas material balance equation in Britannia Gas Condensate field in North Sea Field (reservoir permeability of 5 mD to 100 mD). Giving the uncertainty in inputs, the cumulative probability distribution curve for gas rate has been studied. Atbi et al. (2004) created second-order polynomial response surface models for cumulative gas and plateau length applied in Tiguentourine field (conventional reservoir) in the South East of the Algerian Sahara desert using D-optimal design of experiment. P90 production profiles (gas rate and cumulative gas) were generated using Monte Carlo simulations. Initial reservoir condition, flowing bottom hole pressure, rock fluid properties and other parameters were not considered in their study. Experimental design using a set of comprehensive compositional simulations for ultralow permeability condensate reservoirs (shale plays like the Eagle Ford) has not been reported previously. The one additional difference in this study is also that the focus is primarily on parameters that affect liquid production from condensate plays in shales.

Because the performance of wells producing from these plays varies considerably, identification of what impacts production and uncertainty in recovery given important parameter variability will be useful for screening and early planning phases. In a play like Eagle Ford, fluid compositions also vary from region to region over fairly short distances.

The purpose of this study was to identify parameters that impact production of condensates in hydraulically fractured tight reservoirs and to provide uncertainty estimates over relevant parameter space, including varying fluid compositions. A sensitivity study was used to select important parameters. Second-order response surface models for different times of production and for a minimum economic condensate rate were constructed based on experimental design consisting of compositional simulations. Uncertainty in the recoveries was also studied giving the some probabilistic distributions in the input parameters.

5.2 Methodology

5.2.1 Reservoir Model

All simulations were conducted using GEM, a Computer Modeling Group Compositional simulator. One vertical fracture is placed in the middle of the reservoir with one horizontal well in the X-direction. The fracture height and fracture width were the same as the reservoir height and width, respectively. The dimensions of the reservoir are shown in Figure 5.2.

The reservoir width is 750 feet in the Y-direction and the reservoir height (Z-direction) is 200 feet. Dimensions in Y and Z directions are considered constant for all simulations but the boundary in the X-direction is altered depending on the fracture spacing used in the particular simulation. X-dimension is the same as the fracture spacing with fracture in the middle of the model. The three different fracture spacings are shown in Figure 5.2.

A minimum number of grid blocks necessary to obtain converged results is used. Additional parameters used in simulations are provided in Table 5.1. The reservoir

properties namely matrix permeability, initial reservoir pressure and formation compressibility are varied. Fracture width, fracture orientation, matrix porosity and initial hydrocarbon saturation remain constant. The reservoir temperature varies depending on the reservoir fluids (defined by their initial condensate to gas ratios). Reservoir simulations with conventional grid systems without refinement near the well bore and fractures produce erroneous results (Panja, Conner et al. 2013).

5.2.2 Input Factors

Important input factors which affect the production performance of condensate were chosen from and extensive initial mechanistic/sensitivity study. Nine factors, namely matrix permeability, gas relative permeability exponent, critical condensate saturation, rock compressibility, initial condensate to gas ratio (CGR), initial pressure, flowing bottom hole pressure, fracture permeability and fracture spacing, are examined in this study. Three different values of each factor are selected based on available field data as shown in Table 5.2. The data were gathered from a variety of publicly available documents on Eagle Ford. The CGR values were chosen based on compositions provided by Whitson et al. (2012).

The gas relative permeability exponent is used in the Corey model to prepare Gas-Oil relative permeability curves. Orangi et al. (2011) used a similar approach. The Water-Oil relative permeability curves are kept fixed. Corey models are described in Equations 4.1 to 4.6. Viscosity effects are built into the compositional representation of the fluid. Porosity affects total oil production but does not influence recovery in a significant manner.

5.2.3 Reservoir Fluids

Three different condensate fluids with initial condensate gas ratios of 50, 125 and 200 STB/MMSCF were evaluated in this study. The compositions and the properties for the three distinct fluids are summarized in Table 5.3. The pressure-temperature plots of the three fluids are shown in Figures 5.3 a through c. Red arrows indicate the reservoir temperatures for the reservoir fluids. The compositional data used to create the fluids were partly derived from the Eagle Ford reservoir in situ fluid compositions suggested by Whitson et al.(2012).

Reservoir temperatures (red arrows) for the reservoir fluids were 150^{O}F for initial CGR 50 STB/MMSCF, 250^{O}F for initial CGR 125 STB/MMSCF and 350^{O}F for initial CGR 200 STB/MMSCF. The temperatures in Eagle Ford vary considerably from region to region due to depth and other factors, affecting fluid compositions significantly.

5.2.4 Experimental Design

Determining the suitable experimental design method is key to developing an effective response surface model. The effectiveness of regression models is also dependent on the design of the experiment method. The Box-Behnken (1960) technique, a partial factorial design method is used in this study and is also suitable for second order response surface generation. The technique needs 130 runs for nine input factors. The three absolute values of each input parameter are converted to -1, 0 and +1 using linear relationship except for matrix permeability where logarithmic values are taken. All input parameters are summarized in Table 5.4.

Distributions of input parameters which were used when performing uncertainty analyses are also shown in Table 5.4. The spread in parameter values is similar to the

variation in field values shown in Table 5.2.

5.2.5 Regression Model for Building Response Surfaces

The functional relationships of output with inputs are defined by the second order model as shown in Equation 7.1.

$$ln[f(X_1, \ldots, X_n)] = a_0 + \sum_{k=1}^{n} a_k X_k + \sum_{i=1}^{n} \sum_{j=i}^{n} a_{ij} X_i X_j + \epsilon \qquad (5.1)$$

where,

X_i:The independent inputs

n:Total numbers of the independent inputs, n=9 for this study

a_0:the intercept

a_k and a_{ij}: the coefficients

ϵ : Error term which (absolute value) will be minimized (towards zero) in the multivariate method.

In order to ensure non-negative values of outcomes, regression was performed using logarithms of outcomes. Two types of models, namely time based and rate based models, are used in this study. In the time based model, coefficients for condensate recovery, gas recovery, and CGR after 90 days, 1 year, 5 years, 10 years, 15 years and 20 years are determined. In the rate based model, coefficients for condensate recovery and coefficients for gas recovery are obtained when condensate rate falls to 5 STB/day. Fifty five coefficients are obtained from each model. Well was operated at constant flowing bottom hole pressure (FBHP) although it is variable from simulation to simulation.

5.2.6 Workflow

The workflow for generating the response surfaces is shown in Figure 5.4 and shows each step from creating input files to generating final response surfaces. The Box-Behnken technique for design of experiment with nine factors uses 130 input files for simulation. (These input files are created using nine input factors on three levels.) The absolute values for the three levels of all factors are shown in Table 5.4. A full compositional simulator, GEM from CMG was used in all compositional simulations. All relevant results from output files were collected systematically using combinations of programs like windows batch files and MATLAB® (MathWorks® Inc.). Condensate recoveries, gas recoveries and condensate to gas ratios for different times and for the minimum economic condensate rate are extracted from collected data to fit the second order models as shown in Equation 7.1. Multivariate regressions were performed using MATLAB® programs (MathWorks®Inc.) to obtain all the coefficients of Equation 7.1. This modified multivariate regression approach is very effective in obtaining response surface parameters. The goodness of fit is measured by the values of R^2 and NRMSE (Normalized Root Mean Square Error). The calculation procedures of R^2 and NRMSE are provided in Appendix E.

5.3 Results and Discussion

For time based models of condensate recoveries and gas recoveries, 5, 10, 15 and 20 years of production data are collected from simulations. The minimum economic rate of 5 STB/day of condensate is used for the rate based model. Models are compared with the simulations by plotting them and displaying the values of R^2 and NRMSE in the same plot. Values of R^2 close to unity and low percentage values of NRMSE are indications of

good fits of models with simulations.

Simulation results and corresponding set of results from surrogate models for condensate recoveries are shown in Figures 5.5 a and b.

The time based models for 5 years, 10 years, 15 years and 20 years are shown in Figure 5.5 a and the rate based model for a minimum economic rate of 5 STB/day of condensate is shown in Figure 5.5 b. R^2 values are above 0.9 and NRMSE values are below 5% for all models. Thus, the models are reasonable to accept as surrogate reservoir models to forecast production performance. All coefficients obtained from the regression models are shown in Appendix F.

5.3.1 Validation of the Surrogate Model

Although all models fit very well with surrogate models (based on NRMSE values), validation is essential to verify the robustness of the surrogate models. Surrogate models are generated based on the three levels of values of input factors as referred by the Box-Behnken technique. The models should be effective with the other values of input factors within the range of study without any significant errors. Eighteen values are chosen randomly (using in-built random value generator in Matlab) from each input distribution to validate the models. Trivalue discrete distributions were used for fracture spacing and initial condensate to gas ratio. Simulations were run using those 18 random values of each input factors as shown in Table 5.5. The modeled values of condensate recovery are then compared with simulations to demonstrate the robustness of the surrogate models in Figure 5.6.

The response surfaces predict compositional simulation outcomes reasonably well, especially in the range over most recoveries are expected 5 - 20%. The R^2 and NRMSE

values also indicate the good matches of the simulation results with modeled values. The time based models are better fitted with simulation results than the rate based model. This validation showed that the surrogate models of condensate recoveries from ultralow permeability reservoirs can be used with good confidence to predict condensate values. It is also important to ensure that the range of input variables used from Table 5.2 cover the range of outcomes observed in the field. Comparison of field production for the highest producing (7 wells), median (5 wells) and lowest producing (5 wells) condensate wells in Eagle Ford with simulated values over a range of input parameters is shown in Figures 5.7 a and b.

The cumulative condensate productions were obtained from simulations with non-interfering single fracture and net to gross ratio (NTG) is considered as 0.4 for Eagle Ford. If there are five clusters per stage in a 16-stage well, about 80 possible fractures are expected.

Analysis of the Eagle Ford cumulative production indicates that poor and median wells fall within the 50 to 100 nD permeability range. The highest producing wells are located in the reservoirs with permeability of 500 nD to 2000 nD. It is seen from the figures that a permeability range of over 2000 nD to 10 nD is necessary to represent the performance of rich (200 stb/MMscf) and lean (50 stb/MMscf) condensates.

5.3.2 Forecast and Sensitivity Analysis of Production Outputs

Surrogate models can be used efficiently as forecast and as sensitivity analysis tools. Continuous recovery curves with time are constructed by interpolating the model data of 90 days to 20 years. For set of values of input parameters as shown in Table 5.6, the forecast and as well as the sensitivity of the condensate recovery are illustrated in Figures

5.8a and b. The curves can be extrapolated for forecast beyond 20 years. Condensate recoveries plateau after around 10 years of production for 50 nD to 500 nD reservoirs. It is important to compare the production performances among regions having differences in properties in the same field. As an example, effect of permeability on condensate recovery is shown in Figure 5.8 b. Significantly, higher condensate is recovered from higher permeability region.

This plot shows the strong dependence of permeability on condensate recovery. Similarly, operating a well at different flowing bottom hole pressure changes the recovery of condensate as shown in Figure 5.8 a. Higher flowing bottom hole pressure suppress the liquid drop out inside the reservoir, hence facilitates the production of liquid in vaporized form in the gas phase. The spread in condensate recovery, however, is only about 6-7% compared to variations of about 15% for permeability variation.

5.3.3 Uncertainty Analysis

Given the variations in important input variables, it is important to establish the probability distributions of important outcomes, such as recoveries and calculate P10, P50 and P90 values. Uncertainties in desired outcomes after 5 years, 10 years, 15 years, 20 years and when condensate reaches minimum economic rate of 5 STB/day were investigated. Probability distribution functions (PDF) of outcomes were generated using Monte Carlo simulations on response surfaces. Hierarchies of the input factors based on their impact on outcomes are also prepared. The workflow of the whole procedures is presented in Figure 5.4.

Individual probability distribution function is assigned to each input factor. Random values are chosen from each input distribution using the Monte Carlo method to produce

different values of outcomes from the corresponding response surface models. The process is repeated several times to create multiple realizations of outcomes. Averaging all realizations prepares the final probability distribution function (PDF) of the outcome. PDF provides important statistical information like mean, mode, median, and variance.

A tornado plot is useful in obtaining the hierarchy of the importance of input factors. Using statistical tools, Monte Carlo simulations construct plots of all input factors according to their influence on outcomes. The heavy hitters appear on the top of the chart and factors with the least influence appearing on the bottom. In addition to the hierarchy of the input factors, the plot also displays the range of the outcomes where each factor affects the outcome most. Commercial software *@Risk* from Palisade Corporation is used to prepare PDF and Tornado plots. Each bar in the tornado plot represents the impact of an input on output and provides the range of output where it is affected by that input. Tornado plots are prepared using output values obtained from all iterations of the surrogate model using a sequential ordering and iteration method. The PDF and tornado plots provide sufficient information on uncertainties in production performance from ultralow permeable reservoirs. Although the uncertainty analysis is conducted for different time based models (5 years, 10 years, 15 years and 20 years), the results from time based model of 10 years are discussed here along with results of rate based model. All the model results are summarized in tables.

Prior knowledge for input distribution is required to reflect the field data of reservoir parameters. One practical distribution of each input factor was assigned for the uncertainty analysis. Uniform distribution captures the total heterogeneity in the property, whereas the normal distribution has more data near the mean. The distributions of all

inputs are displayed in Table 5.4. Results of uncertainties in the outcomes are greatly dependent on the type of distribution of input factors. Uniform distributions are selected for all input factors except the matrix permeability. Matrix permeability has lognormal distribution with mean value at 500 nD. Trivalued distributions are selected for the initial CGR and fracture spacing. Lower condensate to gas ratio is observed in field with low reservoir pressure and on the other hand, higher CGR in high pressure reservoir. The initial pressure has segmented uniform distributions depending on the value of initial CGR. For initial CGR 50 STB/MMSCF, range of uniform distribution of initial pressure is 5000 psi to 5500 psi, for initial CGR 125 STB/MMSCF, range of uniform distribution of initial pressure is 5500 psi to 6500 psi and for initial CGR 200 STB/MMSCF, range of uniform distribution of initial pressure is 6500 psi to 8000 psi. All ranges are normalized to between -1 to 1.

The tornado plot indicates that the matrix permeability, formation compressibility, initial reservoir pressure and fracture spacing are the top four factors which have the most influence on the condensate production. Critical condensate saturation, flowing bottom hole pressure and initial CGR are the next the most influential factors on condensate recovery for 10 years of production. Reservoir permeability and rock compressibility emerge as the top two factors that control recovery of condensates over 10 years of production or when an economic limit of 5 STB/day is considered. These findings are consistent with earlier sensitivities published by Orangi et al. (2011) and Whitson and Sunjerga (2012). The significant drawdown in the vicinity of the well for the ultralow permeability formations causes condensate drop out and these reservoirs operate at chronically low condensate to gas ratios over their lifetime. Compressibility has been

established as one of the important governing parameters during primary production of condensates. The range of recoveries for extreme values of these parameters is also shown on the tornado plot. The plot shows that under favorable permeability conditions, 10 times as much condensate is recovered and about 8 times more recovery is realized when compressibility is favorable. These geologic parameters are not easily altered – but the compressibility aspect may present a tradeoff between placing the fractures in brittle zones where fracturing is expected to be more effective versus seeking more ductile (and hence compressible) formations to assist in the primary recovery of condensates. The initial pressure is an important reservoir attribute since higher initial pressures delay approach to dew point and condensate formation in the reservoir. Fracture spacing, which is one of the controllable parameters, appears double recovery when low fracture spacing is realized. This will have economic implications as lower fracture spacing will increase the cost of creating hydraulic fractures. The relative permeability aspects (critical condensate saturation and gas relative permeability exponent) have surprisingly lesser impact, as does the bottom hole pressure. Recoveries are affected when the range of bottom hole pressures are varied over a few thousand psi, but not with the range of 500-1500 psia employed in the study. In Eagle Ford, very few operators hold bottom hole pressures of higher than 1500 psia.

5.3.3.1 Uncertainty in condensate recovery. Uncertainties in condensate recovery after 10 years of production and the hierarchy of input factors are shown in Figures 5.9a and b. The median condensate recovery factor is only around 14% after 10 years of production from ultralow permeable reservoirs. The condensate recovery spreads over a wide range in the probability distribution function (PDF). The range 5- 95% in the PDF

covers 2 to 39% of condensate recovery. The Weibull function closely mimics the distribution.

The uncertainty in the condensate recovery after the condensate rate drops to 5 STB/day is shown in Figures 5.10a and b. Median recovery (P50) when the condensate production reaches an economic limit of 5 stb/day was observed to be about 7%. Beta function best fits the PDF for this recovery function. PDF also predicts that the most probable (mode) condensate recovery is around 2%. The matrix permeability, formation compressibility, reservoir pressure and fracture spacing are the most influential factors. The gas relative permeability exponent, bottom hole pressure, fracture permeability and critical condensate saturation rank in the next four in the tornado plot. The results of uncertainty analysis from 5 years, 10 years, 20 years and rate based models are summarized in Table 5.7. The most influential factors in condensate recovery were matrix permeability, fracture spacing, formation compressibility and initial reservoir pressure for all cases though the orders of the factors change slightly with the models as shown in Table 5.7. Higher matrix permeability always enhances the productivity from reservoirs.

The higher formation compressibility helps to sustain the reservoir pressure minimizing liquid drop out. Fracture permeability, critical condensate saturation, initial CGR and gas relative permeability exponent are next four important factors that affect recovery of condensates.

5.4 Key Findings

Guidelines for quick screening and uncertainty assessment of the performance of condensates in shales are needed. This is because, despite increased drilling, declining

production is being observed in important resource plays like the Eagle Ford. The purpose of this study was to provide such guidance by developing response surface (surrogate) models that emulated full compositional reservoir simulations. The response surfaces were generated by using the Box-Behnken experimental design and a novel multiregression strategy. The models were an excellent proxy for the computationally intensive compositional simulations as evidenced by low root mean square errors and a thorough validation exercise. Development of validated response surfaces allowed performing Monte Carlo simulations for uncertainty assessment. Uncertainty analysis revealed that reservoir permeability, compressibility, fracture spacing and initial pressure were the most significant parameters that affected condensate recovery followed by initial condensate to gas ratio, fracture permeability, gas relative permeability exponent, critical condensate saturation and the bottom hole pressure. The median values of recovery (P50) for 10 year production and for an economic cutoff rate of 5 STB/day of condensate were determined to be about 16% and 12%, respectively.

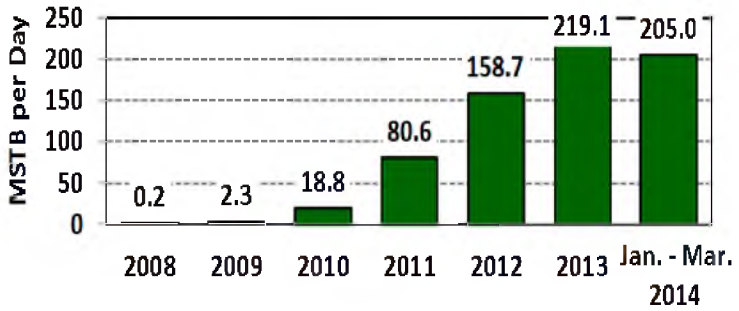

Figure 5.1: Texas Eagle Ford shale condensate production 2008 through April 2014 – from the Texas Railroad Commission.

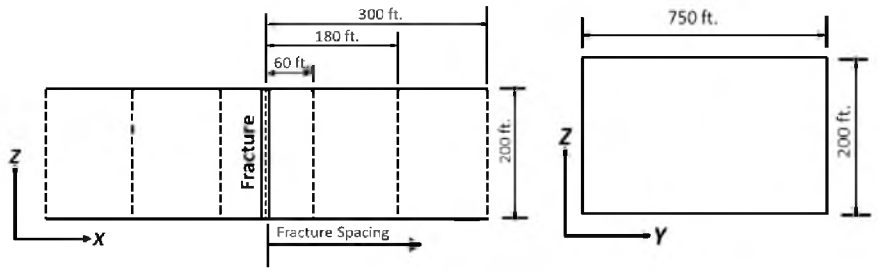

Figure 5.2: The geometry of a simulated reservoir.

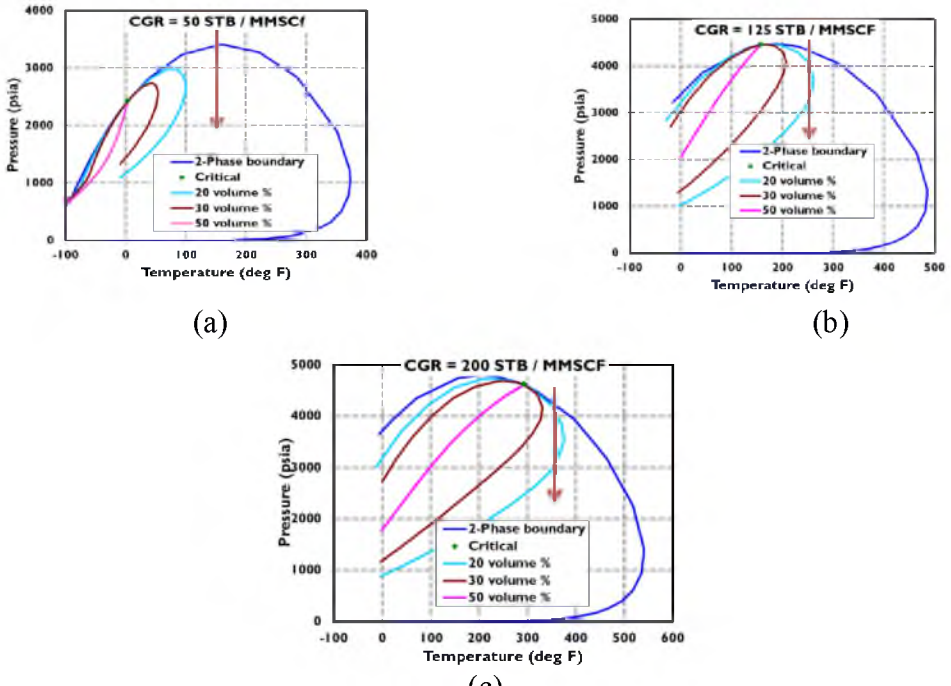

(a) (b)

(c)

Figure 5.3: Pressure-Temperature diagram for three distinct reservoir fluids (a) Initial CGR = 50 STB/MMSCF (b) Initial CGR = 125 STB/MMSCF (c) Initial CGR = 200 STB/MMSCF.

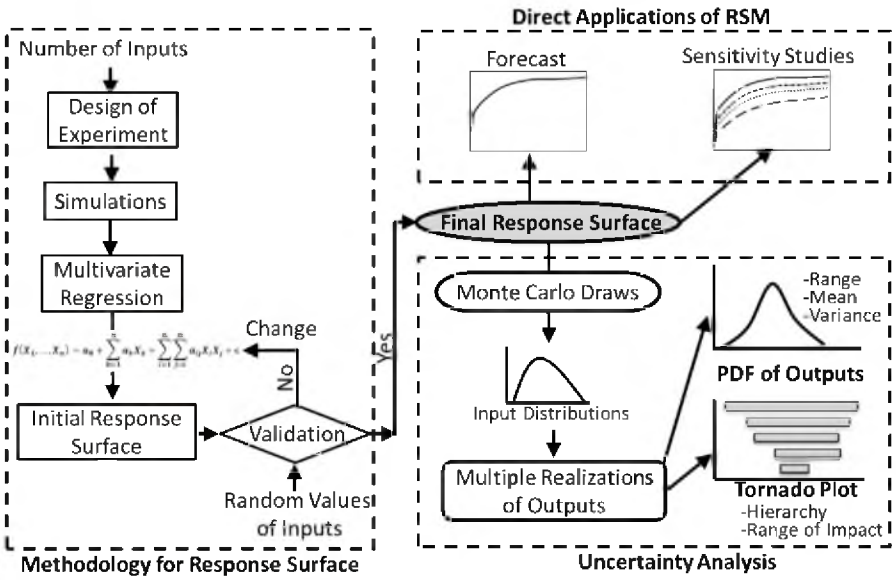

Figure 5.4: Workflow of the methodology to generate response surfaces and to analyze uncertainty in outcomes.

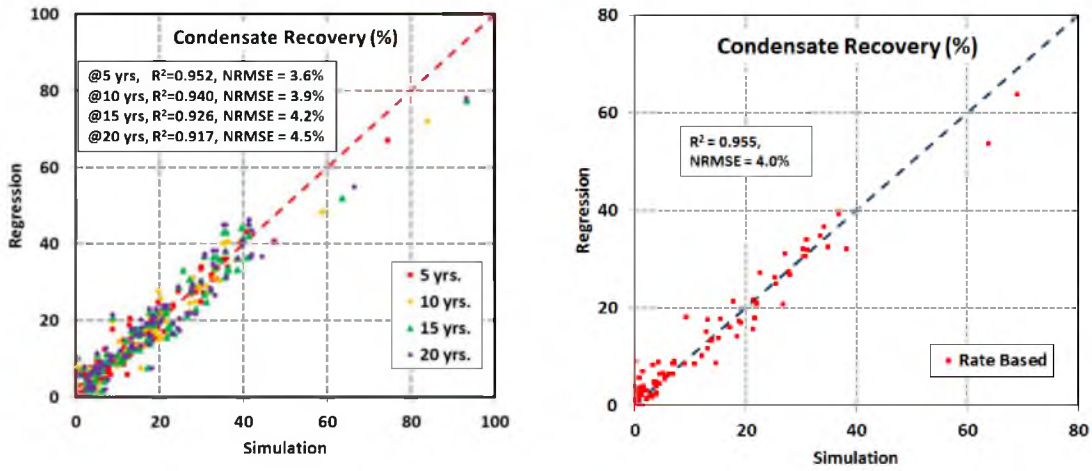

(a) (b)

Figure 5.5: Comparison of regression model with simulation results for (a) Time based condensate recovery and (b) Rate condensate based recovery.

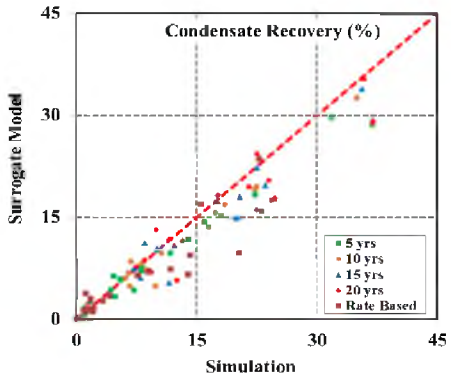

Figure 5.6: Comparison of results from the response surface (surrogate) models of condensate recovery with compositional simulation results for validation.

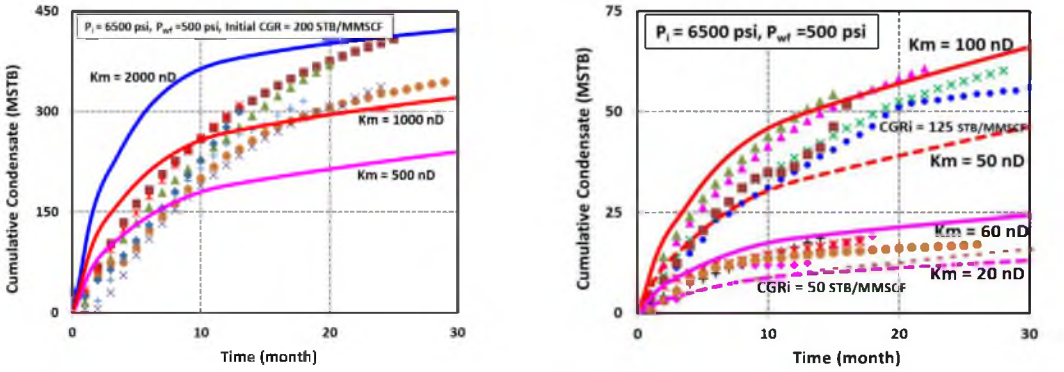

(a) (b)

Figure 5.7: Comparison of Eagle Ford field data with compositional simulations, by varying matrix permeability and initial condensate to gas ratios (a) The highest producing wells (b) Median and the lowest producing wells.

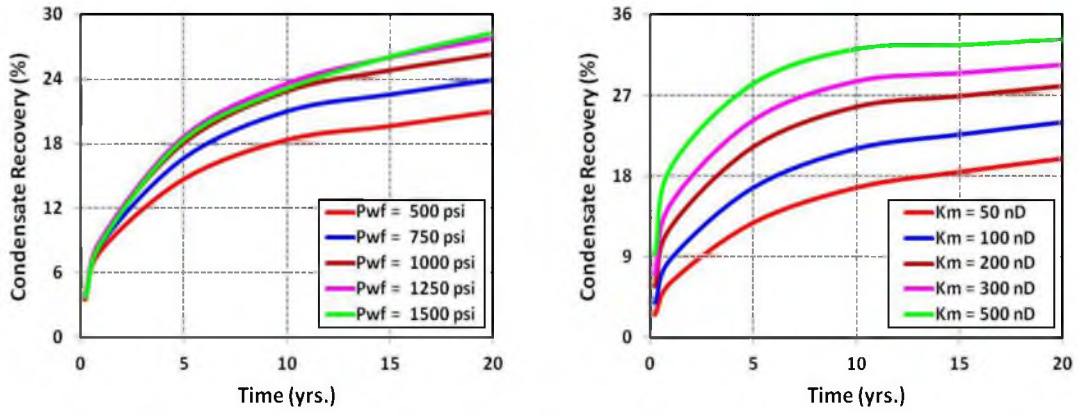

(a) (b)

Figure 5.8: Condensate recovery with time for different (a) Flowing bottom hole pressure and (b) Reservoir permeability.

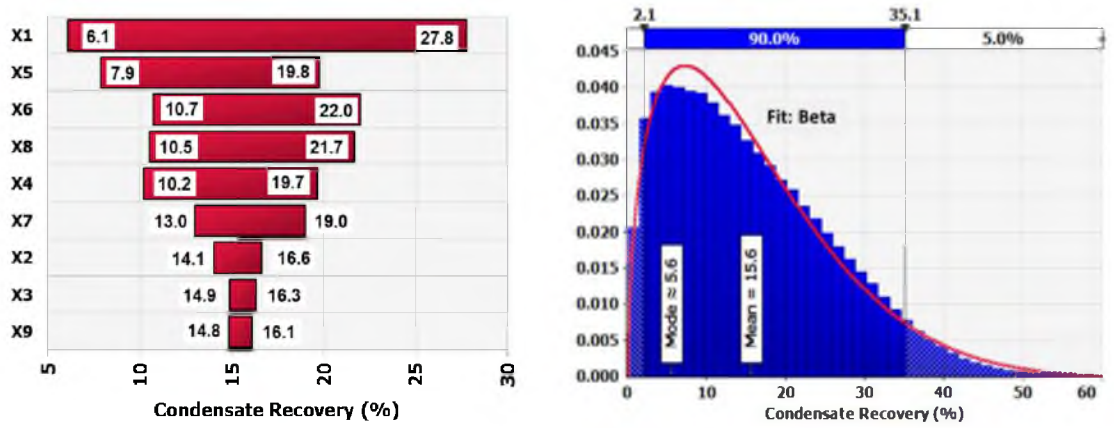

(a) (b)

Figure 5.9: Condensate recovery after 10 years of production (a) Hierarchy of input parameters (b) Probability distribution of output.

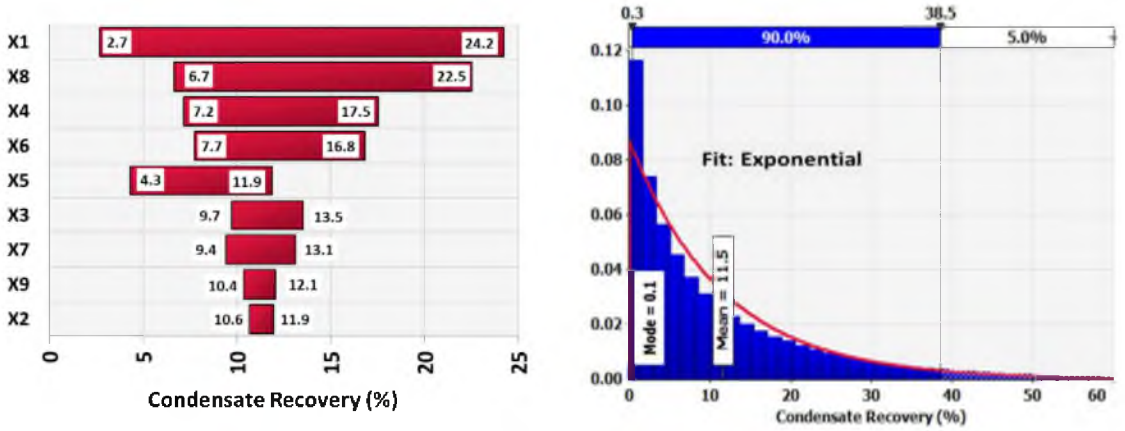

(a) (b)

Figure 5.10: Condensate recovery when condensate rate reaches 5 STB/day (a) Hierarchy of input parameters (b) Probability distribution of output.

Table 5.1**.** Simulation parameters used in the study.

Reservoir Top (ft.)	12000
Reservoir Thickness (ft.)	200
Reservoir Width (ft.)	750
Fracture Width (ft.)	0.05
Fracture Height (ft.)	Reservoir Height
Fracture Half length (ft.)	Reservoir half width
Fracture Orientation	Parallel to YZ plane
Reservoir Porosity (%)	5
Initial Water Saturation (%)	20
Number of grids	Variable depending on Fracture spacing
Minimum Size of grid (ft.)	0.05 (X-direction), 250(Y-direction), 66.67(Z-direction)
Maximum size of grid(ft.)	2 (X-direction), 250 (Y-direction), 66.67 (Z-direction)

Table 5.2**.** Field data from Eagle Ford Shale plays

System/Unit/Zone	h_{avg} (ft.)	ϕ_{avg} (%)	Km Range (md)	$K_{m,avg}$ (md)	S_w (%)	Pore pressure (psi)	GOR (SCF/ STB)
Bakken (condensate)							
Elm Coulee (Middle Bakken)	11	6	.04 - .50	0.04	15 - 25	4800	500
Parshall-Sanish (Middle Bakken)	16	6	.002 - .05	0.02	23	6350	500
Elkhorn Ranch (Upper Bakken Shale)	10	2	.001 - .02	0.01	25	6500	500
Eagle Ford							
Karnes Trough (oil)	150	10	.0011 - .0015	0.001	30	6000	500 - 1000
Hawkville (gas/condensate)	300	10	.0011 - .0015	0.001	15	6000	1000 - 2000
Briscoe Ranch South (gas)	150	10	.0011 - .0015	0.001	30	7200	2000 - 4000
Niobrara (Condensate)							
Hereford Field area	300	8		0.1	45	3500	<2000
Powder River Basin	400	8		0.1	45	4500	<2000
North Park Basin	500	8		0.1	45	4000	<2000

Table 5.3. Composition of three distinct reservoir fluids

Components	Composition (mole fraction)		
	CGR@50	CGR@125	CGR@200
H2S	0.0001	0.0001	0.0001
N2	0.0019	0.0019	0.0019
CO2	0.0286	0.0286	0.0286
C1	0.7173	0.6805	0.6555
C2	0.0916	0.0887	0.0835
C3	0.0513	0.0493	0.0472
iC4	0.0118	0.0114	0.0109
nC4	0.0201	0.0195	0.0189
iC5	0.0092	0.0089	0.0085
nC5	0.0099	0.0135	0.0091
C6	0.0141	0.0135	0.013
C7+	0.0441	0.0841	0.1228
C7+ mol. Wt.	132	148	152
API	49.8	47.1	45.5
Tc (degree F)	3.2	157	293
Pc (psi)	2422	4448	4611

Table 5.4**.** List of input parameters and their distribution for uncertainty analysis.

Variable	Symbol	Minimum (-1)	Medium (0)	Maximum (+1)	Distribution for Uncertainty Analysis
Matrix Permeability, nD	X1	10	225	5000	lognormal
Gas Rel. Permeability Exponent, n_g	X2	1	2	3	Uniform
Critical Condensate Saturation	X3	0.1	0.2	0.3	Uniform
Initial CGR, STB/MMSCF	X4	50	125	200	Tri-Valued discrete
Initial Pressure, psi	X5	5000	6500	8000	Conditional Uniform (depends on X4) Distribution
Fracture Spacing, ft,	X6	60/60	180/180	300/300	Tri-Valued discrete
Fracture Permeability, mD	X7	10	155	300	Uniform
Rock Compressibility, $\log(c_f)$, $\log(psi^{-1})$	X8	-6	-5	-4	Uniform
BHP, psi	X9	500	1000	1500	Uniform

Table 5.5. Random values for validation of surrogate models.

Sr. No	Km (nD)	n_g	S_{oc}	R_{vi} (STB/MMSCF)	P_i (psi)	X_f (ft.)	K_f (mD)	C_f (1/psi)	P_{wf} (psi)
1	112	1.1	0.29	125	7948	180	216	3.3E-05	541
2	526	2.5	0.10	125	6949	300	296	3.9E-05	569
3	17	1.4	0.20	200	6274	180	136	9.6E-05	1357
4	20	2.2	0.19	200	6361	180	160	1.5E-04	1329
5	2345	2.7	0.28	50	7744	300	145	4.2E-06	569
6	212	1.3	0.26	125	6222	60	14	1.0E-05	946
7	104	2.3	0.27	125	7124	60	296	9.9E-05	1315
8	386	2.8	0.17	50	5964	60	238	1.2E-04	866
9	299	1.6	0.14	200	5154	60	190	3.0E-05	759
10	85	1.9	0.15	200	7092	300	290	6.5E-06	1223
11	367	1.7	0.18	125	6396	300	184	1.2E-04	1235
12	10	1.4	0.25	125	6069	180	39	4.7E-05	1459
13	26	1.9	0.16	200	5139	180	19	3.3E-04	892
14	242	1.5	0.29	125	5240	180	63	2.2E-05	1315
15	621	1.7	0.14	50	7708	300	191	4.1E-05	890
16	90	1.1	0.29	125	7266	60	93	7.0E-06	1378
17	22	2.0	0.14	50	6385	300	108	6.2E-06	1258
18	349	2.0	0.22	200	5640	180	266	2.1E-05	1090

Table 5.6. Values of input parameters used in sensitivity studies.

Variable	Sensitivity of Pwf	Sensitivity of Km
K_m (nD)	100	50,100,200,300,500
n_g	3.0	3.0
S_{oc}	0.15	0.15
R_{vi} (STB/MMSCF)	125	125
P_i (Psi)	7500	7500
X_f (ft.)	180	180
K_f (mD)	300	300
C_f (1/psi)	3.3E-05	3.3E-05
P_{wf} (Psi)	500,750,1000,1250,1500	750

Table 5.7. Uncertainty in recoveries and rank of input parameters.

Parameters	Condensate Recovery				Gas Recovery
	5yr	10yr	20 yr	qo=5 STB/day	qo=5 STB/day
Mean (%)	13.3	15.6	17.9	11.5	16.5
Mode (%)	4.8	5.6	7.0	0.1	0.2
P10	2.7	3.5	4.2	0.7	1.4
P50	11.1	13.8	16.2	6.8	11.6
P90	27.1	30.4	33.9	28.9	39.1
5-95% Range in PDF	1.7– 32.1	2.1 – 35.1	2.6 – 39.0	0.3 – 38.5	0.7 – 49.2
Inputs Rank by Effect on Output Mean	Km Xf Pi Cf Rvi Kf ng Pwf Scc	Km Pi Xf Cf Rvi Kf ng Scc Pwf	Km Cf Pi Rvi Xf Kf ng Scc Pwf	Km Cf Rvi Xf Pi Scc Kf Pwf ng	Km Cf Rvi Xf Pi Kf Scc ng Pwf

CHAPTER 6

EXPERIMENTAL DESIGN AND RESPONSE SURFACE METHODS: BLACK OILS

The general procedures are discussed in this work to create surrogate reservoir models for black oil from ultralow permeability reservoirs. The study is then extended to determine the hierarchy of the important factors and to analyze the uncertainty in the production outcomes for given distributions of input factors. Surrogate reservoir models were generated through compiling main factors that most affect oil and gas recovery in ultralow permeability reservoirs. Simulation experiments are designed using partial factorial method. Two different recovery outcomes were sought – one based on a terminal time and the other based on economic rate. Multivariate regression was used to obtain coefficients for the second-order response surface models using the simulated results. Probability density functions (PDF) of recoveries were generated using Monte Carlo simulations with uncertainties in the primary input parameters. The heavy hitters are identified from tornado plot. The order of importance of these factors changed slightly as the type of outcome sought changed. Reservoir permeability, fracture spacing, initial reservoir pressure and the initial gas oil ratio were the most important factors for oil production from shales. Average oil recoveries in the PDFs generated were about 16% after 10 years of production. Coupling production uncertainty with economics provides a strong strategic tool for field development. A probabilistic economic model is developed

to study the profitability and optimum fracture spacing. Twenty five million dollars of NPV is expected from well with 18 fractures in 60 acre well spacing. Abandonment time for well with 18 fractures is approximately 7 years. Nearly 20 fractures in 60 acre well spacing are found to be optimum.

6.1 Background

In the next five years the United States is expected to become the largest producer of oil in large part due to the production of liquids from tight oil reservoirs such as the Bakken or shales like the Eagle Ford. It is well recognized that ultralow permeability reservoirs behave differently even when compared to low permeability reservoirs. There have been questions concerning the storage and production of liquids from such low permeability reservoirs. Importance of the petrophysical parameters can be assessed using parameter sensitivity studies. Clear insight into the geologic and operational factors controlling production of oil/condensate and gas from these reservoirs was developed in this study using experimental design and factorial analysis. Uncertainty in the recoveries was also studied giving the uncertainty in the primary input parameters.

Response surface methodology (RSM) allows for variation of all factors simultaneously to get the maximum interference effect of all important factors on output. Application of the response surface method was started in the early 90s to find the optimal production and uncertainty associated with it (Damsleth, Hage et al. 1992; Egeland, Holden et al. 1992; Aanonsen, Eide et al. 1995). The RSM has been used for various purposes; these include estimating initial hydrocarbon uncertainty (Peng and Gupta 2003), finding an optimal scheme for well placements (Guyaguler and Horne 2001; Manceau, Mezghani et al. 2001; Manceau, Roggero et al. 2002; Landa and

Güyagüler 2003; Carreras, Turner et al. 2006), uncertainty in production and recovery performance (Dejean and Blanc 1999; Chewaroungroaj, Varela et al. 2000; Corre, Thore et al. 2000; Venkataraman 2000; Manceau, Mezghani et al. 2001; Mohaghegh 2006), history matching (Landa and Güyagüler 2003; Yang, Nghiem et al. 2007; Slotte and Smorgrav 2008), and optimizing production to flow through nanopores (Sarma, Durlofsky et al. 2005; Xie, Lee et al. 2013). Effectiveness of RSM has been thoroughly investigated by comparing various design of experiments (DOE) methods and different RSM (Yeten, Castellini et al. 2005) and it has been proved that response surface built through an appropriate DOE is an efficient and fast proxy model for forecasting production performance and analyzing uncertainties (Amorim and Schiozer 2012). Multiple possible 3-D geological models (Peng and Gupta 2004; Peng and Gupta 2005; Mohaghegh, Modavi et al. 2006) were developed with uncertainty of their occurrences (realizations) with input uncertainties using surrogate reservoir model. Models with strong nonlinear effects of key parameters are handled differently; local subdivision is applied to parameter domain (Li and Friedmann 2005) to analyze the uncertainty in production forecast. Amplitude factor and phase factors are adopted to separate out the highly nonlinear effects from the remaining effects to forecast the oil rate and water cut (Li and Firedmann 2005). The pressure and production are studied using field cases by applying surrogate reservoir models which are based on pattern recognition techniques (Mohaghegh, Liu et al. 2012). Recently, RSM has been applied in unconventional fractured shale reservoirs (Dahaghi, Esmaili et al. 2012; Xie, Lee et al. 2013) and tight reservoirs (Khosravi, Fatemi et al. 2011; Khosravi, Rostami et al. 2012). Previous studies have shown that aquifer strength, fracture permeability and block height have a great

impact on oil recovery (Khosravi, Fatemi et al. 2011) for low permeablity fractured reservoirs. Economic applications of risk based model in oil and gas industry are discussed by many researchers (Virine and Rapley 2003; Murtha, Peterson et al. 2007). Economic model is also utilized to optimize fracture spacing (Mendoza, Aular et al. 2011). A wide range of parameters are assigned to study the impacts on production performance from ultralow permeability reservoir. Models are developed for different times and for an economic rate. The methodology to create surrogate black oil reservoir models and to analyze uncertainty of the production outcomes, specifically oil and gas recoveries are discussed in this paper. The generated surrogate models are used in probabilistic economic model to estimate production. We have prepared a model which comprises well cost components and production components.

6.2 Methodology

The same methodology as described in section 5.2 is applied here. All simulations were conducted using CMG-IMEX, a Computer Modeling Group Black oil simulator. A mechanistic study was conducted to choose the most significant petrophysical inputs and operating parameters. Eight factors, namely matrix permeability, gas relative permeability exponent, rock compressibility, initial gas oil ratio, slope of gas oil ratio in PVT, initial pressure, flowing bottom hole pressure and fracture spacing, are selected in this study. The Box-Behnken technique significantly reduces the number of runs (113) for eight input parameters, and is also suitable for second-order response surface generation. All input parameters with their values of three different levels are summarized in Table 6.1. The Corey models for relative permeabilities are used as described in Equations 4.1 to 4.6. The range of each variable is chosen based on observed

data variability in specific fields, on completion data and on how each well operated as shown in Table 5.2. In this study, only gas relative permeability exponent (n_g) is varied, and hence water-oil relative permeabilities are fixed in all simulations.

- The same second-order equation as shown in Equation 5.1 is used except the normal logarithm is replaced by 10 base logarithm in the right hand side. In the time based model, coefficients for Oil Recovery, coefficients for gas recovery and coefficients for GOR after 90 days, 1 year, 5 years, 10 years, 15 years and 20 years are determined.
- In the rate based model, coefficients for Oil Recovery and coefficients for gas recovery are obtained when the oil rate falls to 5 STB per day. Forty five coefficients are obtained from each model.

6.3 Results and Discussion

Oil recoveries and gas recoveries after 5 years, 10 years, 15 years, 20 years and when oil rate reaches minimum economic rate of 5 STB/day are collected from output files generated by simulations. Simulation data are plotted against the data obtained from RSM model for comparison. Oil recoveries and gas recoveries are plotted in Figures 6.1 a and b. Goodness of model fit is measured by calculating coefficient of determination, R^2 and *Normalized Root Mean Square Error (NRMSE)* (see Appendix E).

Figures 6.1 a and b show that both RSM models agree well with the simulation results. All recoveries (oil and gas) fall well over the diagonal line. There are few variations between the simulations and the model. The measurement of fitness in terms of R^2 and NRMSE is provided in Table 6.2. The coefficient of determination, R^2, values indicate a good correlation between RSM models and simulations. The coefficient of

determination, R^2, values are close to unity for time based models, and the data for the rate based model are slight scatter around the diagonal line with reasonably good value of R^2. The predicted recoveries by model and the recoveries from simulation are in considerable agreement. Coefficients of oil recovery, gas recovery and gas oil ratio obtained from the regression models are shown in Appendix F.

6.3.1 Validation of the Surrogate Model

Validation is an important part of model development. Surrogate models are generated based on the set of values of input factors as referred by the Box-Behnken technique. Models should be tested with the other values of input factors within the range of study. Unsatisfactory fit of models will prescribe the modifications in original models. Thirty values are chosen randomly for each input parameter from their range of study to validate the models. Simulations are run using those 30 random values of each input factors. The modeled values are then compared with simulations to demonstrate the robustness of the surrogate models. Oil and gas recoveries for time based models and rate based model are compared with simulation results with randomly chosen input values (as shown in Table 6.3) in Figures 6.2a and b.

The oil and gas recoveries have larger error around the diagonals but the overall fit of the models is satisfactory as indicated by R2 and NRMSE values (Table 6.4). Models of long-term recoveries (after 5 years) and rate based models are more accurate (R2>0.9 and NRMSE<15%) than the short term recovery models. Thus the models for recoveries can be used confidently to predict the production for any input parameters value within the given ranges of study.

The surrogate models of recoveries from ultralow permeability reservoirs can be used

confidently for any values of input factors within the range of study. These models are also useful to study the risk associated with the production that will guide the development of a field.

6.3.2 Forecast and Sensitivity Analysis

Forecast and sensitivity analysis are two of many applications of surrogate models. These applications are very rapid and easy to change the parameters. Any parameter or combination of parameters in the models can be varied deterministically or probabilistically for sensitivity analysis. Forecast of recovery for any time can be estimated from continuous recovery curves prepared by interpolating the available model data (90 days to 20 years) for intermediate time periods. Sensitivities of fracture spacing and initial gas oil ratio on recovery are studied here. All other parameters except the parameter of interest are kept fixed as shown in Table 6.5. The values of input parameters are chosen within the range of study. The results of sensitivity analysis are shown in Figure 6.3a and b. Low fracture spacing improves oil recovery as shown in Figure 6.3 a. Major increase in recovery (approximately 8% at 20 years) is observed when fracture spacing is reduced from 120 feet to 60 feet.

In the case of low fracture spacing, most of the oil in the reservoir portion is exploited and fracture interferes with the adjacent fractures. The stimulated volume is also reduced for low fracture spacing reservoir. Hence smaller reservoir volume is used in recovery factor calculation. The change in oil recovery is not significant (1-2% in 20 years) when fracture spacing increases beyond 180 feet. For ultralow permeable reservoirs, fracture spacing of 180 feet seems to be very high. Transient state flow may persist for the entire well life. Increasing fracture spacing increases the reservoir volume in calculation of

recovery factor. Thus, for same amount of oil recovered during moving boundary transient state flow, recovery factor is less for higher fracture spacing. In Figure 6.3 b, a higher amount of oil is recovered with higher initial gas oil ratio. Higher initial gas oil ratio provides energy in reservoir to sustain pressure for long time. On the other hand, gas production is increased for higher initial gas oil ratio. Higher gas oil ratio helps production of oil by improving the oil mobility with dissolved gas

6.3.3 Uncertainty Analysis

Quantifying the uncertainties in the significant production parameters like oil recovery, gas recovery and gas oil ratio is a primary concern. In the first part of this paper, response surfaces of each production outputs are generated after 5, 10, 15, and 20 years and when the oil rate reaches a minimum economic rate of 5 STB/day. A Monte Carlo method is used to analyze the uncertainty in the production forecast and to establish the hierarchy of the input factors using the response surfaces. A general schematic diagram of the methodology is shown in Figure 5.4.

A single value is drawn randomly from individual input distribution and different outcomes are produced from the corresponding response surfaces. The process is repeated several times to create several realizations that provide a distribution of the outcome. This method is known as Monte Carlo simulation. Multiple realizations are prepared using hundreds of Monte Carlo simulations. It takes a fraction of a minute to complete the simulations. The final probability density function (PDF) of the outcome is proposed by averaging all the realizations. The PDF provides useful information like the range, mean, median and mode of the outcome.

A tornado plot of each outcome is also found in this uncertainty study and indicates

the hierarchy of the inputs. The most significant input factors are found on the top of the tornado plot and those factors with the least effects are at the bottom of the plot. It also provides the ranges of outcomes where each input affects most.

The combined analysis of probability density functions and tornado plots of the output creates a complete picture for the uncertainty analysis regarding the overall output and the impact of each input on the output results. Uncertainty analysis of a time based model after 10 years of production and a rate based model when the oil rate reaches a minimum economic rate of 5 STB/day. Relevant distribution of each input factor is chosen for the Monte Carlo sampling. The distributions of all factors used in the study of the production of black oil from ultralow permeability reservoirs are summarized in Table 6.3. Uniform distribution assures the total heterogeneity in the property; on the other hand, normal distribution collects the most values around the mean. Lognormal distribution is chosen for matrix permeability. The absolute values of the range of each input are shown in Table 6.1. The outputs may vary as the input distribution functions change. Distribution of initial gas oil ratio (X5) is dependent on the distribution initial pressure (X6) and distribution of fracture spacing (X8) on distribution of reservoir permeability (X1). Additional information for distribution of X5 and X8 are given in Table 6.6.

6.3.3.1 Uncertainty in recoveries. The probability density function and tornado plot of the oil and gas recoveries factor after 10 years of production from ultralow permeability reservoirs are shown in Figures 6.4 a and b. The mean and the median of oil recovery factor are only around 16% and 9.5%, respectively. The range 5 – 95% of the density function covers approximately 5 – 35 % of oil recovery. The density function of

the oil recovery closely follows the Inverse Gaussian distribution function.

Fracture spacing and matrix permeability are the two main factors that have the most effect on oil recovery. The detailed results of the uncertainty analysis for all models are recorded in Table 6.7. It is evident from Table 6.7 that the most influential factors in oil recovery are fracture spacing, matrix permeability and initial gas/oil ratio for all cases. The levels of uncertainty change with the production time but the first three main factors remain the same. The oil recoveries are not very strong dependent on rock compressibility, gas relative permeability exponent and flowing bottom hole pressure. The probability density functions and tornado plots of gas recovery factors were also generated in this study. Results of the model for the gas recovery factor after 10 years of production from ultralow permeability reservoirs are shown in Figures 6.5 a and b.

The mean gas recovery factor is only around 18% (median 10.3%) which is close to oil recovery factor of 16%. The range 5 – 95% of the density function covers around 5 – 43% gas recovery. The density function of the gas recovery also follows the Inverse Gaussian distribution function like the oil recovery factor. The gas recovery is most affected by the fracture spacing and matrix permeability.

The mean gas recovery factor is around 24% and is higher than the oil recovery. The range of gas recovery factor for the range 5 – 95% of the density function is very wide from around 3 – 51%. The Beta distribution function is the closest fit for the probability density function. Matrix permeability and the initial gas oil ratio remain the two primary factors that most affect the oil recovery for this case. The detailed results of uncertainty analysis of all models are recorded in Table 6.8. The most influential factors in gas recovery are fracture spacing, matrix permeability and initial gas/oil ratio for all cases

except the rate based models. Fracture spacing, matrix permeability and slope of the gas/oil ratio in PVT are the top three influential factors for gas recovery in the rate based model. The levels of uncertainty change as the production time changes but the first few main factors remain same.

6.3.4 Economic Evaluation

Spreadsheet models for net present value (NPV), economic rate and abandoned time are prepared and models are coupled with *@Risk* software. Cumulative probabilities of NPV for various periods and for abandoned rate are studied. Mean NPV with 50% and 90% confidence intervals are also plotted. The study is then extended to sensitivity of number of fractures on NPV. The capital expenditures like land acquisition, and drilling are dependent on the well spacing. Fracking cost is kept variable based on the number of fractures. The rate of production is not directly calculated using decline curve models. Recoveries (oil and gas) are calculated probabilistically by giving uncertainty in reservoir permeability, initial GOR and initial reservoir pressure in reservoir surrogate models for different time periods and for abandoned rate. Productions for intermediate periods are interpolated. Cumulative productions are obtained from well spacing and initial reservoir conditions. Fracture spacing is determined based on number of fractures and well spacing. A schematic diagram of reservoir with fracture spacing and number of fractures is shown in Figure 6.6. The fracture height is considered to be same as reservoir height. For 60-acre well spacing, horizontal length of well is calculated to be 3485 feet (L_X) with dimension of Y-direction of 750 feet. The pay zone is located 12000 feet below surface and thickness of pay zone is 200 feet. Thus, the horizontal section of well and fracture spacing vary depending on the well spacing. A relationship between number of fractures

and fracture spacing is given in Equation 6.2:

$$2\,n\,x_f = L_x \tag{6.2}$$

Various parameters like cost of land acquisition, leasing, royalty, discount rate etc. are taken from different sources (Hefley, Seydor et al. 2011; Mendoza, Aular et al. 2011). Typical well spacing for an unconventional reservoir is considered 60 acres. Parameters and various costs associated in the economic model are listed in Table 6.9. Total cost of a single horizontal well with 18 hydraulic fractures is estimated to be 7 million dollars. The cost may vary greatly depending on locations of drill site. The prices of crude oil and natural gas for future are taken from Annual Energy Outlook reports published by EIA (EIA 2013; EIA 2014). The gas price is converted to per Mscf from million Btu in model. Economic models are run in Monte Carlo simulation to obtain probabilistic estimation of net present value (NPV). Reservoir permeability is taken as lognormal distribution ranges from 10 nD to 5000 nD with mean of 447 nD and standard deviation of 627 nD. The projections of prices of crude oil and natural gas from AEO 2014 and 2013, respectively, are reproduced in Figure 6.7 a and b.

Initial reservoir pressure is sampled from a uniform distribution between 4000 psi and 6500 psi. Initial gas oil ratio is also taken from a uniform distribution (between 800 SCF/STB and 3000 SCF/STB) conditioned with initial reservoir pressure. Monte Carlo simulations are run to produce 100,000 realizations and then to perform the probabilistic study of economic models. In each iteration, cumulative production curves are built and fitted by following Duong's power law model for long term linear flow (Duong 2011) and then cumulative productions of each year are determined from rate models.

The NPV model for single well reservoir provides probabilistic values with 50% and 90% confidence intervals for different time periods. NPV plays a major role in development of a prospect. The NPV distributions depend on many factors like number of fractures, distribution of reservoir permeability, drilling cost, completion cost, discount rate of currency, oil and gas prices etc. Cumulative probability of NPV with confidence intervals for horizontal well with 18 fractures is shown in Figures 6.8 a and b. Five STB/day of oil production from a single fracture is considered as economic production rate. Cumulative production from well is variable with the number of fractures.

Drawdown applied in well bore will not be practical if the rate drops below economic rate and well will be left abandoned. For a fixed probability, higher NPV is achieved from longer time of production. This fact is obvious because more oil is extracted with time but the rate of production decreases. Rise in average NPV is very slow after 10 years of production. Increase in NPV is only approximately 5 MM$ from 10 years to 20 years of production. The probability curve for rate based NPV falls between 5 year and 10 years and hence well may not be practically producible after 10 years of production. It is observed that 50% confidence interval for economic NPV is 12.8 to 33.4 MM$ (P25 and P75) and 90 % confidence interval for the same is 3.9 to 56.2 MM$.

Time of abandonment (Figure 6.9) is also determined probabilistically in the same Monte Carlo simulations. It is also evident from Figure 6.9 that there is a 95% chance that it will be less than 14 years and greater than 1.6 years. Although, production from wells in conventional reservoirs sustains for a long time, the abandonment time is shorter in this case with reservoir permeability ranging from 10 to 5000 nD with lognormal distribution in 60-acre well spacing.

This prompts producers to exploit more oil from a reservoir in a short time which requires higher fracture density. Higher fracture density leads to higher cost of fracking and completion. Sensitivity of fracture density in NPV is studied here. A comparison of NPV (mean and median) for different time periods and for economic rate is shown in Figures 6.10 a and b. Cost increases with increase of number of fractures but recovery of hydrocarbon also increases as the fracture spacing decreases. Higher amounts of oil and gas are recovered which generate more revenue.

The NPV (mean and median) does not increase significantly with number of fracture for 1 year production. Slow rises of NPV with number of fracture are observed after 1 year production but the oil production rate from each fracture will be not enough for economic production. NPV based on economic rate has almost no improvement after the number of fractures reaches nearly 20. It can be concluded that the 20 fractures (approximately 87 feet fracture spacing) in 60-acre well spacing is optimum for maximum profitability with the parameters used in the study.

6.4 Key Findings

Surrogate reservoir models can be used for a quick assessment of production performance from ultralow permeability reservoir like shales. The methodologies to create surrogate models and to analyze uncertainty of the production outcomes are demonstrated. Very few simulations are needed to generate the surrogate reservoir models. Surrogate models are developed for different times (after 90 days, 1 year, 5 years, 10 years, 15 years and 20 years) and for a minimum economic rate (5 STB/ day). Eight factors, namely, matrix permeability, gas relative permeability exponent, rock compressibility, initial gas oil ratio, slope of gas oil ratio in PVT, initial pressure, flowing

bottom hole pressure and fracture spacing, are selected to study the impacts on oil production from ultralow permeable reservoirs. The accuracy of the surrogate models is in the acceptance range.

The Monte Carlo simulation for uncertainty analysis is a rapid method to quantify risk. For given distributions of input factors, the probability density functions (PDF) of recoveries were generated. The distribution functions for the input factors can be modified easily according to field properties. The hierarchy of the most significant factors is displayed in the tornado plots. The order of these factors changed slightly as the type of model changed.

Reservoir permeability, fracture spacing, initial reservoir pressure and the initial gas/oil ratio were identified as the most important factors for oil production from shales. Average recoveries were about 16% for oil and 24% for gas after 10 years of production. A probabilistic economic model can be used with surrogate reservoir model for development of field and to find optimum fracture spacing. NPV of 25 million dollars can be achieved from well with 18 fractures in 60 acre well spacing. Abandonment time for well with 18 fractures in ultralow permeability reservoir is found to be approximately 7 years which is very short compared to long term production from conventional reservoirs.

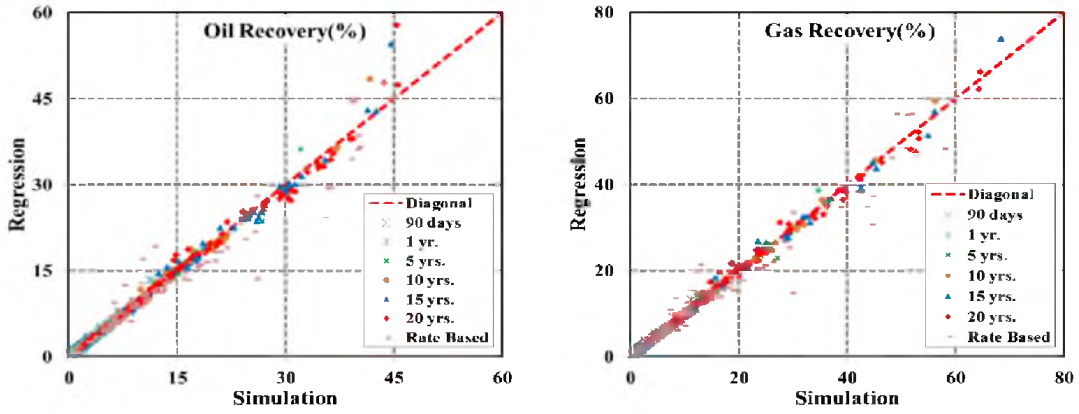

(a) (b)

Figure 6.1. Comparison of regression model with simulation results for (a) Oil recovery and (b) Gas recovery.

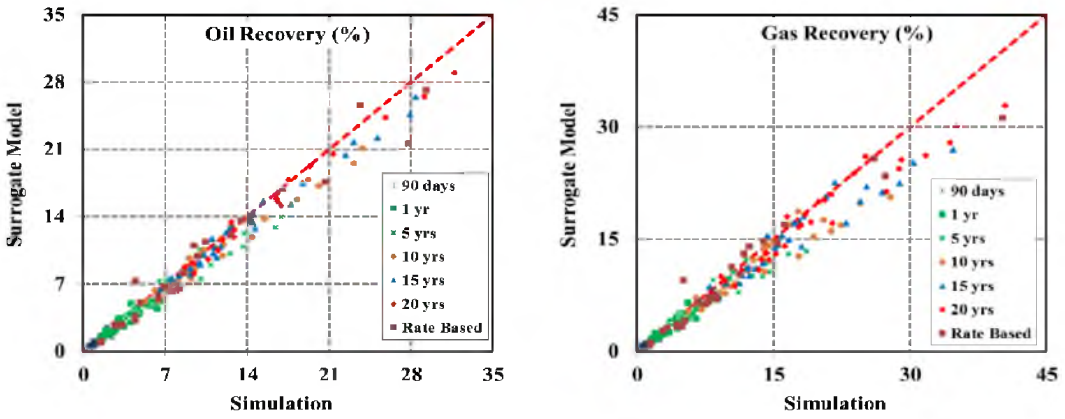

(a) (b)

Figure 6.2. Comparison of surrogate models with simulation results for (a) Oil recovery and (b) Gas recovery.

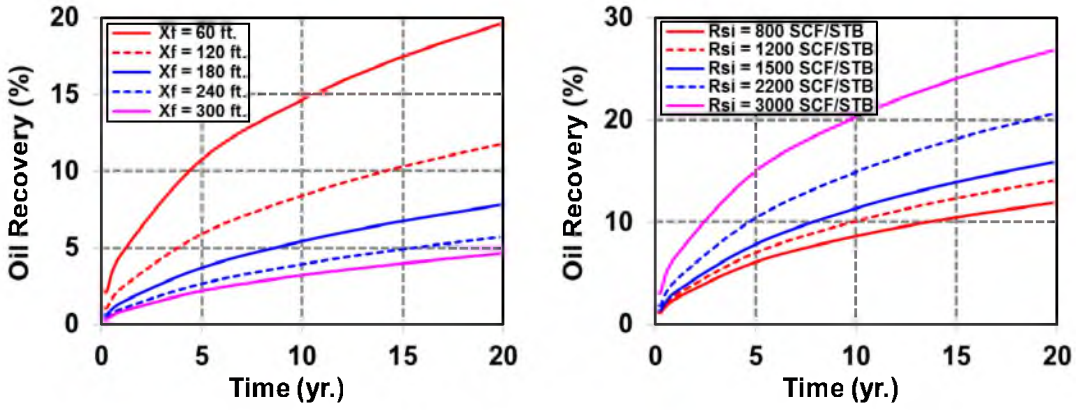

(a) (b)

Figure 6.3. Sensitivity on oil recovery for (a) Fracture spacing and (b) Initial gas oil ratio.

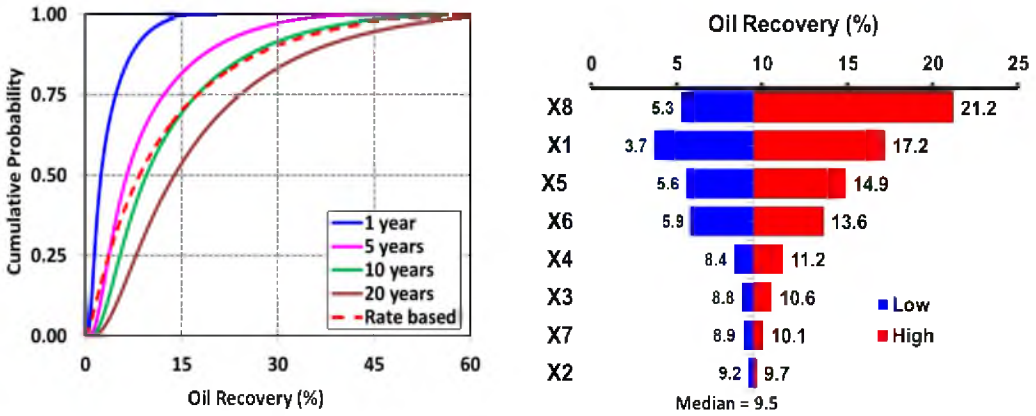

(a) (b)

Figure 6.4. Uncertainty analysis of oil recovery factor by (a) Cumulative probability distribution. (b) Tornado plot for 10 years of production.

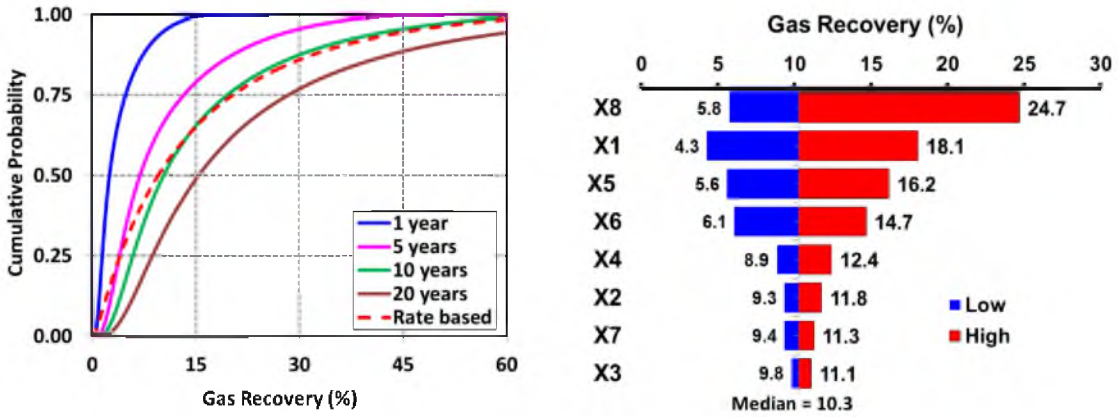

(a) (b)

Figure 6.5. Uncertainty analysis of gas recovery factor by (a) Cumulative probability distribution. (b) Tornado plot for 10 years of production.

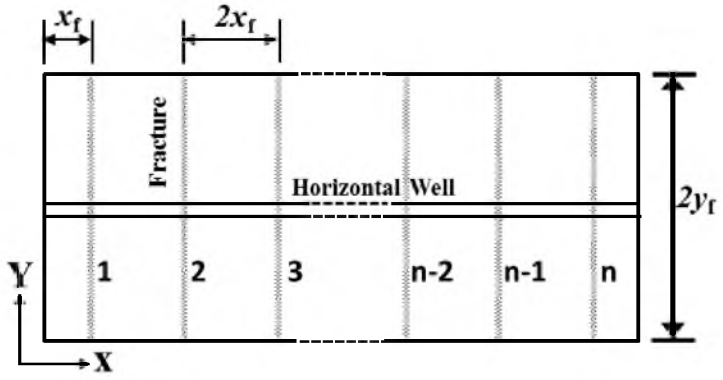

Figure 6.6. Schematic of fracture spacing and number of fractures.

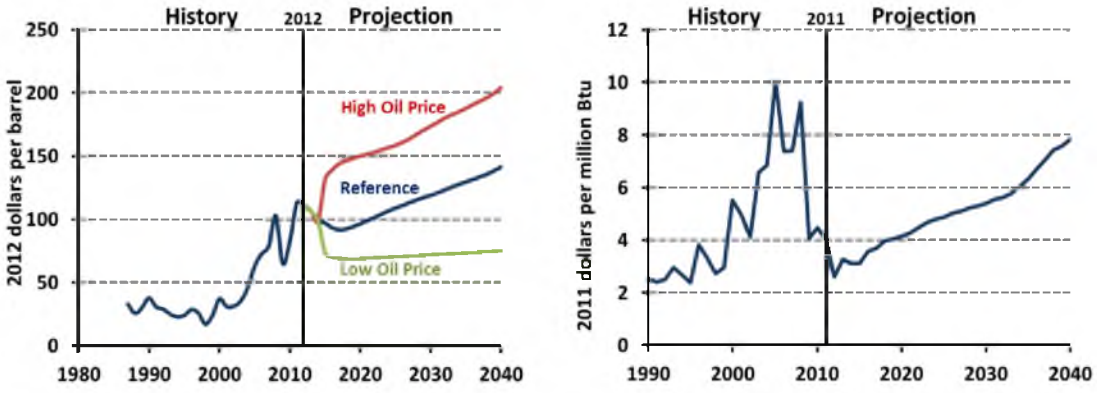

(a) (b)

Figure 6.7. Average annual Brent spot crude oil prices in three cases (AEO 2014) (b) Annual average Henry Hub spot natural gas prices (AEO 2013).

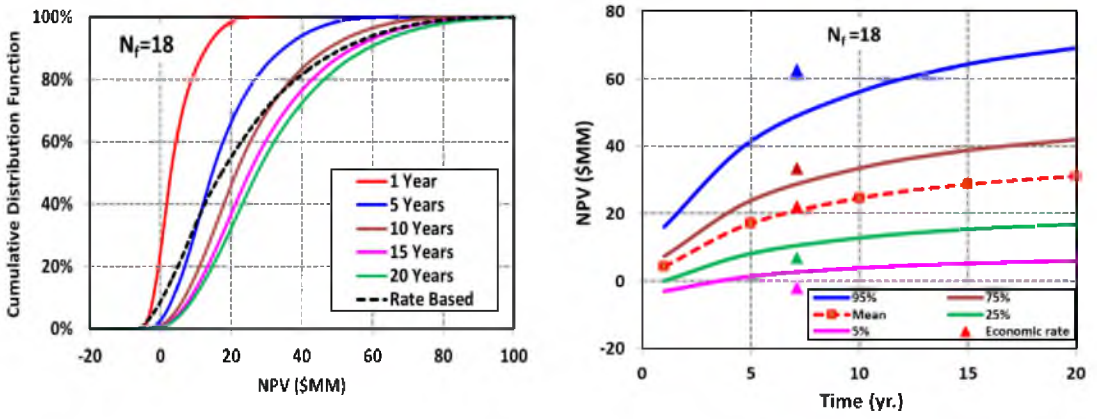

(a) (b)

Figure 6.8. Statistics of investment (a) Cumulative probability of NPV for various periods (b) Mean of NPV with 50% and 90 % confidence interval.

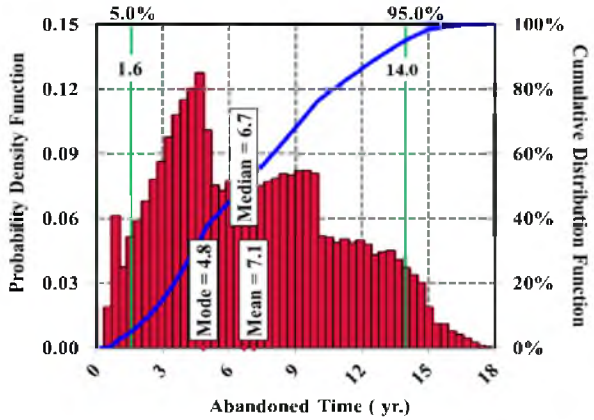

Figure 6.9. Probability of abandoned time for well with 18 fractures when oil rate reaches 5 STB/day/fracture.

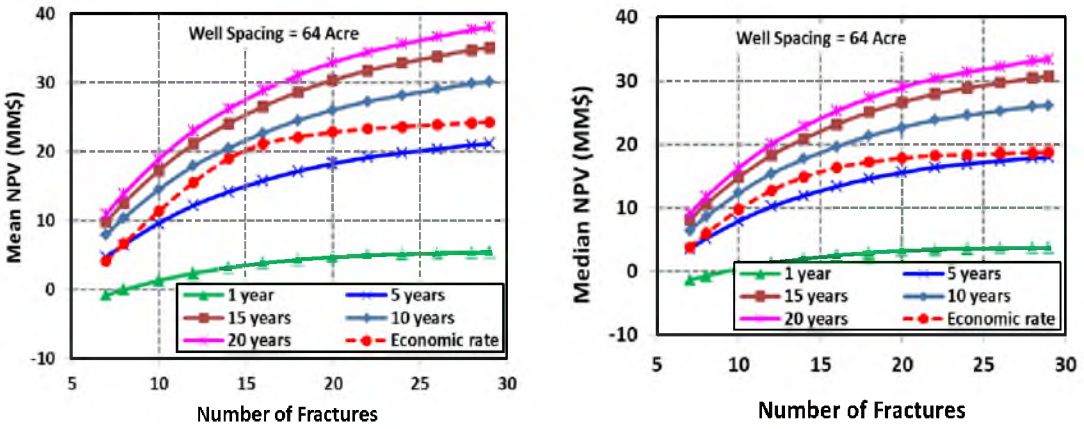

(a) (b)

Figure 6.10. Sensitivity of fracture density on (a) Mean NPV (b) Median.

Table 6.1. List of input parameters and their distribution for uncertainty analysis.

Variable	Symbol	Minimum (-1)	Medium (0)	Maximum (+1)	Distribution for Uncertainty Analysis
Matrix Permeability, $\log(k_m)$, log(nD)	X1	1	2.35	3.70	Lognormal
Gas Rel. Permeability Exponent, n_g	X2	1	2	3	Uniform
Rock Compressibility, $\log(c_f)$, $\log(psi^{-1})$	X3	-6	-5.5	-5	Uniform
dRs/dp, (SCF/STB)/psi	X4	0.50	0.65	0.80	Uniform
Initial Gas Oil Ratio, Rsi, SCF/STB	X5	800	1900	3000	Conditional Uniform (depends on X6)
Initial Pressure, Pi, psi	X6	4000	5250	6500	Uniform
BHP, psi	X7	500	1000	1500	Uniform
Fracture Spacing, foot,	X8	60/60	180/180	300/300	Conditional Tri-Valued (depends on X1)

Table 6.2. Goodness of fit of response surface models.

Models	Oil Recovery (%)		Gas Recovery (%)	
	R^2	NRMSE (%)	R^2	NRMSE (%)
90 days	0.989	1.9	0.983	2.3
1 year	0.986	2.3	0.984	2.5
5 years	0.990	1.8	0.989	1.9
10 years	0.991	1.8	0.994	1.3
15 years	0.986	2.6	0.993	1.5
20 years	0.980	3.4	0.989	2.1
Rate Based	0.989	7.3	0.983	6.9

Table 6.3. Random values of input parameters for validation of surrogate models.

Sr. No.	K_m (nD)	n_g	C_f (1/psi)	dR_s/dp ((SCF/STB)/psi)	R_{si} (SCF/STB)	P_i (psi)	P_{wf} (psi)	X_f (ft.)
1	1496	1.17	1.0E-05	0.62	2069	5738	743	300
2	361	1.27	3.8E-05	0.67	1456	4170	1417	180
3	31	1.35	8.0E-06	0.58	1625	4637	769	60
4	44	1.78	2.0E-05	0.59	1724	4560	1266	60
5	2475	2.66	1.9E-05	0.69	2408	5670	689	300
6	12	2.61	1.4E-05	0.58	2820	6111	787	60
7	210	1.12	2.0E-05	0.75	1775	4861	591	180
8	28	1.80	1.9E-05	0.79	2969	5951	1076	60
9	4390	2.05	6.0E-06	0.72	2531	5688	1183	300
10	840	1.83	5.4E-06	0.60	1460	4017	1047	300
11	225	2.31	4.0E-05	0.68	2106	5505	926	180
12	187	2.26	5.9E-06	0.53	1689	4967	1144	180
13	14	1.58	4.3E-06	0.77	2779	6290	1148	60
14	694	1.86	1.5E-05	0.76	1539	4003	1179	300
15	13	1.03	3.0E-05	0.75	1273	5156	1136	60
16	16	2.97	1.9E-05	0.58	1413	5061	1445	60
17	256	1.33	6.2E-06	0.68	1323	5152	709	180
18	18	1.21	9.4E-06	0.51	2281	5925	1209	60
19	1618	1.74	1.2E-05	0.63	1552	4806	736	300
20	1612	1.40	3.8E-05	0.59	2527	5962	619	300
21	892	1.98	5.7E-06	0.55	1566	5178	1107	300
22	25	1.68	2.9E-05	0.55	1900	4089	950	60
23	604	2.90	1.8E-05	0.63	1614	4440	959	300
24	251	2.84	9.5E-06	0.53	2944	5804	1162	180
25	4237	1.11	6.2E-06	0.68	1710	5184	1270	300
26	565	2.48	1.1E-05	0.64	1966	4382	850	300
27	1448	1.54	1.2E-05	0.71	1393	4853	1162	300
28	168	1.85	5.3E-06	0.71	2676	5518	916	180
29	147	2.10	1.6E-05	0.69	1431	4479	1342	180
30	1692	2.89	6.7E-06	0.51	2672	5846	1333	300

Table 6.4. Validations of oil and gas recovery models.

Models	Oil Recovery (%)		Gas Recovery (%)	
	R^2	NRMSE (%)	R^2	NRMSE (%)
90 days	0.81	17.3	0.86	17.0
1 year	0.85	12.8	0.85	14.7
5 years	0.92	10.4	0.85	13.3
10 years	0.97	7.8	0.89	12.4
15 years	0.98	6.1	0.92	11.1
20 years	0.99	4.8	0.94	9.6
Rate Based	0.97	6.9	0.96	5.8

Table 6.5. Values of input parameters used in sensitivity studies.

Variable	Sensitivity of X_f	Sensitivity of initial GOR
K_m (nD)	100	100
n_g	1.5	1.5
C_f (1/psi)	4* 10^-5.5	4*10^-5.5
dR_s/dp ((SCF/STB)/psi)	0.55	0.55
R_{si} (SCF/STB)	1000	800,1000,1200,1500,3000
P_i (psi)	5000	6000
P_{wf} (psi)	500	500
X_f(ft.)	60,120,180,240,300	120

Table 6.6. Distribution of initial GOR and fracture spacing.

Name Independent Variable	Condition	Distribution of Dependent Variable	Name of Dependent Variable
Initial Pressure, Pi, psi, (X6)	4000 to 4500	Uniform (800,1200)	Initial GOR, SCF/STB(X5)
	4501 to 5500	Uniform (1200,2000)	
	5501 to 6500	Uniform (2000,3000)	
Reservoir Permeability, Km, nD, (X1)	10 to 100	60	Fracture Spacing, ft, (X8)
	101 to 500	180	
	More than 500	300	

Table 6.7. Uncertainty in oil recovery and rank of input parameters

Description	Oil Recovery (%)				
	1 Year	5 Years	10 Years	20 Years	q_o = 5 STB/day
Mean	3.5	9.1	13.0	17.8	12.4
Std. Dev.	3.0	7.7	10.5	13.2	11.9
Mode	1.1	3.3	4.2	7.0	1.6
5%	0.7	1.7	2.5	3.6	0.9
10%	0.9	2.3	3.3	4.8	1.6
50%	2.4	6.4	9.5	13.8	8.4
90%	7.9	20.3	28.0	37.1	29.6
95%	10.1	25.9	35.5	45.8	37.9
Rank of Inputs by Impact on Median Recovery	X_f	K_m	K_m	K_m	K_m
	K_m	X_f	X_f	X_f	R_{si}
	R_{si}	R_{si}	R_{si}	R_{si}	X_f
	dR_s/dp	dR_s/dp	dR_s/dp	dR_s/dp	P_i
	P_i	P_i	P_i	P_i	dR_s/dp
	n_g	C_f	C_f	C_f	C_f
	C_f	n_g	n_g	P_{wf}	P_{wf}
	P_{wf}	P_{wf}	P_{wf}	n_g	n_g

Table 6.8. Uncertainty in gas recovery and rank of Input parameters.

Description	Gas Recovery (%)				
	1 Year	5 Years	10 Years	20 Years	q_o = 5 STB/day
Mean	3.6	10.0	14.9	21.7	14.6
Std. Dev.	3.1	8.6	12.9	18.4	14.7
Mode	1.3	3.4	5.1	7.3	1.5
5%	0.7	1.9	2.9	4.1	1.0
10%	0.9	2.5	3.7	5.4	1.7
50%	2.5	6.9	10.3	15.4	9.5
90%	8.1	22.5	33.4	47.8	35.6
95%	10.4	29.0	43.4	62.3	46.2
Rank of Inputs by Impact on Median Recovery	X_f	X_f	X_f	K_m	K_m
	K_m	K_m	K_m	X_f	R_{si}
	R_{si}	R_{si}	R_{si}	R_{si}	X_f
	dR_s/dp	dR_s/dp	dR_s/dp	dR_s/dp	dR_s/dp
	n_g	n_g	n_g	n_g	P_i
	P_i	P_i	P_{wf}	P_{wf}	n_g
	C_f	P_{wf}	P_i	P_i	C_f
	P_{wf}	C_f	C_f	C_f	P_{wf}

Table 6.9. Parameters and cost in Economic Model for NPV.

Well Spacing (Acre)	60
Royalty (%)	15
Discount rate (%)	10
Fracture extend in Y-direction (ft.)	375
Bottom hole pressure (psi)	500
Decline Curve Analysis Model	Duong's Model
Production cost ($/bbl)	10
Fixed operating Cost ($/month)	3500
Land Acquisition and Leasing (MM$)	0.15
Vertical Drilling(MM$)	1.82
Horizontal Drilling(MM$)	1.22
Completion(MM$)	0.25
Fracking(MM$/fracture)	0.18
Single Well Total (MM$) with 18 fractures	7.08

CHAPTER 7

COMPOSITIONAL AND TEMPERATURE DEPENDENCE OF LIQUIDS PRODUCING SHALES

When the reservoir temperature is near the critical temperature of the fluid, the quality and amount of produced fluids become very sensitive to temperature change and initial fluid compositions. Different types of fluids such as oil, condensate and gas may coexist in different layers of thick reservoirs depending on the temperature and maturity of hydrocarbons. Temperature, pressure and compositional variations in the flow paths inside the reservoirs and in production lines also lead to production comprised of a mixture of various fluids. Effects of temperature shift around the critical point on production of liquids with low to high initial liquid to gas ratio from low permeable fractured reservoirs are studied here. Liquid rates (condensate, volatile oil), instantaneous liquid to gas ratio (LGR) and liquid recovery factors are compared between volatile oil and condensate for identical initial fluid compositions. Liquid recovery was higher from condensate reservoir. Differences between the condensate rate and volatile oil rate are very prominent for 100 nD reservoir compared to 1000 nD reservoir. Operating well at higher flowing bottom hole pressure (FBHP) is preferable for low permeability (100 nD) reservoirs while low FBHP is preferable for higher permeablility (1000 nD) reservoirs in order to recover more liquid. FBHP affects the liquid rates least for higher initial LGR.

7.1 Backgrounds

Reservoir temperature is considered as constant in most reservoir engineering studies. However, while known temperature gradient exists along the depth of the reservoir, there are very few studies on the performance of liquid near critical temperature. This study is intended to investigate the performance of volatile oil and condensate in ultralow permeable reservoirs. In early studies, researchers tried to establish empirical relationships between oil recovery and reservoir fluid properties like initial gas oil ratio (GOR), API gravity and type of reservoir rock for conventional reservoirs. GOR and formation volume factors were predicted for dissolved gas drive reservoir at saturated conditions using compositional simulations (Brinkman and Weinaug 1956). Using empirical relationships, Jacoby et al. (1959) correlated total stock tank oil, separator gas, and recovery by primary depletion with the initial GOR, initial oil gravity, reservoir pressure, and reservoir pressure for saturated volatile oil and rich condensate reservoirs.

Jones-Parra and Reytor (1959) showed that decline in oil rates occurs less from fractured limestone reservoirs with higher initial gas oil ratio (GOR). Produced GOR was proved (Levine and Prats 1961) to be independent of reservoir permeability and well spacing at the same oil recovery for solution gas drive reservoirs. In another study, Prats and Levine (1963) showed that vertically fractured reservoirs produced higher GOR than unfractured reservoirs. Saturations and pressure profiles around well were solved numerically for two-phase flow of gas-condensate and volatile oil in transient conditions and results were compared with field data (Kniazeff and Nvaille 1965). The effect of temperature on the petrophysical properties of rock has been studied extensively, as illustrated below. Pore volume compressibility was increased significantly in

temperatures up to 400° F compared to room temperature (Von Goten and Choudhary 1969) for sandstone rock. Decreases in absolute permeability by 60% (Weinbrandt, Ramey et al. 1975) to near 90% (Afinogenov 1969) were also observed, although causes were not clearly understood since the absolute permeability of rock is independent of fluid properties. Residual oil saturation was reduced with increasing temperature in sandstone, unconsolidated sand and porous Teflon (Edmondson 1965; Davidson 1969; Poston, Ysrael et al. 1970; Lo and Mungan 1973; Weinbrandt, Ramey et al.). Change in irreducible water saturation was found to be dependent on rock; it was increased in sandstone (Sinnokrot, Ramey et al. 1971; Sanyal, Ramey et al. 1973) and unconsolidated sand pack (Poston, Ysrael et al. 1970) but unchanged (Sinnokrot, Ramey et al. 1971) in limestone. Capillary pressure curves moved towards the higher water saturation in sandstone (Sinnokrot, Ramey et al. 1971; Sanyal, Marsden et al. 1974) with the increase in temperature due to a decrease in hysteresis between drainage and imbibitions curves. Many researchers (Poston, Ysrael et al. 1970; Lo and Mungan 1973; Weinbrandt, Ramey et al. 1975; Sufi, Ramey et al. 1982; Torabzadey 1984; Maini and Batycky 1985; Schembre, Tang et al. 2005) have shown that water–oil relative permeability curves changed with increasing temperature due to the change in wettability and reduction of the interfacial tension. Blom et al. (1997) demonstrated that the near critical relative permeability was strongly dependent on non-Darcy flow and significant well impairment occurred due to the combined effect of condensate drop out and non-Darcy flow. Ayala et al. (2007) showed similar results in which they revealed that Fickian flow in fissured tight reservoirs had comparable contribution (compared to Darcy flow) to ultimate recovery of near critical fluid like condensate and the diffusion coefficient is greatly

dependent on fluid composition and properties. After compiling previous studies, Sanyal et al. (1974) concluded that the effects of temperature on petrophysical properties like bulk volume, porosity, absolute permeability, relative permeability, residual oil saturation etc. cannot be neglected for formation evaluations and reservoir performance calculations. Researchers had difficulties to simulate phase behavior of near critical fluids and it is very sensitive to many factors in equation of state like binary interaction coefficients (Arbabi and Firoozabadi 1995). The Watson characterization factor was included (Huang 1985) to improve the PVT data of near critical fluids with nitrogen gas injection in the reservoir. Kossack et al. (1986) proved that the Peng-Robinson equation was inadequate to simulate phase behavior of near critical fluids. Gravity can affect the near critical condensate very strongly and wettability plays a great role during phase separation (Williams and Dawe 1989). Proper characterization of higher molecular fractions (C7 through C20+) of near critical reservoir fluids were necessary (Rosales, Ashford et al. 1992) to match the field GOR, saturation pressure etc. Importance of proper calculations method of Interfacial Tension (IFT) on the gravity drainage contribution on recovery of near critical fluid like condensate was demonstrated (Ceragioli and Masserano 1998).Viscosity and density of near critical fluids were measured (Al-Meshari, Kokal et al. 2007) by designing PVT apparatus suitable for elevated pressure and temperature and these data were used to evaluate the correlations for viscosity used in commercial software. Laboratory experiments proved that an increase in temperature improved the final oil recovery after injecting surfactant and water (Najurieta, Galacho et al. 2001). Fang et al. (1998) discussed the importance of correct fluid characterizations. The near critical fluids in reservoir were successfully

identified (Kyi, Bt Yahaya et al. 2009) by integrating all available formation evaluation data obtained from fields in offshore Malaysia. Various kinds of fluids such as dry gas, gas-condensate and oil are produced from a single play like Eagle Ford shale (depths between 4,000 and 14,000 feet with the average thickness about 475 feet) which is located in South Texas as shown in Figure 7.1. Oil and gas condensate areas are the most attractive zone for producers right now. The near critical fluids like condensates/volatile oils which are found in the juncture of oil and condensate areas are very sensitive on the surface, subsurface and flow paths conditions (temperatures, pressures and initial compositions). The two different fluids are produced from the same initial reservoir fluids with different temperature as shown in Figure 7.2. Reservoir temperature greater than critical point temperature makes condensates and less than critical point produces volatile oils. Reservoir temperatures corresponding to volatile oil and condensate are equally spaced ($25^{O}F$) from the critical temperature. The initial reservoir pressure and flowing bottom hole pressure are kept the same for both fluids. Three different fluids, namely, lean condensate, intermediate condensate and rich condensate with the reservoir temperatures near critical points, are considered for the study. Effect of temperature on relative permeability is not considered because temperature change between volatile oil and condensate is reasonably small for significant change in relative permeability. In this study, production performance (liquid rate, gas rate, instantaneous produced LGR and recovery factors for gas and liquid) for the same initial fluid compositions at different temperatures around the critical point will be investigated.

7.2 Reservoir Model

Single vertical fracture in the middle of the reservoir with one horizontal well is simulated in this study. The reservoir dimensions are kept fixed as 120 ft. in the x-direction (which is considered as the distance between two fractures), 750 ft. in the y-direction, and 200 ft. in the z-direction; with a top depth of 12800 ft. A schematic diagram of the reservoir is shown in Figure 7.3. The simulated portion of the reservoir is marked by the red dashed line. Initial reservoir pressure is chosen to be higher than the initial bubble point/dew point pressure for all three fluids to keep the initial reservoir fluids is in single phase either in liquid phase or gaseous phase. The parameters used in the study are summarized in Table 7.1.

The fracture width and orientation, fracture permeability, initial hydrocarbon saturation, and reservoir porosity are also selected constant for all simulations. Reservoir temperatures are varied in different fluid PVT. The relative permeability curves are shown in Figures 7.4 a and b.

Same relative permeability curves are used for both condensate and volatile oil for small temperature difference between them. The effect of temperature change on relative permeability curves of condensate and volatile with same initial compositions is negligible. Effect of end point saturations are also not considered in this study.

7.3 Reservoir Fluids

Three distinguished fluids are studied here. The initial hydrocarbon liquids to gas ratios (LGR) for three fluids are 98, 142 and 248 STB/MMSCF. The compositional data used to create the fluids were partly taken from Whitson and Sunjerga (2012). The compositions are shown in Table 7.2. The three different fluids are designated as Fluid 1,

Fluid 2 and Fluid 3.

The crititical points of the three fluids and the initial LGR are also displayed in the table. The pressure-temperature plots of the three fluids obtained using Winprop from Computer Modeling Group are shown in Figures 7.5 a, b and c. The critical temperatures increase with increase in the initial LGR. The fluids behave differently depending on the reservoir temperature. Reservoir fluids with the temperature less than the critical point temperature are volatile oil and the same fluid will be condensate if the temperature is above the critical point temperature. The properties of the three different fluids studied here are summarized in Table 7.3. Viscosity of fluid greatly depends on the compositions, temperature and pressure. Viscosity of volatile oil is higher compared to viscosity of condensate for both initial CGR of 98 and 248 STB/MMSCF as shown in Figure 7.6.

7.4 Results and Discussion

All simulations were conducted using GEM, a Computer Modeling Group compositional simulator. Sufficiently fine grids are used to obtain converged results without any grid effects. Initial reservoir pressure of 6500 psi is chosen to keep the reservoir fluid in single phase initially. Liquid rates (i.e., condensate rate and oil rate), instantaneous liquid to gas ratio, gas recovery and liquid recovery are compared between volatile oil and condensate. Pressure profiles inside reservoirs for different times are also compared.

Results for various fluids are presented sequentially from lean condensate (and volatile oil with high gas oil ratio) to rich condensate (and volatile oil with low gas oil ratio). Instantaneous liquid to gas ratio, gas recovery and liquid recovery when economic liquid rate of 5 STB/day is reached are also tabulated. The pressure profile with distance

is a significant parameter to understand the flow inside reservoir, and hence, comparison of pressure profiles between condensate reservoir and volatile oil reservoir are also shown. In this study, simulations are run with constant BHP of 1000 psi and 3000 psi. Wells are normally operated with variable flowing bottom pressure (BHP) with time. Initially well are opened with higher BHP and then pressure is reduced as the reservoir is depleted in course of production. The effect of variable pressure is shown in Figure 7.7. Before discussing the production performances of various fluids, the pressure profiles inside reservoirs are investigated as shown in Figure 7.8.

7.4.1 LGR = 98 STB/MMSCF

The fluid 1 as described in Table 7.2 is considered as lean condensate at 255^{O}F with condensate to gas ratio of 98 STB/MMSCF and volatile oil at 205^{O}F with gas oil ratio of 10205 SCF/STB. The amount of liquid that drops out is very small for lean condensate when pressure drops below dew point pressure.

The liquid flow rates for condensate and volatile oil for two different reservoir permeabilities are shown in Figure 7.9 a and b. There are no significant differences in rates of volatile oil and condensate for 100 nD and 1000 nD reservoirs at flowing bottom hole pressures (FBHP) of 1000 and 3000 psi. The higher liquid rate is obtained when flowing bottom hole pressure is 3000 psi. Higher FBHP enhances the flow of liquid and suppresses the flow of gas. The differences in the liquid flow rates for FBHP of 1000 psi and 3000 psi are subtle at higher reservoir permeability of 1000 nD. The instantaneous liquid to gas ratios (LGR) for volatile oil and condensate are compared in Figures 7.10 a and b. A volatile oil reservoir produces lower liquid to gas ratio (LGR) than a condensate reservoir. Same trend is observed for both 100 nD and 1000 D reservoirs. Lower FBHP

has less effect on LGR between volatile oil and condensate reservoirs. Liquid recoveries are compared in Figures 7.11 a and b. Five to ten percent more liquid is recovered from condensate reservoir than volatile oil reservoir. In lean condensate reservoir, condensate is mainly produced from gas phase than flow of condensate itself in liquid form. Higher gas recoveries yield higher condensate recoveries too compared to oil recoveries from volatile oil reservoir. Lower FBHP helps to recover more liquid and gas from both types of reservoirs for 1000 nD permeable reservoir. A reverse effect is noticed for liquid recoveries from 100 nD reservoir; higher FBHP yields higher recovery of liquid. Higher gas and liquid recoveries are obtained from reservoir permeability of 1000 nD than 100 nD. Up to 5% more gas is recovered from gas condensate reservoir than volatile oil reservoir at the same time. Since gas has higher mobility than liquid at the same pressure, more gas is recovered from a gas condensate reservoir than a volatile oil reservoir because a gas condensate reservoir is initially a gas reservoir at pressure above dew point pressure. FBHP adversely affects the recovery of gas for both kinds of reservoirs. Gas recoveries are almost doubled when FBHP is changed from 3000 psi to 1000 psi.

No differences in pressure profiles are noticed except in the early time of production. Pressure drop is slightly higher for volatile oil reservoir from 100 nD permeable reservoir with FBHP of 3000 psi. The differences in pressure profiles almost diminish for 1000 nD reservoirs.

7.4.2 LGR= 142 STB/MMSCF

The fluid2 behaves as intermediate condensate at 325OF with condensate to gas ratio of 142 STB/MMSCF and volatile oil at 275OF with gas oil ratio of 7042 SCF/STB. The liquid flow rates for condensate and volatile oil for two different reservoir permeabilities

are compared in Figures 7.12 a and b. No significant differences are observed in liquid rates for intermediate condensate and volatile oil. The difference between condensate rates and volatile oil rates at FBHP of 1000 psi is also reduced. Flow rates of both fluids are almost the same at higher reservoir permeabilities of 1000 nD for FBHP of 1000 psi and 3000 psi. The instantaneous liquid to gas ratios (LGR) for volatile oil and condensate are shown in Figures 7.13 a and b. Similar trends like fluid 1 are observed for fluid 2.

A condensate reservoir produces more liquid to gas ratio than volatile oil reservoir for both reservoir permeabilities of 100 nD and 1000 nD. The difference in the LGR between condensate and volatile oil reduces with reducing FBHP at 1000 psi. The flat plateau of LGR prolongs for fluid 2 (intermediate LGR) compared to fluid 1 (low LGR).

Liquid recoveries are presented in Figures 7.14a and b. Substantial differences in liquid recoveries between condensate reservoir and volatile oil reservoir are observed for both permeability (100 nD and 1000 nD). More condensate and volatile oil are recovered at higher FBHP of 3000 psi for 100 nD permeable reservoirs. More hydrocarbons (liquid and gas) are extracted from r reservoirs of higher permeability of 1000 nD. Condensate reservoirs produce more gas than volatile oil reservoirs for reservoir permeabilities of 100 nD and 1000 nD. Effect of FBHP is also clearly noticed for both fluids; higher FBHP restricts flow of gas, and hence less gas is produced.

7.4.3 LGR= 248 STB/MMSCF

The fluid 3 is considered as rich condensate at 387OF with condensate to gas ratio of 248 STB/MMSCF and volatile oil at 337OF with gas oil ratio of 4032 SCF/STB. The gaseous phase contains a large amount of vaporized condensate and the amount of liquid that drops out is high when pressure drops below dew point pressure.

The liquid flow rates for condensate and volatile oil for two different reservoir permeabilities are shown in Figures 7.15 a and b. The differences between condensate rates and volatile oil rates for two different FBHP of 1000 psi and 3000 psi disappear gradually from lean LGR (98 STB/MMSCF) to rich LGR (248 STB/MMSCF). In Figures 7.15 a and b, all rates almost overlap each other. Therefore, FBHP (in the range of 1000 psi to 3000 psi) has the least effect on liquid rate for reservoir permeability of 100 nD and 1000 nD. The instantaneous liquid to gas ratios (LGR) for volatile oil and condensate are shown in Figures 7.16 a and b. The LGR trends are not different from the trends seen in fluid 1 and fluid 2. The differences in the LGR of condensate and volatile oil are less for this fluid with initial LGR of 248 STB/MMSCF. Condensate reservoirs produce a little higher gas than volatile oil reservoirs. But up to 5% more liquid is recovered from condensate reservoirs than volatile oil reservoirs as shown in Figures 7.17a and b. More liquid is recovered from the condensate reservoirs and with higher FHBP for 100 nD reservoir. Differences in the condensates rates and volatile oil rates reduce with increase in reservoir permeability. Gas recoveries, liquid recoveries and produced gas liquid ratio at economic liquid rate of 5 STB/day for 100 nD and 1000 nD permeability reservoirs at different flowing bottom hole pressure (1000 psi and 3000 psi) for three different fluids are summarized in Table 7.4.

Condensate reservoirs take a longer time to reach the economic rate of 5 STB/day than the volatile oil reservoirs. More liquid and gas are recovered from condensate reservoirs compared to volatile oil reservoirs by the time liquid rates reach the economic rate, although produced instantaneous LGRs are almost same for both reservoirs. Liquid rates from lower permeability (100 nD) reservoirs (with condensate or volatile oil) reach

the economic rate limit more quickly than the higher permeability (1000 nD) reservoirs (except the fluid 2 at FBHP of 3000 psi) but more gas and liquid are recovered from higher permeability reservoirs. This can be explained by analyzing the liquid rates. Initial liquid rates are higher for 1000 nD reservoir (liquid rates near 60 to 80 STB/day) compared to very low rates of near 15 to 20 STB/day from 100 nD reservoirs. Therefore, liquid rates more quickly reach to 5 STB/day from 15 STB/rate (initial rate) for 100 nD reservoir than the initial rates from 60 STB/day to 5STB/day in the case of 1000 nD reservoirs.

In the case of gas condensate reservoirs, the reservoir is filled with gas initially when reservoir pressure is above dew point pressure. Gas phase contains the liquid condensate as volatilized form. Condensate drops out inside the reservoir when the reservoir pressure declines below dew point pressure. The amount of condensate drop out depends on the richness of volatilized condensate in the gas phase, i.e., initial condensate to gas ratio. Amount of condensate dropout inside the reservoir is meager in the case of lean condensate fluid; hence condensate is produced mainly from the gas phase. For rich condensate fluid, a sufficient amount of condensate is produced on the surface from liquid phase as well as from gas phase. On the other hand, volatile oil reservoir is initially oil reservoir with high dissolved gas inside the oil. Gas evolves out of oil phase when pressure drops below bubble point pressure. Condensate production mainly comes from gas phase for condensate reservoir and in the case of volatile oil reservoir; oil is mainly produced from the oil phase itself. Having greater mobility, gas always dominates the flow for both type of reservoirs (volatile oil and condensate), and hence comparatively more condensate (in volatilized form in gas phase inside reservoir but liquid form at

separator) is produced from a gas-condensate reservoir than oil production (liquid from inside reservoir as well as separator) from volatile oil reservoirs. The facts are reflected in the results (in rate, liquid to gas ratio and recovery factors). The difference in the amount is again dependent on the initial conditions of the fluids.

7.4.4 Comparison Among Various Fluids

The amounts of hydrocarbon initially in place are varied for various fluids. Initial hydrocarbon (condensate, volatile oil and gas) in place for fluid 1, fluid 2 and fluid 3 for both types of reservoirs (condensate reservoir and volatile oil reservoirs) are shown in Figure 7.18. Amounts of initial liquids increase with increasing initial gas to liquid ratio as clearly shown in Figure 7.18. Liquid recoveries and gas recoveries for different reservoir conditions with various fluids are plotted in Figures 7.19 a and b. The highest liquid volumes (condensate and volatile oil) are recovered from the reservoir which is initially filled with fluid 2 (initial LGR of 142 STB/MMSCF). For the reservoir with a lesser initial LGR fluid (fluid1), there is less volatilized condensate in the gas phase in the condensate reservoir and higher gas in the oil phase in the volatile oil reservoir. Condensate is mainly produced from gas phase (for condensate reservoirs) leaving some amount of condensate inside the reservoir and volatile oil is produced from the oil phase mostly (for volatile oil reservoirs). If condensate saturation exceeds the critical saturation, condensate starts flowing as liquid phase with gas phase. The relative flow rates depend on the condensate saturation, i.e., amount of condensate drop out inside the reservoir. Less gas flow rates yield less condensate but enhance the flow of condensate as liquid phase. Therefore, there is an optimum initial LGR where maximum condensate is recovered cumulatively from phases, gas and liquid. It is evident from Figures 7.19 a and

b that the optimum initial LGR (for maximum liquid recovery) is 142 STB/MMSCF, i.e., fluid 2.

7.5 Key Findings

Results have a strong impact on production strategy. When combined with economic constraints, they will have an even bigger impact on field development strategy.

Conclusions are summarized here:

- Higher gas and liquid recovery are obtained for a higher permeability reservoir.
- Differences between condensate rate and volatile oil rate are far less for higher permeability reservoirs.
- To recover more liquid and less gas, operating wells at higher FBHP is better for 100 nD and transition observed between 100 nD and 1000 nD. Lower FBHP is preferable for 1000 nD permeability reservoir.
- Liquid rate, liquid recovery and gas recovery are higher for condensate at the same conditions.
- Decline rate of liquid for condensate is low
- Higher LGR is produced from condensate reservoir.
- FBHP affects the liquid rates least for higher LGR fluid.
- The effect of temperature shift is more pronounced for lean LGR.
- Production of liquid is not directly proportional to initial LGR present in the reservoir; optimum initial LGR was observed which yielded highest recovery of liquid.

Finally, from the above summary, it can be concluded that condensate reservoirs perform better than the volatile oil reservoirs in terms of rate, liquid to gas ratio and recovery in the same conditions.

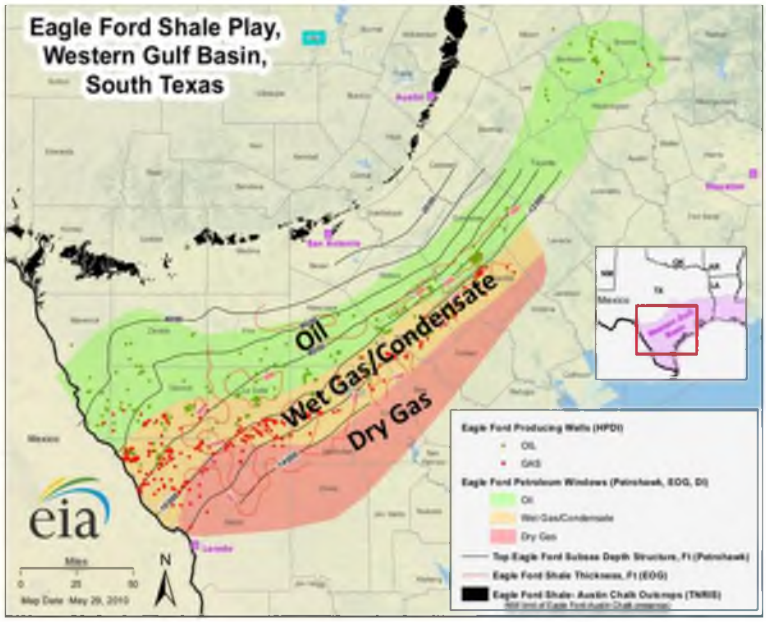

Figure 7.1. Various hydrocarbon fluids windows in Eagle Ford Shale, Texas.

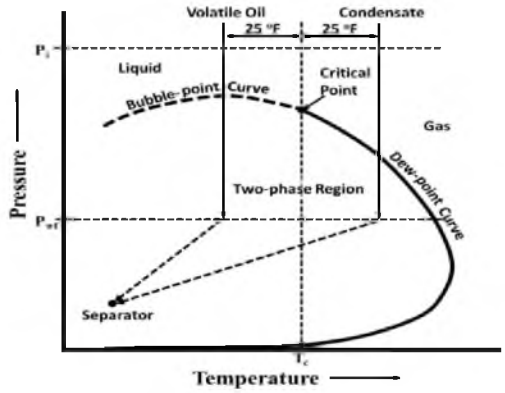

Figure 7.2. Different fluid production paths in Pressure-Temperature diagram.

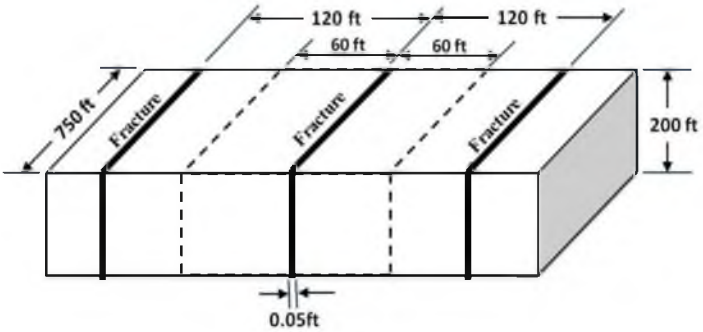

Figure 7.3. Schematic diagram of reservoir model.

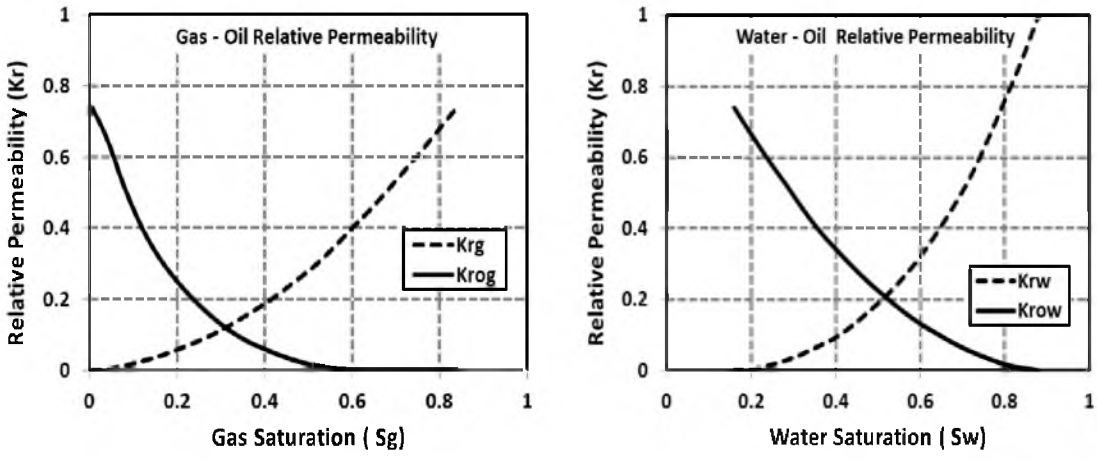

(a) (b)

Figure 7.4. Relative permeability curves (a) Gas-Oil relative permeability (b) Water-Oil relative permeability.

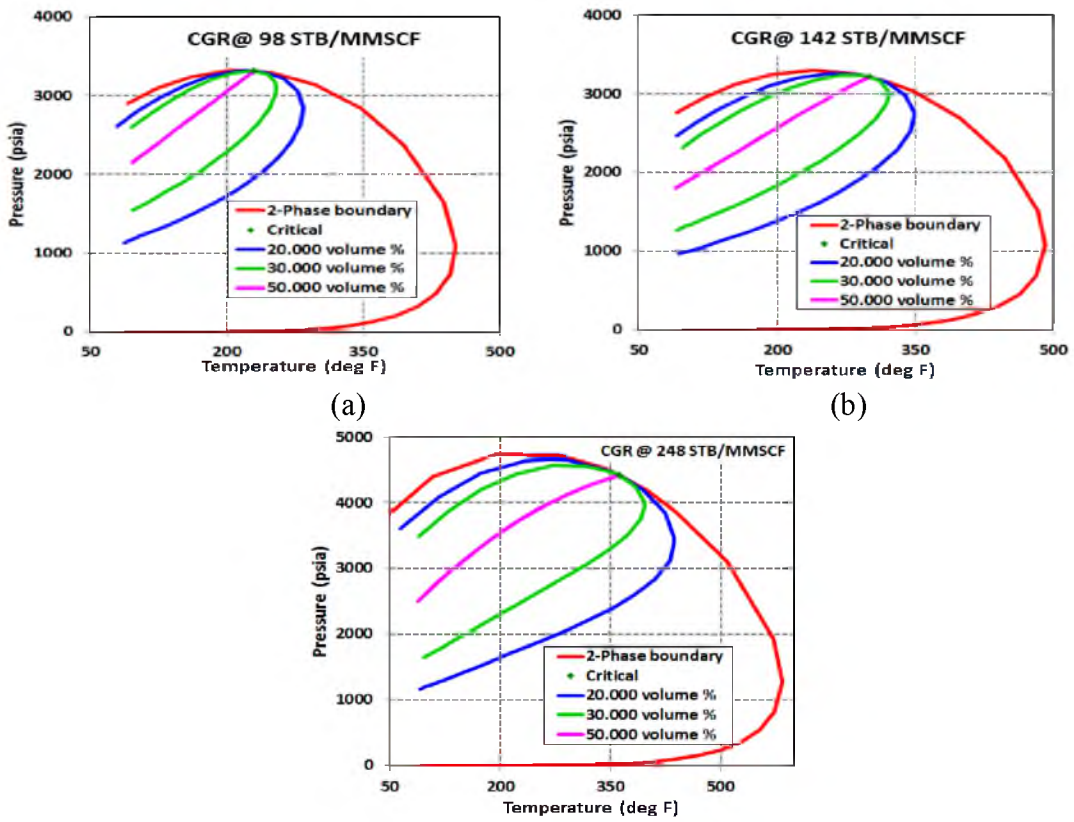

(a) (b)

(c)

Figure 7.5. Fluid Pressure-Volume-Temperature (PVT) diagram for three different fluids (a) Lean condensate (b) Intermediate condensate (c) Rich condensate.

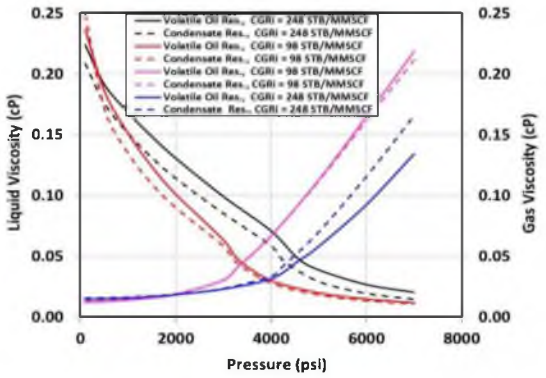

Figure 7.6. Pressure dependence of liquid and gas viscosities of various fluids.

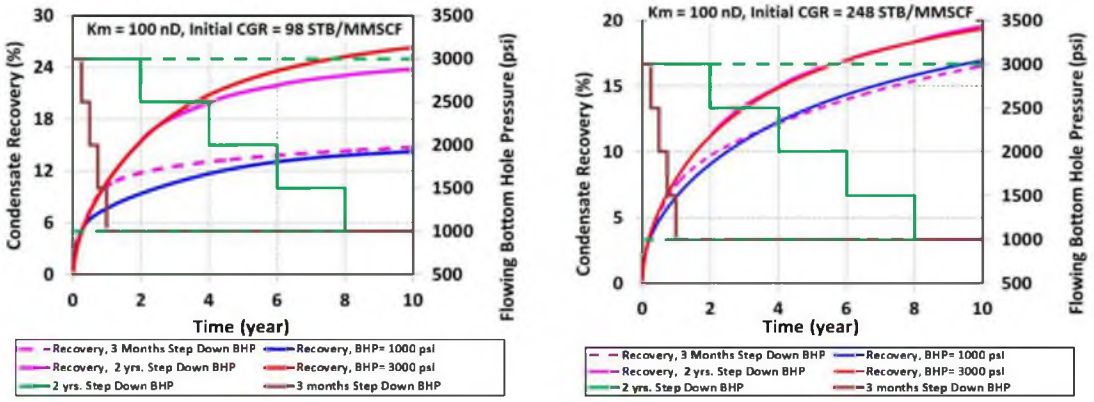

(a) (b)

Figure 7.7. Condensate recovery for various ways of operating bottom hole pressure for reservoir fluids with initial CGR of (a) 98 STB/MMSCF (b) 248 STB/MMSCF.

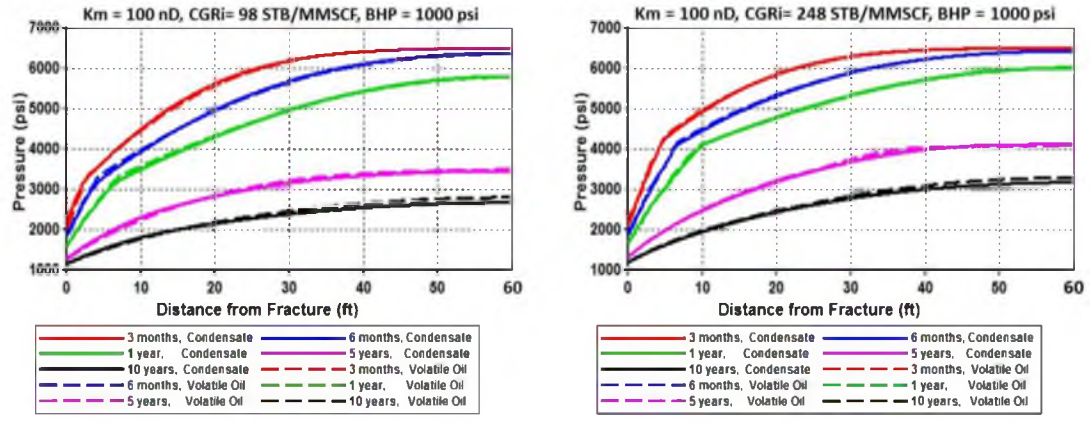

(a) (b)

Figure 7.8. Comparison of pressure profile inside reservoir for condensate and volatile oil with initial CGR of (a) 98 STB/MMSCF (b) 248 STB/MMSCF.

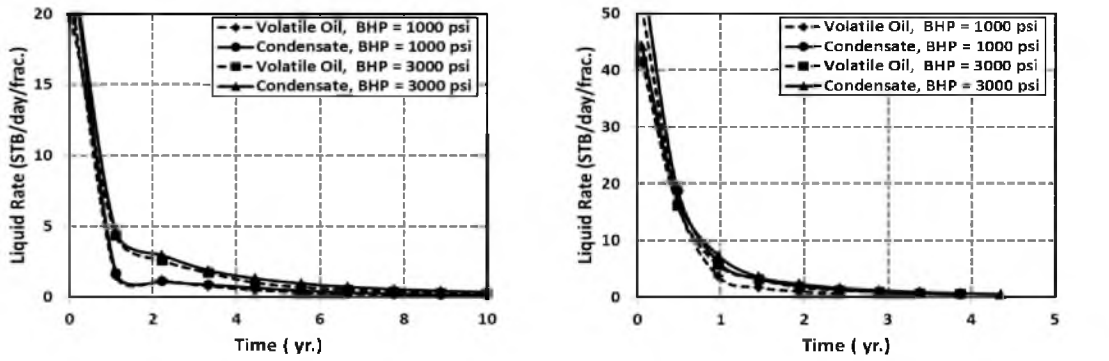

Figure 7.9. Flow rates of lean gas condensates and volatile oil of initial liquid gas ratio 98 STB/MMSCF for reservoir permeabilities (a) 100 nD (b) 1000 nD.

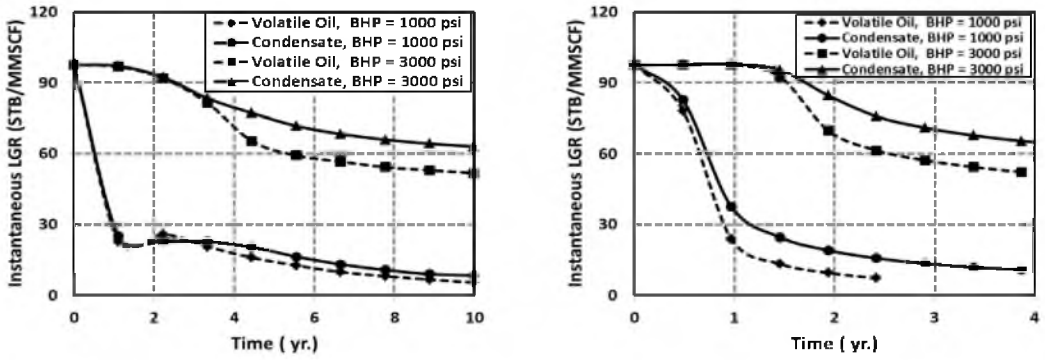

Figure 7.10. Instantaneous liquid to gas ratio from lean gas condensates and volatile oil reservoirs of initial liquid gas ratio 98 STB/MMSCF for reservoir permeabilities (a) 100 nD (b) 1000 nD.

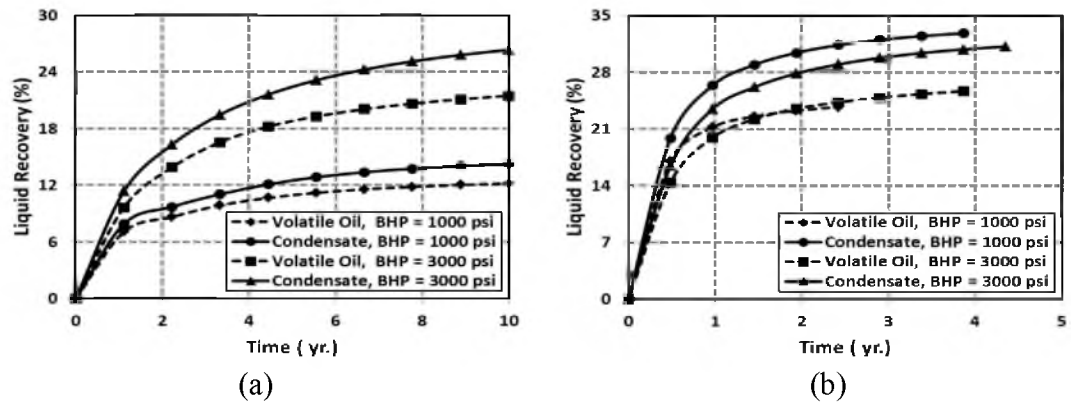

Figure 7.11. Liquid recoveries from lean gas condensates and volatile oil reservoirs of initial liquid gas ratio 98 STB/MMSCF for reservoir permeabilities (a) 100 nD (b) 1000 nD.

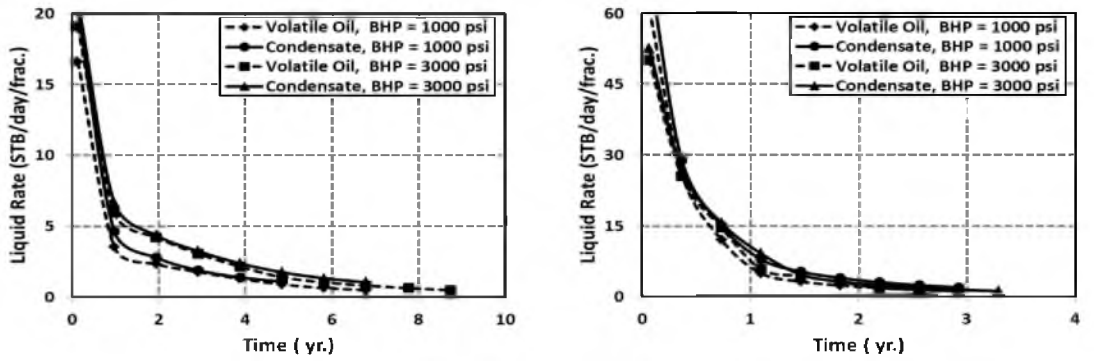

Figure 7.12. Flow rates of lean gas condensates and volatile oil of initial liquid gas ratio 142 STB/MMSCF for reservoir permeabilities (a) 100 nD (b) 1000 nD.

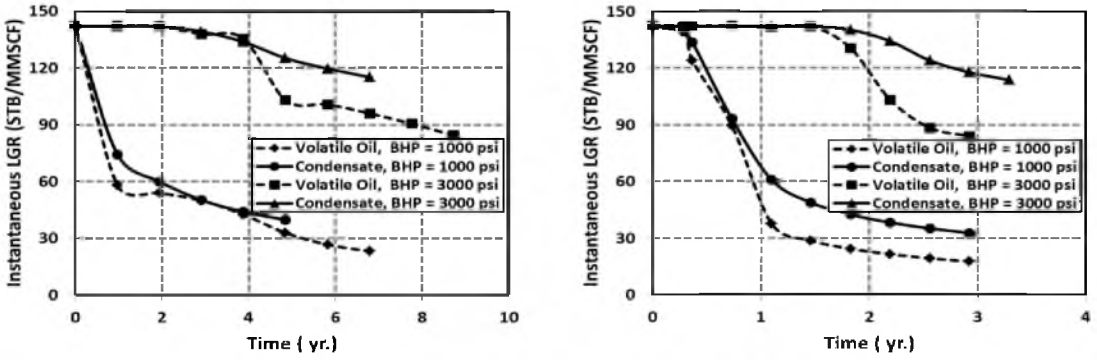

Figure 7.13. Instantaneous liquid to gas ratio from lean gas condensates and volatile oil reservoirs of initial liquid gas ratio 142 STB/MMSCF for reservoir permeabilities (a) 100 nD (b) 1000 nD .

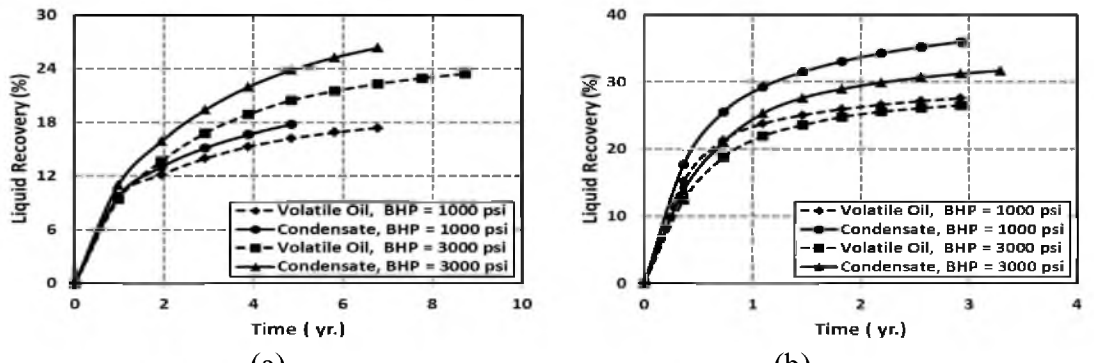

Figure 7.14. Liquid recoveries from lean gas condensates and volatile oil reservoirs of initial liquid gas ratio 142 STB/MMSCF for reservoir permeabilities (a) 100 nD (b) 1000 nD.

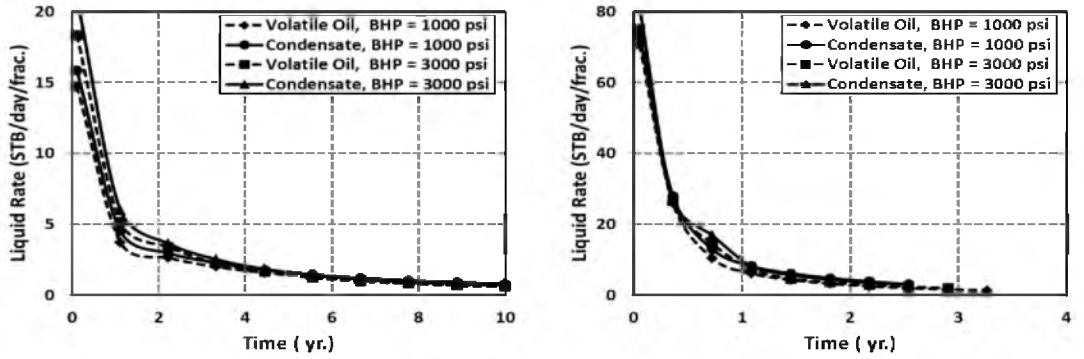

Figure 7.15. Flow rates of lean gas condensates and volatile oil of initial liquid gas ratio 248 STB/MMSCF for reservoir permeabilities (a) 100 nD (b) 1000 nD.

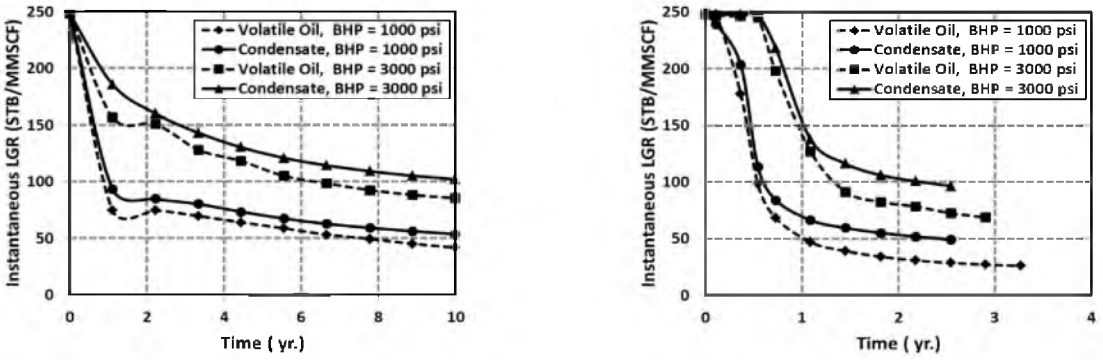

Figure 7.16. Instantaneous liquid to gas ratio from lean gas condensates and volatile oil reservoirs of initial liquid gas ratio 248 STB/MMSCF for reservoir permeabilities (a) 100 nD (b) 1000 nD.

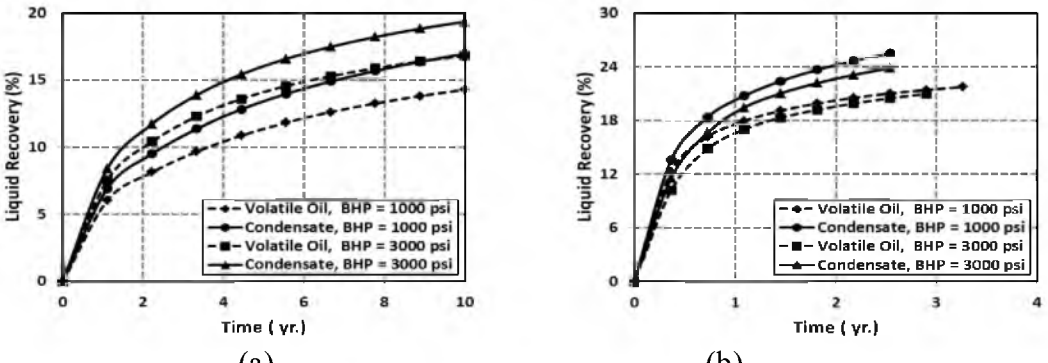

Figure 7.17. Liquid recoveries from lean gas condensates and volatile oil reservoirs of initial liquid gas ratio 248 STB/MMSCF for reservoir permeabilities (a) 100 nD (b) 1000 nD.

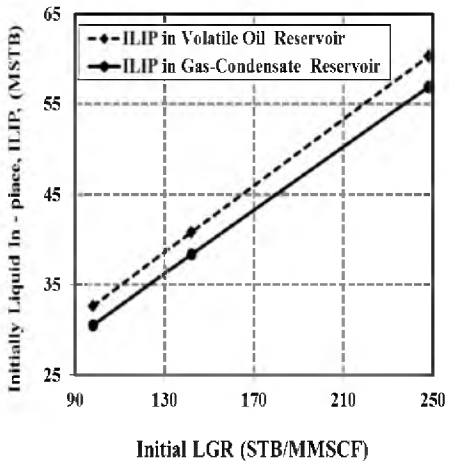

Figure 7.18. Initial gas and liquid in place for simulated reservoir volume with various fluid and reservoir conditions.

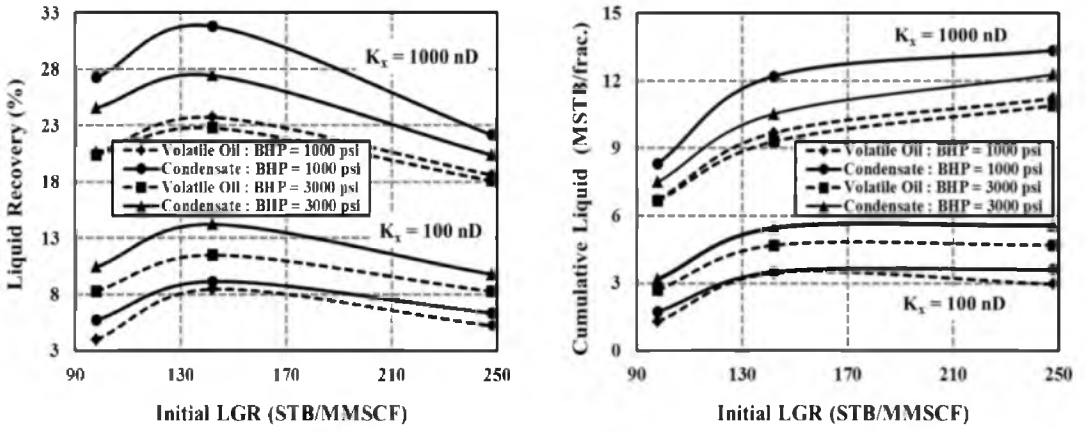

(a) (b)

Figure 7.19. Recoveries for fluid 1, fluid 2 and fluid 3 in different reservoir conditions and FBHP (a) Liquid recovery (b) Cumulative liquid production.

Table 7.1. Summary of Reservoir model parameters and operational parameters.

Reservoir Top (ft):	12800
Reservoir Dimension, X(ft), Y(ft), Z(ft)	120, 750, 200
Matrix Permeability, kx, ky, kz (nD):	100,1000
Matrix Permeability, kz (nD):	0.1 kx
Fracture Permeability (mD):	kfx = kfy = kfz = 300
Fracture Width (ft):	0.05
Fracture Orientation	Parallel to YZ plane
Initial Reservoir Pressure (psi):	6500
Initial HC Saturation:	84% (Single phase)
Reservoir Porosity:	5%
Flowing Bottom hole Pressure (psi):	1000, 3000
Simulation time	10 years

Table 7.2. Compositions of three different reservoir fluids.

Components	Compositions (mole %)		
	Fluid 1	Fluid 2	Fluid 3
C1	61.92	57.98	64.68
C2	14.08	13.00	8.27
C3	8.35	8.20	4.63
iC4	0.97	1.93	1.07
nC4	3.41	4.43	1.82
iC5	0.84	1.75	0.83
nC5	1.48	2.25	0.89
FC6	1.79	1.69	1.27
C7	1.58	1.38	2.37
C8	1.22	1.12	1.96
C9	0.94	0.84	1.62
C10+	3.11	5.12	7.82
CO2	0.18	0.18	2.58
N2	0.13	0.13	0.17
H2S	0.00	0.00	0.01
LGR (STB/MMSCF)	98	142	248
Tc (F)	230	300	362
Pc (psi)	3312	3214	4417

Table 7.3. Summary of properties of three different fluids

Fluid	LGR (STB/MMSCF)	Critical Temp. (F)	Reservoir Temp.(F)	Fluid Type
Fluid1	98	230	255/205	Lean Condensate / Volatile Oil
Fluid2	142	300	325/275	Intermediate Condensate / Volatile Oil
Fluid3	248	362	387/337	Rich Condensate / Volatile Oil

Table 7.4. Performances of various liquids at economic rate.

Kx (nD)	BHP (psi)	Fluid Type	Time (yr.) to reach 5 STB/day			LGRp/LGRi			R_{fl} (%)			R_{fg} (%)		
			Fluid 1	Fluid 2	Fluid 3	Fluid 1	Fluid 2	Fluid 3	Fluid 1	Fluid 2	Fluid 3	Fluid 1	Fluid 2	Fluid 3
1000	1000	Volatile Oil	0.83	1.09	1.30	0.32	0.27	0.17	20.6	23.7	18.6	24.9	29.7	33.7
		Condensate	1.10	1.53	1.76	0.33	0.33	0.22	27.3	31.8	22.2	34.0	41.0	43.3
	3000	Volatile Oil	1.05	1.27	1.39	1.00	1.00	0.39	20.4	22.8	18.1	20.4	22.8	21.0
		Condensate	1.13	1.42	1.62	1.00	1.00	0.44	24.6	27.4	20.4	24.6	27.4	23.6
100	1000	Volatile Oil	0.22	0.64	0.69	0.40	0.48	0.31	4.0	8.4	5.2	5.1	11.4	10.6
		Condensate	0.33	0.86	0.92	0.39	0.54	0.38	5.7	9.1	6.3	7.5	13.3	13.0
	3000	Volatile Oil	0.85	1.41	1.19	1.00	1.00	0.64	8.3	11.5	8.2	8.3	11.5	9.8
		Condensate	0.95	1.57	1.49	1.00	1.00	0.71	10.4	14.2	9.8	10.4	14.2	11.6

CHAPTER 8

CHARACTERIZATION OF PRODUCING GAS OIL RATIO

Many factors like fluid properties, reservoir properties, operational and completion parameters affect oil recovery from reservoirs. Amount of gas dissolved inside reservoir oil is a leading factor to establish production strategy. Gas is always produced with oil as dissolved gas, in addition to flow of free gas from reservoir. Gas production is controlled and kept in the desired production window by maintaining the flowing bottom hole pressure. Initial reservoir pressure (P_i) and flowing bottom hole pressure (P_{wf}) are varied to study a wide range of reservoir and production conditions. The oil rates, recovery factor and produced GOR are the key production parameters for this study. A single characteristic factor affecting the produced gas oil ratio is found to be $(1- R_{sw}/R_{sb}) (1- P_{wf}/P_b) /(1-P_{wf}/P_i)$. Produced GOR increases with time when this factor exceeds certain value, on the other hand, little or no deviations from its initial gas oil ratio are also observed for lower value of the factor. Applicability of this factor is validated by comparing simulation data with field data. Deviation of gas oil ratio from its initial value is higher for low permeability reservoirs. Higher gas and oil are recovered from reservoirs with higher initial gas oil ratio (GOR).

8.1 Backgrounds

Obtaining higher estimated ultimate recovery (EUR) of oil is the primary concern of E&P Company. Dissolved gas helps to improve the mobility of oil by making the oil lighter. Black oil (except heavy oil) contains a certain amount of dissolved gas inside which, in turn, evolves when the reservoir pressure drops below bubble point pressure in the course of production. Gas flows more easily through a porous medium than oil because of its higher mobility and starts dominating the two-phase flow by suppressing the flow of oil. On the other hand, free gas sustains the pressure in the reservoir. Produced gas oil ratio gradually increases with time as the reservoir pressure declines in the reservoir.

The increase in the GOR and the decline of the oil rate with time were first explained by Millikan (1926) who compiled field data and also discussed the drawdown effect on the produced GOR. Different possible ways to control producing gas oil ratio to optimize the ultimate recovery without compensating with rate of production were demonstrated (Marsh and Robinson 1929; Sullivan 1937) incorporating field data. The multiphase black oil flow equation (Muskat 1945) was solved numerically (Arps and Roberts 1955) for initial gas oil ratios up to 2000 SCF/STB to obtain oil recovery. The method was validated by comparing the results with actual field data. It was concluded that a definite relationship could be established between oil recovery and reservoir fluid properties such as initial gas oil ratio, API gravity and the type of reservoir rock. Compositional simulations have been used (Brinkman and Weinaug 1956) to predict the GOR and formation volume factors for a dissolved gas drive reservoir at saturated conditions. Jones et al. (1959) developed a material balance method incorporating gravity segregation.

They showed the effect of GOR on production from fractured limestone reservoirs. Their results proved that oil rates declined less at higher initial GORs. Levine and Prats (1961) concluded that the produced GOR is independent of reservoir permeability. This was done by numerically solving partial differential equations that described solution gas drive reservoirs. Another study by Prats and Levine (1963) showed that the produced GOR for a vertically fractured reservoir is higher than for an unfractured reservoir. A new method to forecast GOR dependent on oil rate and consistent with reservoir mechanisms was developed (Lawal, Uwaga et al. 2006). Laboratory experiments (Busahmin and Maini 2010) showed that the performance of a foamy heavy oil system is affected negatively with an increase in the initial GOR which seems to be counter-intuitive. Ultralow permeable reservoirs like shales behave differently from conventional reservoirs with higher reservoir permeability.

In this study, we attempted to characterize the qualitative behavior of produced GOR from ultralow permeability fractured reservoirs like shales. We also investigated the effect of dissolved gas oil ratio on production performance for different reservoir permeabilities and flowing bottom hole pressures.

8.2 Experimental Design and Preliminary Screening

Based on field data available for Eagle Ford from Railroad Commissions of Texas, different initial gas oil ratios (300, 500, 1000, 1500, 2000 and 2500 SCF/STB) are selected to represent various reservoir fluids. An ultralow permeable reservoir (10, 100, 1000 and 5000 nD) with one horizontal well and one vertical fracture located in the middle of the reservoir is simulated. The fracture height and fracture width are equal to the reservoir height and width, respectively. The reservoir is extended to 2000 ft. in the x-

direction, 750 ft. in the y-direction, and 200 ft. in the z-direction with a top depth of 12800 ft. The properties of the reservoir are summarized in Table 8.1. The matrix permeability, initial reservoir pressure, flowing bottom hole pressure and fluid properties are varied. Different categories are shown in Table 8.2 and discussed here. The fracture permeability, fracture width, fracture orientation, matrix porosity and initial hydrocarbon saturation remain constant. Minimum grid block size (Panja, Conner et al. 2013) is used to obtain converged results to get rid of any grid effects.

The simulations are designed such a way that the difference between initial reservoir pressure (P_i) and flowing bottom hole pressure (P_{wf}) are same for all runs. The location of bubble point pressure (P_b) with respect to flowing bottom hole pressure (P_{wf}) and initial reservoir pressure (P_i) is a significant factor in the production performance of oil and gas. Initially we divided the simulations into various categories to inquire the factor(s) which would characterize the qualitative behavior of production performance mainly gas oil ratio. The term f_p and GCI are described later.

8.2.1 Constant Pressure Differences

The difference between initial reservoir pressure and bubble point pressure (P_i-P_b) and the difference between bubble point pressure and flowing bottom hole pressure (P_b-P_{wf}) are kept constant for serial numbers 1 to 3 as shown in Table 8.2. This is known as constant pressure difference (Δp) case.

8.2.2 Constant End Pressures

For serial numbers 4 to 6 in Table 8.2, initial reservoir pressure (P_i) and flowing bottom hole pressure (P_{wf}) are constant. This can be called constant boundary pressures

(or constant P) cases. In constant pressure cases (serial no. 4 to 6 in Table 2), the difference between initial reservoir pressure and bubble point pressure (P_i-P_b) and the difference between bubble point pressure and flowing bottom hole pressure (P_b-P_{wf}) vary depending on the location of bubble point pressures.

8.2.3 Special Cases

Serial number 7 to 18 are special cases to study the effect of characteristic factor. Value of factor, GCI which is described later varies from near zero to one as shown in Table 8.2.

8.3 Factor to Predict Qualitative Behavior of Produced Gas Oil Ratio

After the preliminary screening of the results, it is observed that constant pressures (initial, bubble point or bottom hole pressures), constant pressure differences and constant ratio of pressure differences are not the valid criteria for characterizing the performance (oil rate, GOR and oil recovery) but combining them in a particular manner can exhibit a conclusive relationship which can predict qualitative behavior of production performance. The ratio of pressure differences (f_p) is first examined as shown by Equation 8.1.

$$f_p = \frac{(P_b - P_{wf})}{(P_i - P_{wf})} \tag{8.1}$$

The value of f_p varies greatly depending on the relation locations of P_i, P_b and P_{wf}. The locations of initial reservoir pressure, bubble point pressure and flowing bottom hole pressure lead to three different possibilities for the ratio of pressure difference as

described in Figures 8.1 a to c.

The physical conditions pertaining in each case are summarized below:

(a) case 1, operation above bubble point pressure, initially undersaturated reservoir

(b) case 2, operation below bubble point pressure, initially undersaturated reservoir

(c) case 3, operation below bubble point pressure, initially saturated reservoir.

Operating well near bubble point pressure suppresses gas production but it also yields very low oil rate which is not economic. The most practical location of the initial reservoir pressure, bubble point pressure and flowing bottom hole pressure for economic production is case 2. Wells are normally operated well below the bubble point pressure to obtain the economic production rate.

The oil rate and oil recovery can be explained using ratio of pressure difference factor (f_p) (shown in Equation 8.1) but without incorporation of gas oil ratio into the factor is ineffective to correctly predict the behavior of the produced gas oil ratio. The depletion of long transient state reservoir can be represented by the distance between the bubble point pressure and flowing bottom hole pressure (P_{wf}) since the average reservoir pressure for this kind of reservoir is not representative. The difference in the gas oil ratios at P_{wf} and GOR at P_b is one characteristic parameter to predict the behavior of produced gas oil ratio from ultralow permeable fractured reservoir. All these factors are accommodated with Equation 8.1 into a single characteristic factor, gas oil ratio characteristic index (GCI) as given by Equation 8.2.

$$GCI = \left(1 - \frac{R_{sw}}{R_{sb}}\right)\frac{\left(1 - \frac{P_{wf}}{P_b}\right)}{\left(1 - \frac{P_{wf}}{P_i}\right)} \tag{8.2}$$

The factor, *GCI, can* be used only when flowing bottom hole pressure is less than the bubble point pressure. When flowing bottom hole pressure is above the bubble point pressure, the well produces initial gas oil ratio because the reservoir is undersaturated. The value of GCI is presented in Table 8.2 for the different cases in this study. The effect of this factor is clearly observed in the qualitative behavior of produced gas oil ratio which is discussed later.

It is desired to operate wells to control the gas oil ratio. Hence, prescribing flowing bottom hole pressure is one quest of this study. GCI can also be utilized to propose the flowing bottom hole pressure to operate wells in a manner to optimize the gas oil ratio. The flowing bottom hole pressure can be controlled to maintain desired produced gas oil ratio by setting the value of GCI. Assuming that the dissolved gas oil ratio varies linearly with pressure for saturated reservoir, the following formula for the flowing bottom hole pressure is derived as shown in Equation 8.3.

$$\frac{P_{wf}}{P_b} = \left[1 - 0.5\left(\frac{P_b}{P_i}\right)GCI\right] - \sqrt{\left[1 - 0.5\left(\frac{P_b}{P_i}\right)GCI\right]^2 - (1 - GCI)} \qquad (8.3)$$

Knowing the initial reservoir pressure and bubble point pressure of reservoir fluid, the value of flowing bottom hole pressure is prescribed using Equation 8.3 to maintain desired produced GOR. The variation of P_{wf}/P_b with the factor, f is shown in Figure 8.2.

The relationship between P_{wf}/P_b and GCI are established for various ratios of P_b/P_i. It is clear that P_{wf}/P_b is inversely prportional to GCI. Higher value of GCI predicts lower value of P_{wf}/P_b, i.e., lower value of flowing bottom hole pressure compared to bubble point pressure which leads to production of more gas. The curve approaches linear when

P_b/P_i moves towards unity. Little or no deviation of produced GOR compared to initial GOR is observed if well is operated at the pressure higher than 0.5 P_b to 0.7P_b depending on the P_b/P_i fraction. For example, if any well in a reservoir with initial pressure of 5500 psi and bubble point pressure of 3500 psi must be operated at pressure higher than about 0.65 P_b, i.e., 2275 psi (as predicted by the equation 8.3 and Figure 8.2), to keep the produced GOR near to initial GOR, but rate of oil production may not be economic for this high flowing bottom hole pressure (2275 psi).

If factor value of 0.6 is a chosen , the flowing bottom hole pressuse is near 0.3 P_b, i.e., 1050 psi, which will enhance the rate of oil production in expense of higher produced GOR. Optimization of oil rate depends on the operators considering many factors like ability to handle gas, long term production strategy etc.

8.3.1 Validation of the Factor, GCI

Comparisons of field data from Eagle Ford with simulation results are shown in Figure 8.3. The production data are collected from Railroad Commissions of Texas but the reservoir and fluid parameters like initial reservoir pressure, bubble point pressure, initial gas oil ratio and operating conditions are not available. These parameters are generated by superimposing simulated gas rate and oil rate with field data as shown in Figure 8.3.

As the oil rates are not very much affected by the initial gas oil ratio for the reservoirs of 50 to 200 nD permeability, superimposing gas rates with the field data is also necessary to generate the reservoir conditions and operational parameters. The parameters as shown in Table 8.3 are reproduced from the superimpositions.

Two different flowing bottom hole pressures are investigated for each field case. It

should be noted that the rates are for noninterfering single fracture and net to gross ratio (NTG) is considered as 0.4 for Eagle Ford. If there are five clusters per stage in a 16-stage well, with about 80 possible fractures, the rate for 50 nd to 450 nD reservoirs is expected to be between 2.5 mstb/month and about 5 mstb/month in the first year. This depends on the initial dissolved GOR, drawdown, bubble point pressure and a number of other factors. Analysis of the Eagle Ford oil rate indicates that the reservoirs fall within the 50 to 450 nD permeability range. The GOR values for Eagle Ford are much more variable from 300 to 1650 SCF/STB.

GCI is calculated for each case as shown in Table 8.3. Ratio of cumulative GOR and initial ratio produced from JP Head Bower C Unit and Meyer Unit are less compared to the same from Hawn Holt and Davenport unit as shown in Figure 8.4. These performances are also correctly predicted by GCI. The values of GCI for JP Head Bower C Unit and Meyer Unit (0.34 to 0.55) are less than the values of GCI for Hawn Holt and Davenport unit (0.58 to 0.80). Higher GCI indicates that increase in gas oil ratio with respect to initial gas oil ratio is higher.

Although the initial gas oil ratio of Hawn Holt is 300 SCF/STB only, the rise of gas oil ratio (ratio of GOR and initial GOR) with time is higher than the other field. This performance also confirms that initial GOR is not the only factor to decide behavior of the produced GOR. GCI can be used reliably to analyze qualitative behavior of produced GOR.

8.4 Result and Discussion

The matrix permeabilities chosen for this study are 10 nD, 100 nD, 1000 nD and 5000 nD. A total of 72 simulations are run to investigate the effect of dissolved gas oil ratio

curve and operation parameters on production performance in terms of oil rate, oil recovery and produced gas oil ratio. Commercial simulator IMEX, a Computer Modeling Group Black Oil simulator, is used to conduct the study.

8.4.1 Effect of Initial Gas Oil Ratio (Rsi)

The effect of initial gas oil ratio on produced GOR, oil rate and oil recovery are discussed for three different initial gas oil ratios (500, 1000 and 2000 SCF/STB) while ratio of pressure difference is kept constant at 0.0625 although GCI varies. Slope of dissolved gas oil ratio curve of 0.4 and four reservoir permeabilities (10,100, 1000 and 5000 nD) are considered. The effect of initial gas oil ratio on cumulative gas oil ratio is shown in Figures 8.5 a and b for the ratio of pressure difference of 0.0625.

It is intuitive that higher GOR is produced from reservoirs with higher initial gas oil ratio. The deviation of GOR from initial GOR is not noticeable with different matrix permeabilities for very low value of GCI (0.007 to 0.07). The differences in the oil rate for different initial GORs are not significant for lower matrix permeability (10 and 100 nD). Higher oil rate is achieved with higher initial GOR and with higher reservoir permeability. Higher initial gas dissolved in oil phase always supports the production by sustaining the reservoir pressure for long time. The mobility of oil is also improved with dissolved gas by making oil phase lighter. Simultaneously, more gas is produced on the surface as dissolved and free gas. Higher initial GOR finally enhances the oil rate in cost of higher gas production. The oil recovery is also improved from higher initial GOR as evident in Figures 8.6a and b for the ratio of pressure difference of 0.0625.

The initial GOR effect on oil recovery is very much noticeable for higher permeability reservoirs (5000 and 1000 nD). The highest oil recovery is obtained from a

reservoir with initial GOR of 2000 SCF/STB and reservoir permeability of 5000nD. As described earlier, the higher initial dissolved gas provides higher energy in the reservoir, thus helping to produce more oil. The lowest amount of oil is recovered from the reservoir with initial GOR of 500 SCF/STB. The effect of initial gas oil ratio on oil recovery is not very prominent for 10 nD reservoir.

8.4.2 Effect of GCI

The effect on GCI is already established in earlier sections with validation with field data. The factor GCI is of particular interest for quantitative analysis of produced gas oil ratio. Behavior of produced GOR is dependent not only on the operating conditions but also on the fluid properties and initial reservoir conditions. The qualitative nature of produced GOR cannot be explained solely by the ratio of pressure difference, f_p. The factor, f_p is useful to explain the oil rate and oil recovery only for different initial GOR. Produced GOR is normalized with initial GOR to compare among the fluids having different initial GOR (500, 1000 and 2000 SCF/STB) in the same scale. As shown in the Figure 8.2, the deviations of produced GOR depend on value of GCI. The simulated results are analyzed here for various GCI.

8.4.3 Little or No Deviation of GOR

Produced GORs have neutral deviation when produced GORs vary within ±2% of initial GOR. The neutral deviations are depicted in Figures 8.7a and b. The neutral or little deviations are found when the factor (GCI) is not greater than 0.07. A special case for neutral deviation can be identified when the flowing bottom hole pressure is above the bubble point pressure, i.e., reservoir is in undersaturated conditions. Neutral deviation

occurs when the flowing bottom hole pressure is close to bubble point pressure. A sufficient amount of gas does not evolve out of oil phase and the oil phase contains initial amount of dissolved gas only.

8.4.4 Positive Deviation of GOR

Positive deviation of GOR is commonly observed in the field. Positive deviations of produced GOR are shown in Figures 8.8a and b. Positive deviation is noticed when a large portion of reservoir is below bubble point pressure and flowing bottom hole pressure is sufficiently below bubble point pressure. In these reservoir conditions, gas and oil in both phases flow simultaneously. The values of GCI are greater than 0.2 for positive deviation. Effect of GCI on cumulative gas oil ratio in terms of deviations is summarized in Table 8.4.

8.5 Key Findings

The complex behaviors of produced GOR, oil rate and oil recovery from ultralow permeable fractured reservoir are illustrated with various PVT varying important parameters like initial dissolved GOR slope of dissolved GOR, operating conditions and reservoir conditions. The following conclusions are made:

Effect of R_{si}

- Higher initial dissolved gas oil ratio yields higher produced GORs.
- Effect on oil rate is not very significant.
- Higher oil recovery is obtained from higher initial GOR and higher reservoir permeability.

Effect of Gas Oil Ratio Characteristic Index (GCI)

- No or little deviations of produced GOR are observed when f is less than 0.07.
- Positive deviations of produced GOR are observed when f is greater than 0.2.
- More deviations (positive and negative) are noticed from the reservoir with the lower permeability reservoir.

GCI is effective measure of the qualitative behavior of produced gas oil ratio accommodating reservoir conditions, fluid properties and operating condition. A well can be operated to produce desired GOR by using the value of GCI prescribed for a particular GOR window. The value of GCI is very specific to the other parameters like relative permeability, critical gas saturation, porosity of reservoir etc. but its characteristic application on produced GOR should be the same.

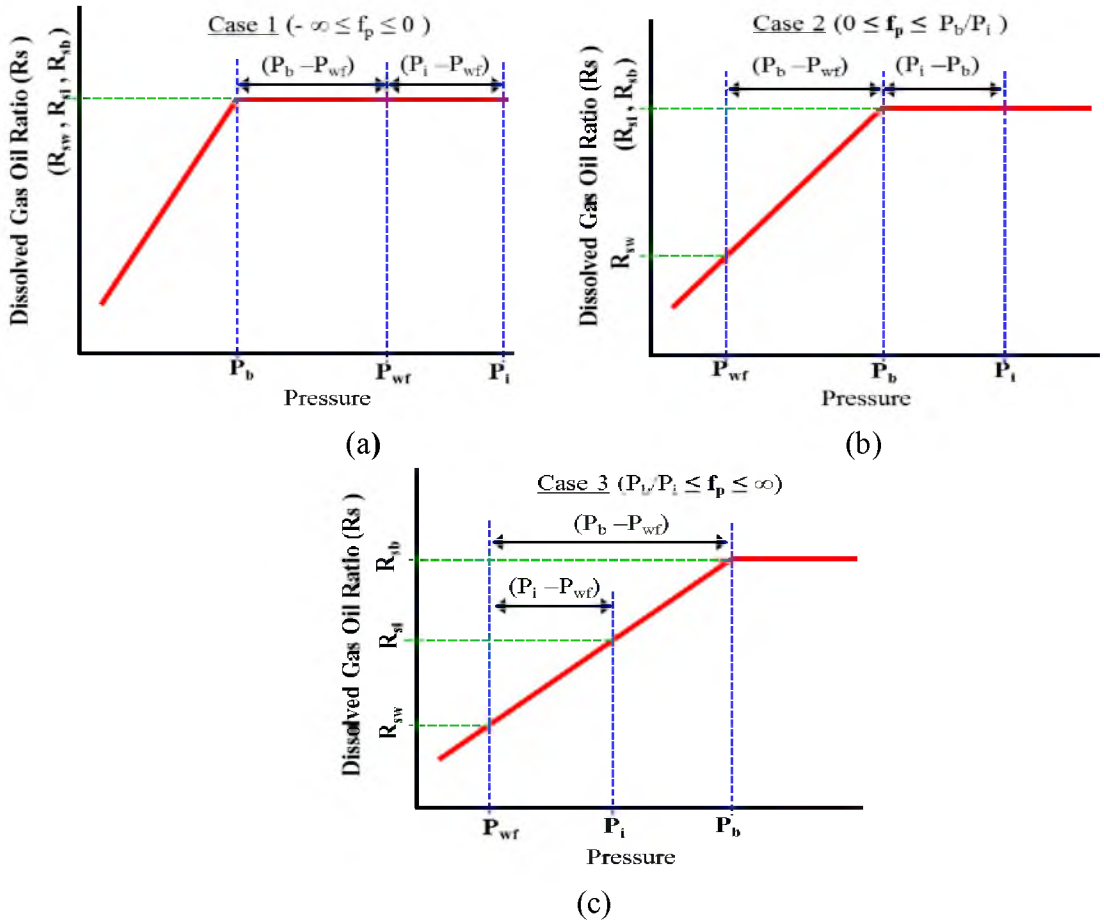

Figure 8.1: The relative locations of initial reservoir pressure, bubble point pressure and flowing bottom hole pressure on Rs-PVT diagram (a) case 1(b) case 2 and (c) case 3.

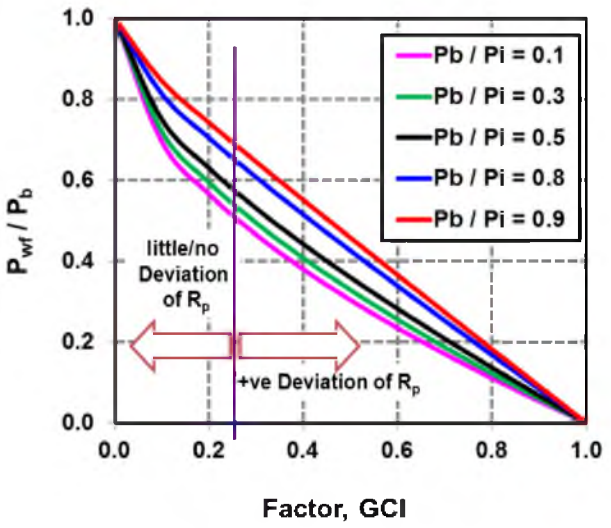

Figure 8.2: Variability of Pwf/Pb with the factor GCI.

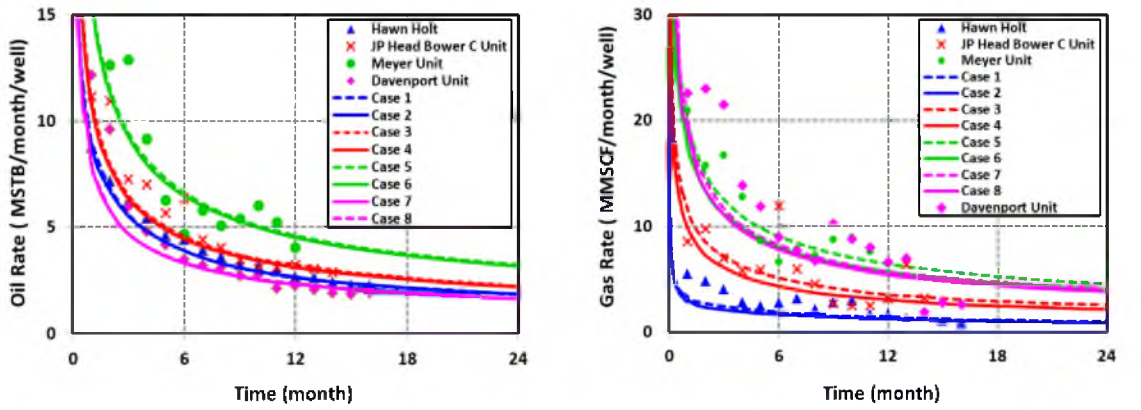

(a) (b)

Figure 8.3: Superimposition of field data with simulation results for (a) Oil rate (b) Gas rate**.**

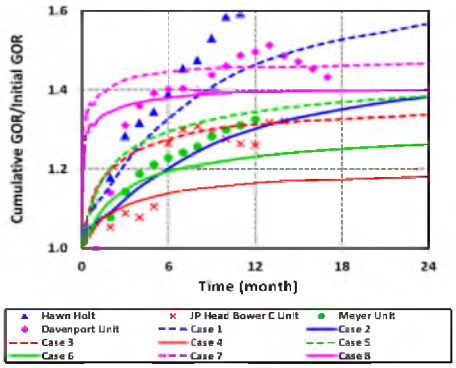

Figure 8.4: Comparison of GOR behavior between field data and simulated results.

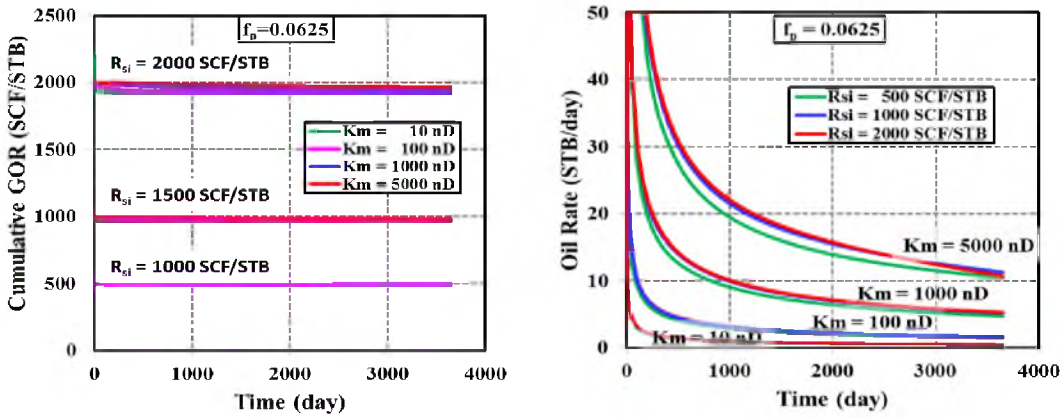

(a) (b)

Figure 8.5: Effect of initial gas oil ratio on cumulative gas oil ratio with constat fp of 0.0625 and two different slopes of dissolved gas oil ratio of (a) 0.4 (b) 0.8.

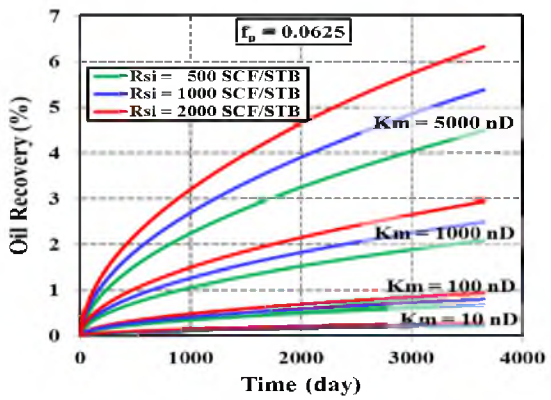

Figure 8.6: Effect of initial gas oil ratio on oil recovery with constant fp of 0.0625.

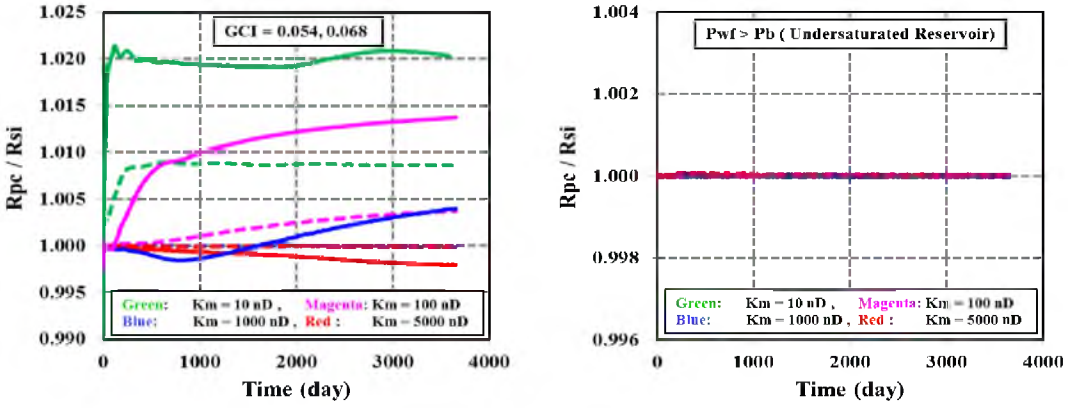

(a) (b)

Figure 8.7: Cumulative gas oil ratio for (a) GCI of 0.054, 0.068 (b) Undersaturated reservoir.

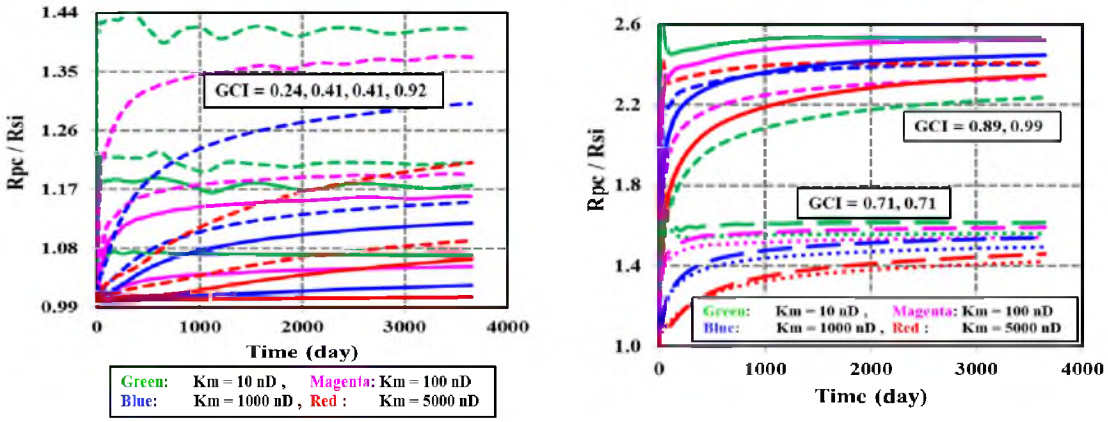

(a) (b)

Figure 8.8: Positive deviation of cumulative gas oil ratio for GCI of (a) 0.24, 0.41, 0.41, 0.92 and (b) 0.89, 0.99.

Table 8.1. Reservoir and completion parameters used in all of the simulations.

Reservoir Top (ft):	12800
Matrix Permeability, k_m (nD):	10,100,1000,5000,
Reservoir Dimensions X(ft), Y(ft), Z(ft):	1000, 750, 200
Fracture Permeability (mD):	$k_{fx} = k_{fy} = 150$; $k_{fz} = 300$
Fracture Width (ft):	0.05
Fracture Height (ft)	Reservoir Height
Fracture Orientation	Parallel to YZ plane
Initial Oil Saturation (%):	84
Reservoir Porosity (%):	5

Table 8.2. Design of experiments for characterizing gas oil ratio

Sr. No.	R_{sb} (SCF/STB)	P_i (psi)	P_b (psi)	P_{wf} (psi)	$(P_i - P_b)$ (psi)	$(P_b - P_{wf})$ (psi)	$(P_i - P_{wf})$ (psi)	f_p	GCI
1	500	5765	1265	965	4500	300	4800	0.0625	0.0683
2	1000	7015	2515	2215	4500	300	4800	0.0625	0.0209
3	2000	9515	5015	4715	4500	300	4800	0.0625	0.0071
4	500	5300	1265	500	4035	765	4800	0.1594	0.4085
5	1000	5300	2515	500	2785	2015	4800	0.4198	0.7129
6	2000	5300	5015	500	285	4515	4800	0.9406	0.8976
7	500	6017	1265	1217	4752	48	4800	0.0100	0.0018
8	2000	9767	5015	4967	4752	48	4800	0.0100	0.0002
9	2000	9863	5015	5063	4848	-	4800	-	-
10	500	6113	1265	1313	4848	-	4800	-	-
11	1000	6650	2515	1850	4135	665	4800	0.1385	0.0974
12	790	6000	1990	1200	4010	790	4800	0.1646	0.1984
13	2500	8500	6265	3700	2235	2565	4800	0.5344	0.2975
14	500	5200	1265	400	3935	865	4800	0.1802	0.5124
15	1000	5500	2515	700	2985	1815	4800	0.3781	0.6002
16	1000	5150	2515	350	2635	2165	4800	0.4510	0.7997
17	500	4865	1265	65	3600	1200	4800	0.2500	0.9227
18	2000	4871	5015	71	-144	4944	4800	1.0300	0.9891

Table 8.3. Plausible parameters for various leases in Eagle Ford.

Lease Unit	Simulation Case	Pi (psi)	Rsi (SCF/STB)	Pb (psi)	Pwf (psi)	Permeability (nD)	GCI
Hawn Holt	1	3000	300	765	100	450	0.80
	2	3000	300	765	200	450	0.60
JP Head Bower C	3	5300	800	2015	650	200	0.53
	4	5300	800	2015	950	200	0.34
Meyer	5	5300	950	2390	750	400	0.55
	6	5300	950	2390	1000	400	0.42
Davenport	7	8000	1650	4140	1000	50	0.66
	8	8000	1650	4140	1250	50	0.58

Table 8.4. Effect of GCI on cumulative GOR

Range of GCI	Comments Cumulative GOR
Below 0.07	No or little Deviation
Above 0.2	Positive Deviation

CHAPTER 9

CONCLUSION

9.1 Original Contributions

The following original contributions are made on achievement of all research objectives.

1. **Development of a new rapid forecasting tool for transient state flow in ultralow permeablity fractured reservoir**

   It has the capability to replace the simulation for fractured reservoir after converting it to an iterative technique. Quick sensitivity study of parameters like matrix permeability, relative permeability, flowing bottom hole pressure, initial pressure, matrix porosity, fluid properties can be conducted using the proposed model for unconventional reservoirs without running any simulations.

2. **Quantitative analysis of the effect of grid refinement on important simulator outcomes in liquid rich unconventional reservoirs.**

   The grid size necessary to achieve converging results are quantified using a set of empirical relationships which are functions of dimensionless fracture conductivity. Correlations are developed based on a generic reservoir model with one horizontal well and one vertical planar fracture in the middle of the reservoir for a given geometry , set of fluids (wet gas, gas-condensate and black oil) , fluid-rock properties, and reservoir matrix permeability.

3. **Performance of sensitivity studies of important geological properties, fluid properties, rock fluid properties, completion parameters and operating parameters on production of liquids from shales.**

   Matrix permeability, rock compressibility, fluid properties and fracture spacing are identified as the key parameters for production of oil from ultralow permeable reservoir.

4. **Development of surrogate reservoir models for a quick assessment of production performance from ultralow permeability black oil and condensate reservoirs.**

   A set of quadratic multivariable response surfaces is generated for recovery factors and gas oil ratio or condensate to gas ratio for different times and for economic production condition by using the Box-Behnken experimental design and multi regression optimization method. The models are an excellent proxy for the computationally intensive compositional simulations or black oil simulations and can also be utilized for sensitivity and uncertainty studies.

5. **Quantification of risk of production performance by preparing the probability density functions (PDF) of production outcomes and the hierarchy of the most significant input factors.**

   Uncertainty in production is assessed by Monte Carlo simulations in the validated response surfaces to generate probability density functions. Reservoir permeability, fracture spacing and initial pressure are identified as the most significant parameters for liquids production from shales. Risk in the investment to develop fields is evaluated by a probabilistic economic model.

6. **Analyses of the production performances of near critical fluids-condensates and**

volatile oils.

Sensitivity of temperature and initial fluid compositions on production of near the critical fluids like volatile oil and gas-condensate is studied. Optimum initial liquid to gas ratio is obtained to produce highest liquid recovery. More liquid is produced from gas-condensate reservoir with less decline rate. Choking of well in controlled manner is preferable to extract highest amount of liquid from reservoirs.

7. **Development of a single characteristic factor to analyze qualitative behavior of produced GOR.**

An effective measure of the qualitative behavior of produced gas oil ratio is modeled by developing single characteristic factor accommodating reservoir conditions, fluid properties and operating condition. Well operating pressure to control gas production is dictated by the relationship relating characteristic factor.

9.2 Recommendations for Future Work

Multiple wells and fractures can be incorporated into models because well and fracture interferences are of prime importance for low well spacing used in unconventional plays. The study can be extended to more robust full field models considering geological faults and natural fracture interactions with hydraulic fractures. Inclusion of a geostatistical model for reservoir parameters, geomechanical properties of fractures and stress dependency may improve the understanding of production from shales. Calculations of thermodynamic equilibrium using classical EOS models like Peng Robinson may not be applicable in nanostructure medium. There is a great concern for storagability in ultralow permeability and porosity reservoirs (like shales) which leads to study the multiphysics like diffusion of hydrocarbon in nanopore. Application of Darcy's

law which is widely used for flow in porous medium is questionable for flow in nanopore. A new kind of flow equations should be developed incorporating diffusion and adsorption.

APPENDIX A

CONVENTIONAL VERSUS UNCONVENTIONAL RESERVOIRS

An unconventional reservoir behaves differently than conventional reservoir. The long transient state in an unconventional fractured reservoir is demonstrated through the pressure profile with distance in Figure A.1. It is evident that low permeability reservoir has transient flow condition with moving boundary even after 5 years of production for a 2000 feet long reservoir with matrix permeability of 1000 nD (0.001 mD). However, initial pressure front of a reservoir with 1 mD matrix permeability reaches the reservoir boundary very quickly in 3 days. A reservoir having 100 nD permeability does not see the outer boundary in 10 years. Approximate time for initial pressure front to reach 300 feet for different permeability reservoirs is also shown in Figure A.1.

Low permeability (100 nD) reservoir takes more than 5 years to reach 300 feet, whereas 1 mD reservoir reaches the distance in 9 hours only.

The average pressure and produced condensate/gas ratio (CGR) are two parameters that are used to characterize production performance from conventional gas condensate reservoir. The behavior of these two parameters is totally different for unconventional reservoirs as shown in Figures A.1 b and A.2. The average reservoir pressure declines to the bottom hole pressure in 3 years for 1 mD matrix permeability reservoir whereas it does not decline significantly for 1000 nD matrix permeability reservoir even after 10

years. On the other hand, the produced gas condensate ratio (GCR) starts increasing sharply after a short while for low permeability (0.001 mD) reservoirs. A reservoir produces higher GCR than initial volatilized condensate gas ratio when the average pressure is above the dew point pressure.

Trends of the produced GCR can be explained by the fact that when flowing bottom hole pressure is below dew point pressure, saturated regions (R_1 and R_2) are formed near fracture. In the saturated regions, condensates drop out from gas phase and form a liquid phase near the fracture. After dropping out some amount of condensates from the gas phase, gas holds more gas than condensate than its initial volatilized condensate content and more gas to condensate is produced at the surface. The saturated region near fracture is very small compared to the entire reservoir and an unsaturated region is also formed next to a saturated region, but a major portion of the reservoir stays at its initial conditions, and thus the average reservoir pressure calculated from volume balance yields higher value.

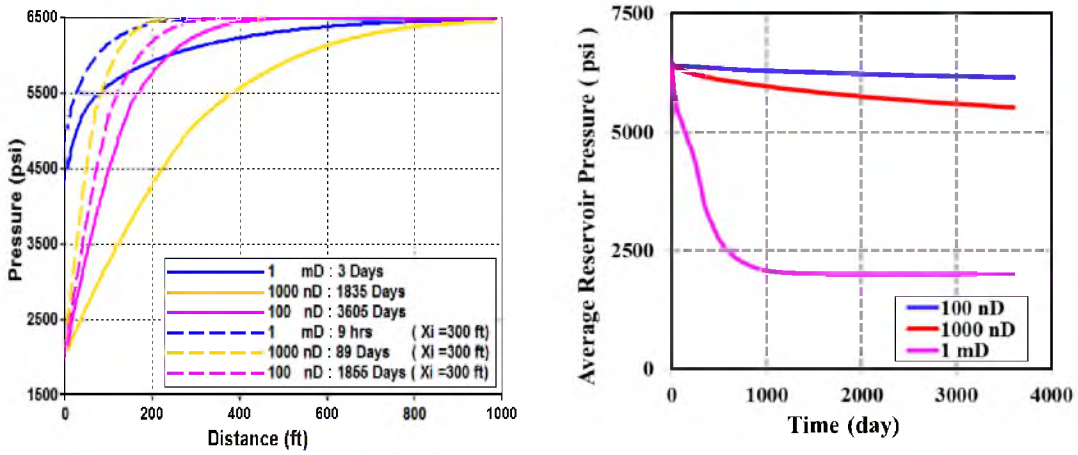

(a) (b)

Figure A.1: Pressure properties near fracture region for different permeabilities (a) Pressure profiles (b) Average reservoir pressure.

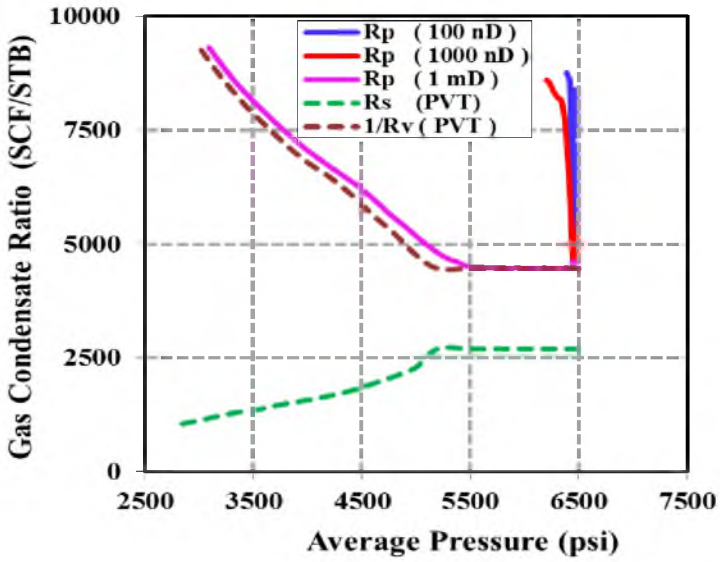

Figure A.2: Comparison of produced GCR for different permeability reservoirs.

APPENDIX B

PSEUDOPRESSURE CALCULATION

B.1 Region 1

The upper limit of the integration, p1, is not known in the peudopressure calculation in the region 1. Determining the flowing condensate to gas ratio (R_{vf}) at the outer edge of the region 1 where reservoir pressure is P_1 is the key factor. Fevang and Whitson (1996) considered constant flowing condensate to gas ratio (R_{vf}) in the region1 and this R_{vf} is equal to the flowing condensate to gas ratio (R_v) at the pressure P_1. Few researchers (1996) assumed that the same R_{vf} is produced in the well stream and therefore the produced gas-condensate ratio (R_p) is inversely equal to the flowing condensate to gas ratio at the pressure p_1. Produced gas condensate ratio (R_p) can be obtained from field production data(Fevang and Whitson 1996) or can be calculated from modified Muskat-Taylor material balance method (Guehria 2000). R_{vf} was also calculated by material balance (Mott 2002; Xiao and Al-Muraikhi 2004; Bonyadi, Rahimpour et al. 2012) in the region 1. The p_1 is calculated finally from the following relationship:

$$R_v(P_1)\text{from PVT table} = \frac{1}{R_p \text{ or } R_{vf}\text{from MB}} \qquad (B.1)$$

In the pseudopressure calculation in the region 1, another main concern is to calculate the relative permeability of gas (k_{rg}) and condensate (k_{ro}). The relative permeabilities krg

and kro are not directly function of pressure. It can easily be shown that for two-phase flow, ratio of relative permeability (Fetkovich, Guerrero et al. 1986) can be expressed as shown in Equation B.2.

$$\frac{K_{rg}}{K_{ro}}(P) = \left(\frac{R_p - R_s}{1 - R_v R_p}\right)\frac{\mu_g B_{gd}}{\mu_o B_o} \qquad (B.2)$$

If produced gas condensate ratio (R_p) is known, the right hand side of Equation B.2 can be calculated using PVT data. The relative permeability curves and their ratio can be plotted readily from PVT data. Once ratio is known, individual value of relative permeability can be obtained from mapping the value in relative permeability curves as shown in Figure B.1. The procedure is shown through the green solid line. The other parameters in the pseudopressure of region 1 are accessed from PVT data as the functions of pressure.

B.2 Region 2

In the region 2, only gas relative permeability is an unknown parameter. The lower limit of integration, P_1 is already calculated in the previous section and upper limit is dew point pressure which is known from PVT data. Other parameters except gas relative permeability as the functions of pressure are obtained from PVT. To calculate the K_{rg}, condensate saturation (S_c) must be known. Condensate saturation with pressure can be obtained from Constant Volume Depletion (CVD) data (Fevang and Whitson 1996).

$$S_c(p) = V_{roCVD}(1 - S_w) \qquad (B.3)$$

where, $\quad V_{roCVD} = \frac{V_o(p)}{V_d}$

If V_{roCVD} data are not available, the following method is followed (Fevang and Whitson 1996):

$$(V_{roCVD})_k = \frac{N_{k-1} - G_{k-1}\,(R_v)_k}{1 - (R_s R_v)_k}(B_o)_k \qquad (B.4)$$

$$N_{k-1} = \left(\frac{V_{roCVD}}{B_o} + \frac{1 - V_{roCVD}}{B_{gd}} R_v\right)_{k-1} \qquad (B.5)$$

$$G_{k-1} = \left(\frac{V_{roCVD}}{B_o} R_s + \frac{1 - V_{roCVD}}{B_{gd}}\right)_{k-1} \qquad (B.6)$$

The calculation starts from $(V_{roCVD})_0 = 0$ at $p = p_{dew}$

where k represents the current calculation stage and k-1 represents previous stage.

Once condensate saturation is known at particular pressure, gas relative permeability (k_{rg}) is taken from Figure B.1.

B.3 Region 3

Region 3 contains connate water and gas. Therefore gas saturation as well as relative permeability is constant. Gas relative permeability is calculated from Gas-Water relative permeability curves at the connate water saturation**.** Other parameters are obtained directly from PVT data as the function of pressure.

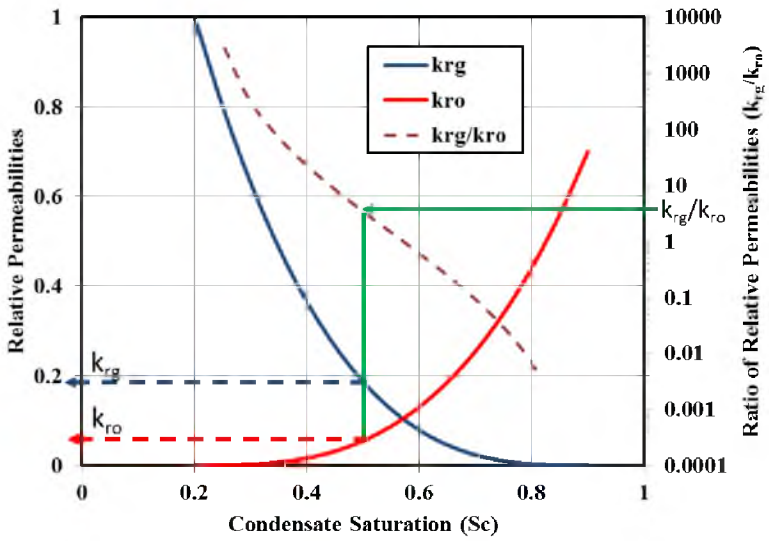

Figure B.1: Relative permeabilities of gas and condensate and ratio of relative permeabilities.

APPENDIX C

DEPLETION STAGES

Depending on pressure depletion inside the reservoir, one or more regions may coexist. Limit of integration will change depending on the depletion stage at the time. The different depletion stages for illustration are shown in Figure C.1. The reservoir may have six different stages with time. In Figure C.1, various stages are designated as S_1, S_2, S_3, S_{4E}, S_{4L}, S_5 and S_6. There are two conditions of stage 4; one is early stage (4E) and another is later depletion stage (4L). Later depletion stage of 4E appears after stage 5.

Dew point pressure (P_{dew}) of the reservoir is considered constant to its initial dew point pressure. The outer boundary pressure of region 1 (P_1) is constant for a long time as long as the gas phase holds sufficient volatilized condensate. The pressure P_1 stays constant when the reservoir is undersaturated and produces GOR equal to the initial GOR ($1/R_{vi}$). The well can be operated as constant flowing bottom hole pressure (P_{wf}) or constant flow rate. In the case of constant flow rate operation, the flowing bottom hole pressure (P_{wf}) changes with time. The bottom hole pressure (P_{wf}) decreases slowly to keep constant flow rate. The reservoir boundary pressure (P_e) also declines with time as reservoir fluid is extracted from reservoir. Reservoir pressure at any point at any time is bounded by the flowing bottom hole pressure (P_{wf}) and the reservoir boundary pressure (P_e). This is shown by the hashed section in the Figure C.1. Coexistence of different regions in each stage is explained in Figure C.2. If the initial flowing bottom hole

pressure is above the dew point pressure, reservoir only contains gas (region 3), this depletion state is designated as stage 1. In the second depletion stage, flowing bottom hole pressure (P_{wf}) drops below dew point pressure (P_{dew}) but reservoir outer boundary pressure (P_e) is above dew point pressure. Region 2 appears near the fracture or well with region 3 in the outer portion of the reservoir. All three kinds of regions (region 1, 2 and 3) exist in the depletion state 3. Pressure near fracture drops enough to generate sufficient mobile condensate. When both flowing bottom hole pressure (P_{wf}) and reservoir outer boundary pressure (P_e) are below dew point pressure, the entire reservoir contains gas and condensate and region 3 disappears. This depletion state is called stage 4. Condensate saturation is above the critical condensate saturation throughout the reservoir (region 1) in the depletion stage 5. In the depletion stage 6, condensate saturation is below the critical condensate saturation in the reservoir (region 2). No condensates flow from the reservoir and the gas only flows with very lean volatilized condensate. The various regions in the different depletion stages are summarized in Table C.1. It is a primary concern to determine the depletion stage at any time to calculate the pseudopressure. The limits of the integration change with the depletion stage. Limits of integration for various stages in calculations of pseudopressure are summarized in Table C.2.

In this study, the external boundary pressure is always considered as initial reservoir pressure. For constant bottom hole pressure operation, the lower limit (P_{wf}) of integration is also constant.

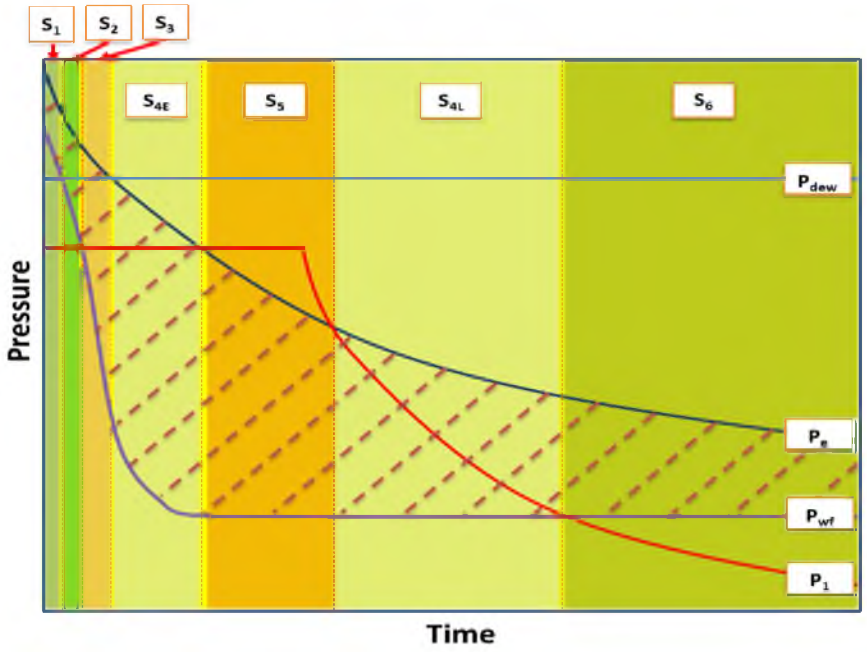

Figure C.1: Pressure depletion and different depletion stages with time.

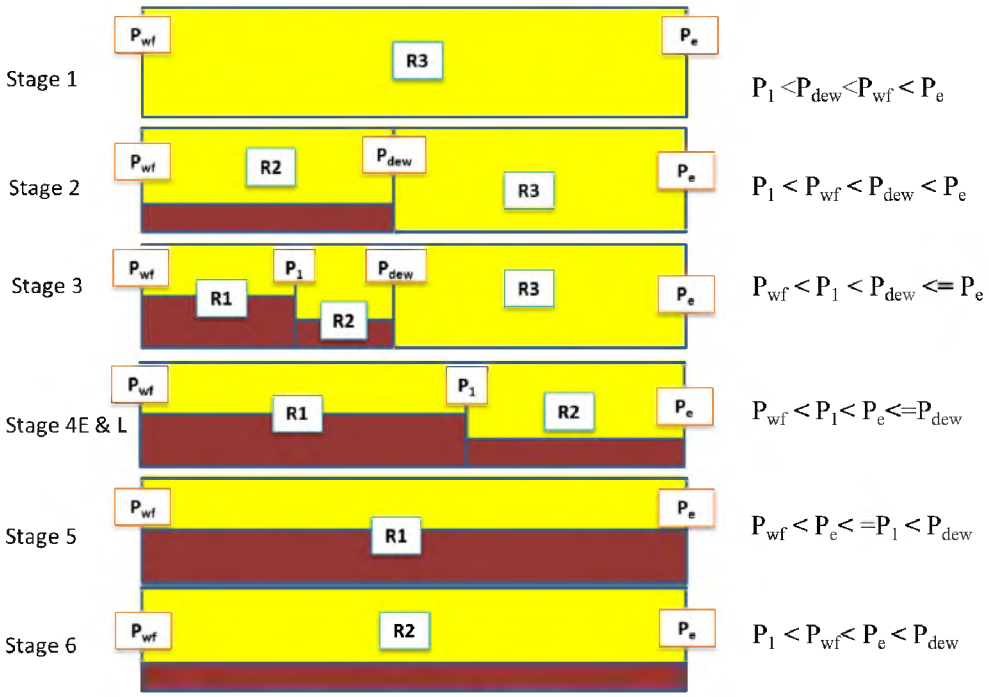

Figure C.2: Appearance and disappearance of different depletion stages.

Table C.1. Physical conditions of different stages of depletion.

Stage	R1	R2	R3
1	-	-	√
2	-	√	√
3	√	√	√
4E,L	√	√	-
5	√	-	-
6	-	√	-

Table C.2. Limits of integration for pseudopressure calculations.

Stage	R1		R2		R3	
	Lower	Upper	Lower	Upper	Lower	Upper
1	-	-	-	-	P_{wf}	P_e
2	-	-	P_{wf}	P_{dew}	P_{dew}	P_e
3	P_{wf}	P_1	P_1	P_{dew}	P_{Dew}	P_e
4E	P_{wf}	P_1	P_1	P_e	-	-
5	P_{wf}	P_e	-	-	-	-
4L	P_{wf}	P_1	P_1	P_e	-	-
6	-	-	P_{wf}	P_e	-	-

APPENDIX D

GRID SYSTEM

Ten different types of grid systems are used in the study. Snapshots of each grid system are displayed in Figure D.1 through D.3 with necessary magnifications. The number of grid cells is progressively increased in the x-direction by refining the near fracture area. The grids are refined linearly. Grid system 1 consists of 4 grids on each side of the fracture. Grid system 10 has the highest resolution with 95 cells on each side of the fracture.

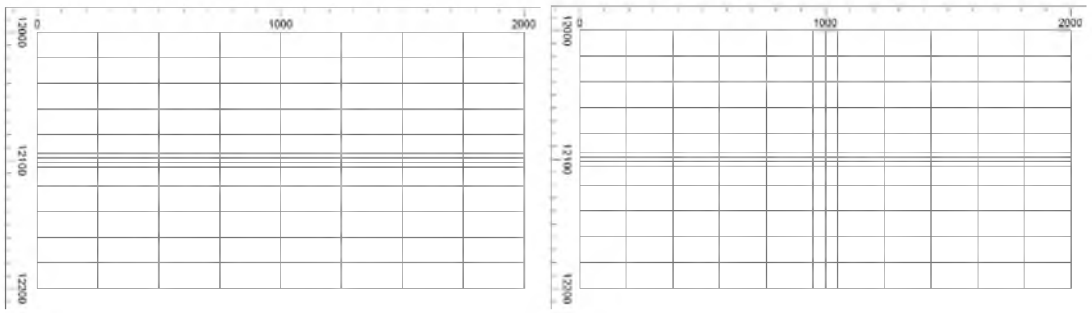

Figure D.1: Snapshots of coarse grid systems (a) Grid system 1 (b) Grid system 2.

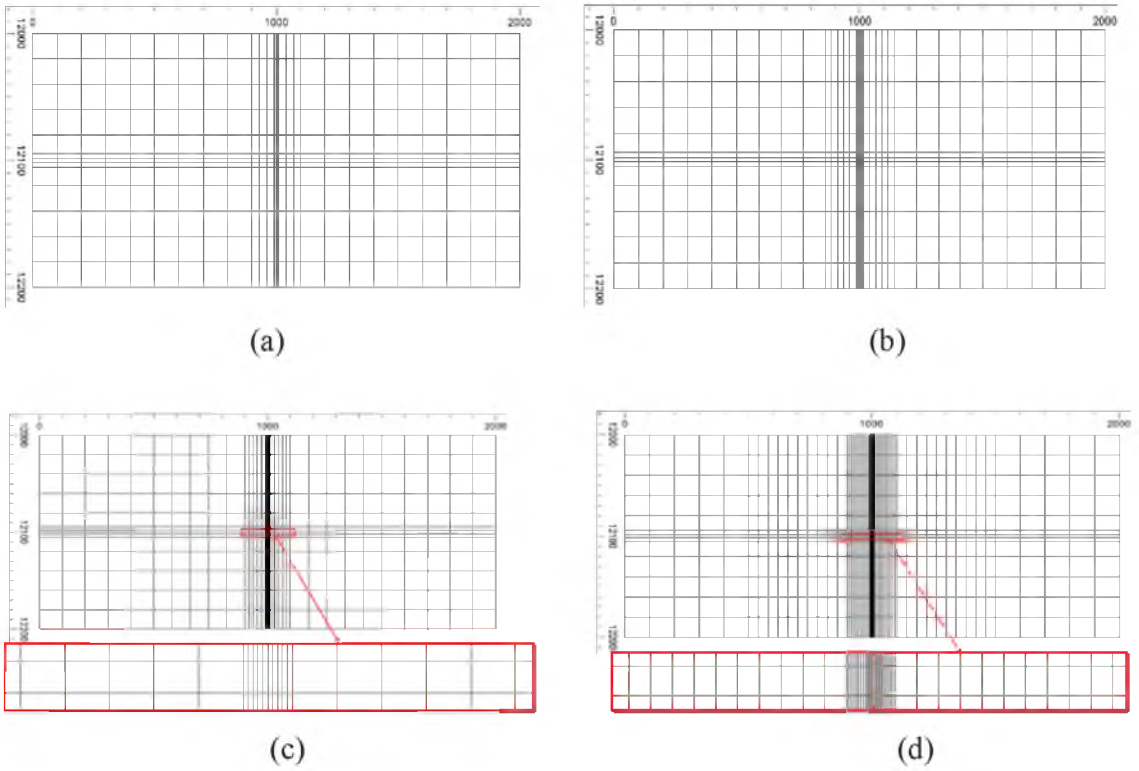

Figure D.2: Snapshots of medium refined grid systems (a) Grid system 3 (b) Grid system 4 (c) Grid System 5 (d) Grid System 6.

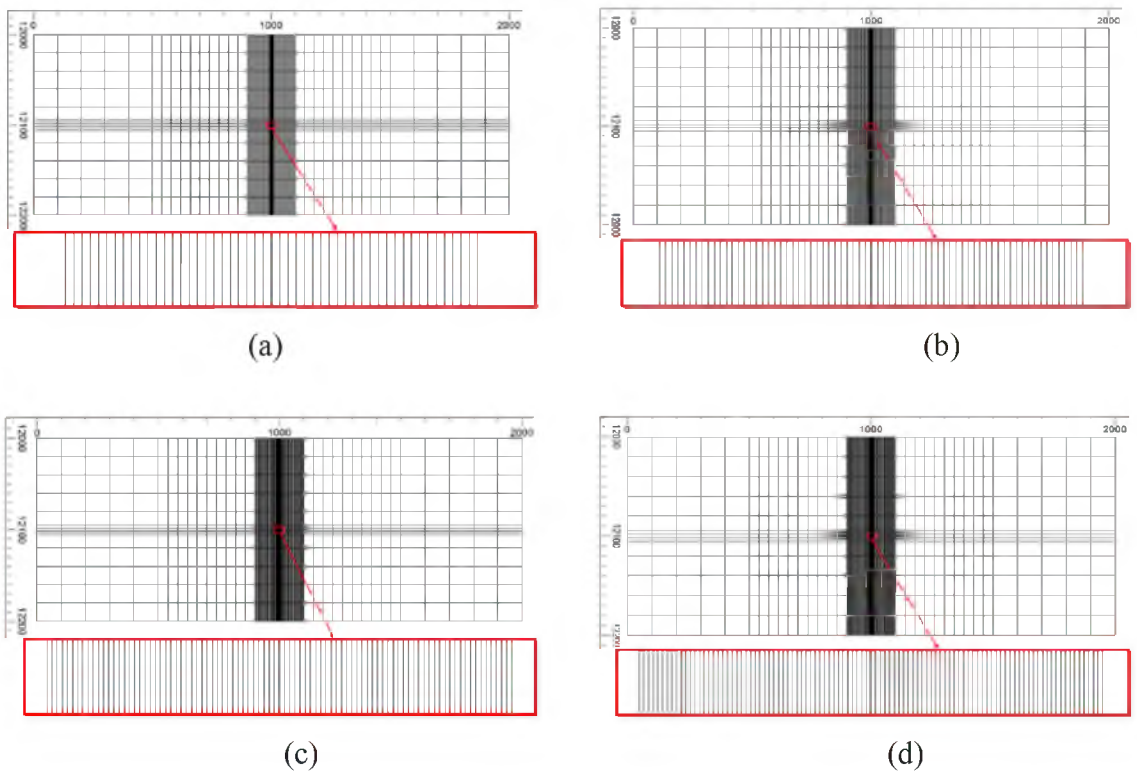

Figure D.3: Snapshots of finely refined grid systems (a) Grid system 7 (b) Grid system 8 (c) Grid System 9 (d) Grid System 10.

APPENDIX E

GOODNESS OF FIT

Goodness of fit is measured with a variety of statistical calculations. The coefficient of determination (R^2) and normalized root mean square error (NRMSE) are considered in this study. The brief descriptions of both calculations are given here.

R^2, the coefficient of determination is defined as:

$$R^2 = 1 - \frac{SS_{res}}{SS_{tot}} \qquad (E.1)$$

where,

$SS_{res} = \sum_{i=1}^{n}\left(Y_{obs,i} - Y_{model,i}\right)^2$, the residual sum of squares

$SS_{tot} = \sum_{i=1}^{n}\left(\bar{Y}_{obs} - Y_{model,i}\right)^2$, the total sum of squares

$\bar{Y}_{obs} = \frac{1}{n}\sum_{i=1}^{n} Y_{obs,i}$, the mean of observed values

The range of R^2 values is from 0 to 1. The values close to unity are concluded as the better fit of the model curve with observed data.

The NRMSE is defined as follows:

$$NRMSE = \frac{RMSE}{Y_{obs,max} - Y_{obs,min}} \qquad (E.2)$$

where,

$$\mathrm{RMSE} = \sqrt{\frac{\sum_{i=1}^{n}\left(Y_{obs,i} - Y_{model,i}\right)^2}{n}} \qquad (E.3)$$

Yobs: observed values

Ymodel: modeled values

Yobs,max: maximum value of observed data.

Yobs,min: minimum value of observed data.

The percentage values of the NRMSE are normally calculated for better interpretation. The smaller percentage values are interpreted as the better fit of the model curve with observed data.

APPENDIX F

COEFFICIENTS OF REGRESSION MODELS

Table F.1. The coefficients of condensate recovery.

Sr. No.	Name	90 Days Model	1 year Model	5 year Model	10 year Model	15 year Model	20 year Model	Rate Based Model
1	a_0	0.916	1.501	2.187	2.491	2.561	2.600	1.379
2	a_1	1.548	1.571	1.375	1.252	1.172	1.115	2.399
3	a_2	0.132	0.204	0.267	0.291	0.304	0.311	0.198
4	a_3	-0.073	-0.094	-0.088	-0.115	-0.111	-0.110	-0.271
5	a_4	0.035	0.103	0.189	0.210	0.235	0.246	0.442
6	a_5	0.553	0.580	0.624	0.628	0.626	0.623	0.846
7	a_6	-0.788	-0.755	-0.580	-0.464	-0.414	-0.373	-0.691
8	a_7	0.147	-0.063	-0.244	-0.279	-0.304	-0.309	-0.320
9	a_8	0.686	0.776	0.777	0.798	0.819	0.835	1.272
10	a_9	0.067	0.088	0.121	0.124	0.127	0.128	0.086
11	a_{11}	-0.136	-0.127	-0.232	-0.293	-0.272	-0.260	-0.611
12	a_{12}	-0.193	-0.154	-0.166	-0.168	-0.172	-0.165	-0.101
13	a_{13}	0.075	0.126	0.136	0.139	0.154	0.151	0.170
14	a_{14}	-0.067	-0.046	-0.064	-0.050	-0.071	-0.069	-0.341
15	a_{15}	-0.229	-0.274	-0.324	-0.334	-0.343	-0.344	-0.470
16	a_{16}	0.042	0.130	0.267	0.284	0.277	0.283	0.322
17	a_{17}	0.500	0.270	0.054	-0.010	-0.023	-0.047	0.252
18	a_{18}	-0.371	-0.352	-0.322	-0.307	-0.294	-0.298	-0.452
19	a_{19}	-0.065	-0.051	-0.035	-0.030	-0.030	-0.026	-0.018
20	a_{22}	0.237	0.186	0.064	-0.004	-0.032	-0.050	-0.027
21	a_{23}	0.029	0.016	0.057	0.048	0.030	0.028	-0.043
22	a_{24}	-0.076	-0.152	-0.174	-0.212	-0.237	-0.251	0.019
23	a_{25}	0.077	0.094	0.089	0.078	0.070	0.065	0.106
24	a_{26}	-0.008	-0.005	0.024	0.056	0.079	0.099	-0.013
25	a_{27}	0.152	0.232	0.234	0.226	0.229	0.238	0.659
26	a_{28}	-0.127	-0.120	-0.165	-0.182	-0.191	-0.196	-0.155
27	a_{29}	-0.046	-0.056	-0.108	-0.122	-0.112	-0.107	-0.051

Table F.1 continued

28	a_{33}	-0.036	-0.011	0.011	0.004	0.020	0.033	0.043
29	a_{34}	-0.023	-0.015	0.023	0.000	-0.014	-0.022	-0.028
30	a_{35}	-0.021	-0.049	-0.089	-0.084	-0.082	-0.077	-0.068
31	a_{36}	0.000	-0.004	-0.054	-0.093	-0.071	-0.067	-0.071
32	a_{37}	0.007	0.018	0.014	-0.005	-0.008	-0.010	-0.037
33	a_{38}	0.027	0.064	0.120	0.162	0.175	0.183	0.112
34	a_{39}	0.030	0.049	0.038	0.035	0.024	0.022	0.045
35	a_{44}	0.158	0.134	0.120	0.095	0.106	0.117	0.234
36	a_{45}	-0.040	-0.130	-0.243	-0.269	-0.291	-0.305	0.061
37	a_{46}	0.000	-0.002	0.004	0.028	0.042	0.055	0.106
38	a_{47}	0.052	0.056	0.099	0.053	0.052	0.045	0.143
39	a_{48}	-0.098	-0.186	-0.280	-0.294	-0.304	-0.311	-0.156
40	a_{49}	-0.048	-0.066	-0.075	-0.108	-0.119	-0.125	-0.039
41	a_{55}	0.109	0.063	-0.085	-0.157	-0.167	-0.175	-0.060
42	a_{56}	0.000	0.022	0.129	0.165	0.187	0.197	0.119
43	a_{57}	0.177	0.255	0.276	0.235	0.227	0.224	0.198
44	a_{58}	-0.067	-0.100	-0.137	-0.132	-0.119	-0.112	-0.237
45	a_{59}	-0.054	-0.059	-0.057	-0.050	-0.045	-0.047	-0.008
46	a_{66}	0.235	0.189	0.078	0.021	0.014	0.015	0.140
47	a_{67}	0.008	0.016	0.052	0.065	0.047	0.039	-0.007
48	a_{68}	-0.067	-0.075	0.000	0.008	-0.001	0.005	0.073
49	a_{69}	0.002	-0.001	-0.011	-0.026	-0.021	-0.018	-0.004
50	a_{77}	-0.284	-0.070	0.065	0.073	0.093	0.109	-0.002
51	a_{78}	0.391	0.456	0.386	0.342	0.304	0.275	0.489
52	a_{79}	0.045	0.060	0.150	0.165	0.172	0.177	0.460
53	a_{88}	0.182	0.145	0.073	0.021	0.040	0.055	0.438
54	a_{89}	-0.053	-0.061	0.029	0.094	0.134	0.162	0.148
55	a_{99}	-0.083	-0.072	-0.093	-0.104	-0.092	-0.078	-0.159

Table F.2. The coefficients of gas recovery from gas-condensate reservoir

Sr. No.	Name	90 Days Model	1 year Model	5 year Model	10 year Model	15 year Model	20 year Model	Rate Based Model
1	a_0	1.63	2.42	3.28	3.64	3.85	3.98	2.25
2	a_1	1.14	1.25	1.16	1.04	0.97	0.91	2.36
3	a_2	-0.155	-0.155	-0.096	-0.061	-0.038	-0.023	-0.016
4	a_3	0.042	0.045	0.046	0.034	0.026	0.021	-0.244
5	a_4	-0.031	-0.029	-0.024	-0.022	-0.023	-0.023	0.596
6	a_5	0.105	0.042	0.030	0.025	0.023	0.024	0.544
7	a_6	-0.803	-0.783	-0.685	-0.584	-0.515	-0.462	-0.685
8	a_7	0.557	0.425	0.254	0.158	0.098	0.059	0.040
9	a_8	0.162	0.184	0.094	0.058	0.040	0.032	0.996
10	a_9	-0.055	-0.058	-0.036	-0.043	-0.047	-0.049	0.028
11	a_{11}	-0.197	-0.165	-0.281	-0.368	-0.416	-0.445	-0.681
12	a_{12}	0.029	-0.001	0.072	0.090	0.093	0.092	-0.026
13	a_{13}	-0.025	-0.007	-0.001	-0.015	-0.021	-0.021	0.136
14	a_{14}	0.010	0.009	0.005	0.021	0.027	0.027	-0.315
15	a_{15}	0.103	0.042	0.033	0.037	0.037	0.037	-0.513
16	a_{16}	0.025	0.112	0.296	0.350	0.370	0.380	0.377
17	a_{17}	0.293	0.245	0.184	0.125	0.083	0.056	0.249
18	a_{18}	0.047	0.034	0.075	0.097	0.110	0.117	-0.350
19	a_{19}	-0.004	-0.010	-0.010	-0.014	-0.018	-0.019	-0.004
20	a_{22}	0.249	0.261	0.193	0.138	0.092	0.061	0.036
21	a_{23}	-0.011	0.000	-0.002	-0.005	-0.005	-0.007	-0.041
22	a_{24}	-0.028	-0.023	-0.023	-0.018	-0.021	-0.023	-0.101
23	a_{25}	0.046	0.000	-0.065	-0.066	-0.067	-0.066	0.075
24	a_{26}	0.001	0.000	-0.025	-0.055	-0.047	-0.036	0.000
25	a_{27}	-0.119	-0.059	0.017	0.024	0.048	0.062	0.497
26	a_{28}	-0.016	0.000	0.003	-0.036	-0.064	-0.083	-0.079
27	a_{29}	0.019	0.009	0.013	0.006	0.004	0.003	-0.044
28	a_{33}	-0.055	-0.039	0.000	-0.001	-0.005	-0.007	-0.027
29	a_{34}	0.005	-0.004	-0.008	-0.052	-0.075	-0.089	0.055
30	a_{35}	-0.025	-0.027	-0.052	-0.051	-0.042	-0.033	-0.082
31	a_{36}	0.000	0.000	0.002	0.011	0.014	0.017	-0.070
32	a_{37}	0.040	0.036	0.026	0.016	0.008	0.002	0.006
33	a_{38}	-0.029	-0.042	-0.049	-0.002	0.025	0.045	0.112
34	a_{39}	-0.016	-0.007	-0.001	-0.003	-0.002	-0.003	0.066
35	a_{44}	0.011	0.016	0.015	0.006	0.004	0.004	-0.033
36	a_{45}	0.008	0.004	-0.002	-0.006	-0.005	-0.005	-0.083
37	a_{46}	0.000	-0.001	-0.010	-0.016	-0.016	-0.017	0.099
38	a_{47}	-0.015	-0.008	0.018	0.008	0.001	0.000	0.207
39	a_{48}	-0.019	-0.017	-0.011	0.029	0.048	0.059	-0.349

Table F.2 continued

40	a_{49}	-0.012	0.004	0.000	0.005	0.005	0.007	-0.063
41	a_{55}	0.234	0.278	0.218	0.156	0.115	0.088	0.009
42	a_{56}	0.000	-0.001	-0.002	-0.009	-0.013	-0.014	0.117
43	a_{57}	-0.218	-0.166	-0.080	-0.055	-0.042	-0.033	-0.054
44	a_{58}	0.090	0.037	-0.024	-0.024	-0.026	-0.029	-0.186
45	a_{59}	0.044	0.028	0.024	0.028	0.028	0.029	0.035
46	a_{66}	0.260	0.223	0.182	0.132	0.081	0.046	0.089
47	a_{67}	-0.001	-0.005	0.012	0.040	0.026	0.014	-0.023
48	a_{68}	-0.003	-0.036	-0.049	-0.037	-0.029	-0.022	0.057
49	a_{69}	0.000	0.000	0.008	0.015	0.018	0.020	-0.014
50	a_{77}	-0.505	-0.407	-0.293	-0.244	-0.224	-0.212	-0.280
51	a_{78}	-0.031	-0.054	-0.125	-0.110	-0.109	-0.110	0.202
52	a_{79}	-0.026	-0.010	0.096	0.102	0.108	0.112	0.471
53	a_{88}	0.132	0.133	0.053	-0.006	-0.036	-0.053	0.319
54	a_{89}	0.003	0.020	0.146	0.230	0.277	0.309	0.156
55	a_{99}	-0.044	-0.054	-0.058	-0.078	-0.091	-0.098	-0.239

Table F.3. The coefficients of condensate to gas ratio.

Sr. No.	Name	90 Days Model	1 year Model	5 year Model	10 year Model	15 year Model	20 year Model	Rate Based Model
1	a_0	3.634	3.612	3.542	2.566	2.237	2.291	3.702
2	a_1	0.393	0.030	-0.411	-0.518	-0.467	-0.625	-0.323
3	a_2	0.473	0.446	0.407	0.343	0.272	0.180	0.247
4	a_3	-0.181	-0.239	-0.161	-0.080	-0.062	-0.107	-0.126
5	a_4	0.901	1.099	1.370	1.510	1.735	1.779	0.648
6	a_5	0.646	0.640	0.506	0.439	0.434	0.404	0.255
7	a_6	0.077	0.153	0.606	0.468	0.423	0.428	-0.033
8	a_7	-0.557	-0.709	-0.712	-0.451	-0.354	-0.259	-0.565
9	a_8	0.749	0.622	0.646	0.803	0.910	0.934	0.291
10	a_9	0.068	0.252	0.239	0.261	0.343	0.255	0.066
11	a_{11}	0.221	-0.184	-0.327	0.266	0.316	0.349	-0.180
12	a_{12}	-0.240	-0.050	-0.314	-0.434	-0.457	-0.058	-0.163
13	a_{13}	0.143	0.343	0.046	0.344	0.354	0.333	0.139
14	a_{14}	-0.089	0.071	0.379	0.499	0.326	0.289	-0.051
15	a_{15}	-0.345	-0.472	-0.601	-0.485	-0.493	-0.591	-0.161
16	a_{16}	0.099	0.241	0.023	-0.333	-0.376	-0.431	0.004
17	a_{17}	0.089	-0.418	-0.653	-0.815	-0.562	-0.497	-0.194
18	a_{18}	-0.391	-0.237	0.036	0.170	0.244	0.244	-0.102
19	a_{19}	-0.052	0.004	0.058	0.099	0.073	-0.064	0.003
20	a_{22}	-0.012	-0.284	-0.494	-0.462	-0.570	-0.623	-0.392
21	a_{23}	0.046	-0.118	0.021	-0.039	-0.091	-0.153	-0.111
22	a_{24}	-0.247	-0.193	-0.356	-0.879	-0.302	-0.664	-0.011
23	a_{25}	0.141	0.194	0.144	0.047	0.025	0.011	0.060
24	a_{26}	-0.018	0.017	0.215	0.189	0.325	0.289	0.000
25	a_{27}	0.427	0.303	0.004	-0.242	0.008	-0.020	0.183
26	a_{28}	-0.103	-0.077	-0.165	-0.080	-0.025	-0.011	-0.055
27	a_{29}	-0.182	-0.044	-0.255	-0.383	0.307	-0.192	0.056
28	a_{33}	0.079	0.049	-0.059	0.139	0.222	0.077	0.064
29	a_{34}	0.104	0.208	0.218	0.176	0.002	0.009	-0.205
30	a_{35}	0.005	-0.080	-0.085	-0.222	-0.059	0.015	0.009
31	a_{36}	0.100	-0.098	-0.203	-0.068	-0.117	-0.294	-0.308
32	a_{37}	-0.017	-0.013	0.042	-0.017	-0.047	0.044	-0.023
33	a_{38}	0.239	0.347	0.377	0.225	-0.005	-0.013	-0.071
34	a_{39}	-0.066	0.173	0.049	-0.029	0.061	0.109	-0.137
35	a_{44}	-0.118	-0.254	-0.355	-0.204	-0.362	-0.288	-0.012
36	a_{45}	-0.410	-0.639	-0.353	-0.357	-0.807	-0.601	-0.052
37	a_{46}	0.006	-0.047	-0.474	-0.519	-0.220	-0.410	0.099
38	a_{47}	0.077	0.199	0.337	0.264	0.456	0.390	0.156
39	a_{48}	-0.281	-0.443	-0.619	-0.719	-0.932	-0.975	0.048

Table F.3 continued

40	a_{49}	0.134	-0.229	-0.239	-0.456	-1.017	-0.540	0.055
41	a_{55}	-0.167	-0.447	-0.806	-0.491	-0.336	-0.403	-0.367
42	a_{56}	0.002	0.140	0.741	0.687	0.413	0.313	0.077
43	a_{57}	0.534	0.501	0.211	0.028	0.110	0.096	0.382
44	a_{58}	-0.111	-0.201	-0.161	-0.045	-0.016	0.003	-0.084
45	a_{59}	-0.107	-0.028	-0.032	0.102	-0.147	-0.067	-0.029
46	a_{66}	-0.068	-0.146	-0.473	-0.140	0.247	0.280	-0.070
47	a_{67}	0.018	0.112	0.119	-0.279	-0.045	-0.278	0.052
48	a_{68}	-0.163	-0.078	-0.128	-0.301	-0.372	-0.345	-0.007
49	a_{69}	-0.019	-0.001	-0.005	-0.071	0.098	0.052	0.202
50	a_{77}	0.473	0.547	0.422	0.616	0.606	0.572	0.483
51	a_{78}	0.618	0.648	0.417	0.269	0.200	0.129	0.477
52	a_{79}	0.100	0.075	0.040	0.030	0.040	0.020	0.032
53	a_{88}	0.040	-0.116	-0.037	0.361	0.525	0.477	-0.035
54	a_{89}	-0.118	-0.117	-0.157	-0.161	-0.163	-0.166	-0.090
55	a_{99}	0.031	0.024	-0.052	0.138	0.059	0.171	0.018

Figure F.1. The coefficients of oil recovery.

Sr. No.	Name	90 Days Model	1 year Model	5 year Model	10 year Model	15 year Model	20 year Model	Rate Based Model
1	a_0	-0.106	0.325	0.766	0.947	1.045	1.111	0.941
2	a_1	0.374	0.442	0.495	0.504	0.505	0.502	0.943
3	a_2	-0.033	-0.031	-0.025	-0.022	-0.018	-0.015	-0.025
4	a_3	0.040	0.041	0.043	0.042	0.043	0.045	0.098
5	a_4	-0.090	-0.087	-0.083	-0.081	-0.077	-0.073	-0.106
6	a_5	0.176	0.179	0.186	0.187	0.186	0.185	0.348
7	a_6	0.101	0.086	0.072	0.066	0.064	0.061	0.148
8	a_7	-0.033	-0.034	-0.034	-0.035	-0.035	-0.034	-0.066
9	a_8	-0.336	-0.337	-0.327	-0.312	-0.300	-0.291	-0.170
10	a_{11}	-0.060	-0.079	-0.105	-0.119	-0.127	-0.133	-0.349
11	a_{12}	-0.005	-0.017	-0.027	-0.023	-0.018	-0.014	0.036
12	a_{13}	-0.004	0.007	0.006	-0.001	-0.004	-0.006	0.008
13	a_{14}	0.011	0.007	-0.018	-0.020	-0.015	-0.007	0.047
14	a_{15}	-0.023	-0.019	0.013	0.033	0.034	0.030	-0.039
15	a_{16}	0.041	0.035	0.001	-0.011	-0.016	-0.020	-0.046
16	a_{17}	0.009	0.004	-0.005	-0.007	-0.006	-0.006	0.025
17	a_{18}	0.009	0.033	0.042	0.060	0.080	0.096	0.127
18	a_{22}	0.018	0.008	0.002	-0.001	-0.001	-0.001	-0.009
19	a_{23}	0.009	0.000	-0.002	-0.004	-0.005	-0.004	-0.013
20	a_{24}	0.016	-0.003	0.000	-0.003	-0.003	-0.002	-0.008
21	a_{25}	-0.031	-0.021	-0.013	-0.009	-0.007	-0.006	-0.009
22	a_{26}	0.021	0.005	0.004	0.000	0.000	0.000	0.003
23	a_{27}	0.010	0.002	0.004	0.002	0.003	0.003	-0.013
24	a_{28}	0.091	0.056	0.028	0.020	0.016	0.012	0.019
25	a_{33}	0.013	0.012	0.014	0.014	0.016	0.017	0.037
26	a_{34}	0.017	0.012	0.013	0.008	0.009	0.010	0.022
27	a_{35}	-0.024	-0.033	-0.039	-0.039	-0.040	-0.042	-0.092
28	a_{36}	0.013	0.010	0.011	0.009	0.010	0.012	0.035
29	a_{37}	0.006	0.004	0.006	0.003	0.003	0.003	0.004
30	a_{38}	0.000	-0.001	-0.006	-0.003	0.000	0.002	0.005
31	a_{44}	0.033	0.024	0.023	0.020	0.019	0.018	0.053
32	a_{45}	-0.059	-0.052	-0.041	-0.036	-0.034	-0.033	-0.054
33	a_{46}	0.018	0.006	0.007	0.003	0.005	0.007	0.036
34	a_{47}	-0.003	-0.012	-0.010	-0.013	-0.012	-0.012	-0.032
35	a_{48}	0.000	0.000	-0.001	0.002	0.001	0.000	-0.003
36	a_{55}	0.061	0.038	0.017	-0.001	-0.010	-0.015	-0.054
37	a_{56}	0.008	0.001	-0.005	-0.007	-0.009	-0.010	-0.068
38	a_{57}	0.016	0.017	0.021	0.025	0.026	0.028	0.059
39	a_{58}	0.001	0.001	-0.007	-0.015	-0.018	-0.017	0.005

Table F.4 continued

40	a_{66}	-0.010	-0.010	-0.008	-0.008	-0.006	-0.004	-0.051
41	a_{67}	0.015	0.009	0.009	0.007	0.006	0.006	0.015
42	a_{68}	-0.001	0.000	0.006	0.013	0.016	0.019	-0.006
43	a_{77}	0.000	-0.003	-0.003	-0.003	-0.001	0.000	-0.018
44	a_{78}	0.000	0.000	0.000	0.002	0.002	0.002	0.001
45	a_{88}	0.146	0.134	0.118	0.102	0.092	0.087	0.071

Table F.5. The coefficients of gas recovery from oil reservoir.

Sr. No.	Name	90 Days Model	1 year Model	5 year Model	10 year Model	15 year Model	20 year Model	Rate Based Model
1	a_0	-0.108	0.330	0.802	0.992	1.099	1.172	0.986
2	a_1	0.365	0.413	0.459	0.479	0.490	0.497	0.968
3	a_2	-0.044	-0.058	-0.067	-0.070	-0.071	-0.072	-0.076
4	a_3	0.039	0.034	0.030	0.027	0.026	0.026	0.086
5	a_4	-0.089	-0.092	-0.091	-0.091	-0.090	-0.089	-0.120
6	a_5	0.175	0.189	0.209	0.220	0.225	0.228	0.384
7	a_6	0.099	0.075	0.055	0.048	0.045	0.043	0.135
8	a_7	-0.035	-0.042	-0.049	-0.052	-0.054	-0.056	-0.087
9	a_8	-0.334	-0.335	-0.333	-0.326	-0.321	-0.316	-0.155
10	a_{11}	-0.052	-0.061	-0.099	-0.111	-0.113	-0.115	-0.329
11	a_{12}	0.024	0.013	-0.013	-0.022	-0.026	-0.031	0.026
12	a_{13}	0.000	0.017	0.016	0.006	0.001	-0.002	0.003
13	a_{14}	0.020	0.016	-0.010	-0.018	-0.021	-0.022	0.044
14	a_{15}	-0.036	-0.041	-0.011	0.024	0.041	0.050	-0.024
15	a_{16}	0.049	0.048	0.013	-0.001	-0.006	-0.009	-0.046
16	a_{17}	0.015	0.016	0.006	0.001	-0.002	-0.004	0.021
17	a_{18}	0.010	0.034	0.033	0.030	0.038	0.053	0.122
18	a_{22}	0.029	0.025	0.019	0.018	0.018	0.019	0.009
19	a_{23}	0.014	0.015	0.014	0.012	0.012	0.013	0.000
20	a_{24}	0.026	0.017	0.015	0.013	0.011	0.011	0.009
21	a_{25}	-0.047	-0.043	-0.042	-0.040	-0.039	-0.038	-0.041
22	a_{26}	0.032	0.026	0.020	0.017	0.015	0.014	0.016
23	a_{27}	0.015	0.015	0.015	0.014	0.014	0.014	0.000
24	a_{28}	0.104	0.071	0.044	0.038	0.034	0.033	0.023
25	a_{33}	0.012	0.012	0.011	0.010	0.009	0.010	0.035
26	a_{34}	0.017	0.015	0.012	0.011	0.010	0.010	0.024
27	a_{35}	-0.025	-0.035	-0.043	-0.045	-0.046	-0.048	-0.097
28	a_{36}	0.013	0.013	0.011	0.009	0.009	0.010	0.034
29	a_{37}	0.007	0.008	0.008	0.008	0.009	0.009	0.008
30	a_{38}	0.000	0.000	-0.002	-0.001	0.001	0.003	0.003
31	a_{44}	0.031	0.025	0.019	0.018	0.017	0.017	0.052
32	a_{45}	-0.056	-0.050	-0.040	-0.033	-0.029	-0.027	-0.054
33	a_{46}	0.018	0.012	0.008	0.007	0.007	0.007	0.038
34	a_{47}	-0.002	-0.009	-0.014	-0.015	-0.016	-0.016	-0.034
35	a_{48}	0.000	0.000	0.000	0.002	0.004	0.005	-0.003
36	a_{55}	0.060	0.036	0.001	-0.020	-0.031	-0.039	-0.071
37	a_{56}	0.005	-0.007	-0.016	-0.018	-0.019	-0.020	-0.073
38	a_{57}	0.015	0.014	0.018	0.022	0.026	0.028	0.054
39	a_{58}	0.001	0.000	-0.010	-0.024	-0.033	-0.038	0.007

Table F.5 continued

40	a_{66}	-0.009	-0.004	-0.004	-0.004	-0.003	-0.002	-0.049
41	a_{67}	0.017	0.014	0.013	0.012	0.011	0.011	0.019
42	a_{68}	-0.001	0.000	0.005	0.009	0.011	0.013	-0.010
43	a_{77}	-0.001	-0.002	-0.004	-0.004	-0.003	-0.002	-0.019
44	a_{78}	0.000	0.000	0.003	0.005	0.006	0.007	-0.002
45	a_{88}	0.147	0.138	0.127	0.117	0.110	0.106	0.093

Table F.6. The coefficients of gas oil ratio

Sr. No.	Name	90 Days Model	1 year Model	5 year Model	10 year Model	15 year Model	20 year Model	Rate Based Model
1	a_0	3.277	3.304	3.314	3.358	3.379	3.391	3.359
2	a_1	-0.032	-0.043	-0.022	0.019	0.057	0.101	0.125
3	a_2	-0.025	-0.041	-0.049	-0.065	-0.079	-0.076	-0.077
4	a_3	-0.006	-0.016	-0.014	-0.021	-0.027	-0.031	-0.017
5	a_4	-0.003	-0.011	-0.009	-0.022	-0.029	-0.031	-0.012
6	a_5	0.291	0.308	0.326	0.344	0.358	0.370	0.355
7	a_6	-0.008	-0.021	-0.013	-0.017	-0.014	-0.014	-0.012
8	a_7	-0.009	-0.017	-0.014	-0.026	-0.031	-0.034	-0.032
9	a_8	0.002	0.001	-0.025	-0.048	-0.065	-0.083	-0.013
10	a_{11}	0.029	0.011	0.012	0.023	0.049	0.063	0.138
11	a_{12}	0.048	-0.010	-0.038	-0.055	-0.062	-0.166	-0.078
12	a_{13}	0.029	0.024	0.006	0.003	0.000	0.002	-0.007
13	a_{14}	0.029	0.020	0.001	-0.018	-0.056	-0.096	-0.056
14	a_{15}	-0.028	-0.033	-0.011	0.060	0.125	0.161	0.113
15	a_{16}	0.036	0.024	0.012	0.010	0.015	0.020	0.010
16	a_{17}	0.036	0.026	0.005	-0.002	-0.010	-0.015	-0.056
17	a_{18}	0.000	0.001	-0.042	-0.125	-0.156	-0.161	0.009
18	a_{22}	0.018	0.016	0.029	0.015	0.018	0.013	0.020
19	a_{23}	0.013	0.025	-0.011	0.013	0.015	0.029	0.026
20	a_{24}	0.023	0.012	0.033	0.038	0.014	0.000	-0.004
21	a_{25}	-0.031	-0.025	-0.036	-0.036	-0.034	-0.032	-0.035
22	a_{26}	0.021	0.032	-0.007	0.008	0.001	0.004	0.015
23	a_{27}	0.014	0.019	-0.022	0.012	0.004	0.010	0.019
24	a_{28}	0.016	0.018	0.012	0.030	0.035	0.059	0.012
25	a_{33}	0.000	0.000	0.006	-0.008	-0.017	-0.019	-0.005
26	a_{34}	0.004	0.003	-0.002	0.002	-0.004	-0.005	0.006
27	a_{35}	-0.003	-0.004	-0.007	-0.008	-0.007	-0.005	-0.005
28	a_{36}	0.004	0.003	0.010	-0.008	-0.004	-0.012	-0.005
29	a_{37}	0.003	0.005	0.012	0.002	0.008	0.007	0.008
30	a_{38}	0.000	0.002	0.012	-0.001	-0.005	0.000	-0.007
31	a_{44}	-0.004	-0.003	0.008	-0.004	-0.005	0.002	0.015
32	a_{45}	0.014	0.019	0.016	0.023	0.030	0.027	0.012
33	a_{46}	0.008	0.007	0.008	-0.010	-0.003	-0.010	-0.002
34	a_{47}	0.004	0.000	-0.005	-0.011	-0.007	-0.006	-0.007
35	a_{48}	0.000	0.002	0.000	0.002	0.022	0.045	0.003
36	a_{55}	-0.090	-0.100	-0.103	-0.118	-0.123	-0.130	-0.128
37	a_{56}	0.007	0.003	0.004	0.007	0.010	0.012	0.013
38	a_{57}	-0.003	-0.005	-0.002	0.002	0.010	0.000	-0.002
39	a_{58}	0.000	-0.001	-0.013	-0.037	-0.068	-0.097	-0.029

Table F.6 continued

40	a_{66}	0.003	0.008	0.013	-0.001	-0.007	-0.007	-0.005
41	a_{67}	0.006	0.007	0.024	0.003	0.003	0.003	0.005
42	a_{68}	0.000	0.000	-0.003	-0.010	-0.013	-0.010	-0.005
43	a_{77}	0.002	0.003	0.010	-0.002	-0.009	-0.009	-0.006
44	a_{78}	0.000	0.000	0.011	0.008	0.006	0.012	0.002
45	a_{88}	0.004	0.008	0.035	0.038	0.041	0.055	0.036

REFERENCES

Aanonsen, S. I., Eide, A. L., et al. 1995. Optimizing Reservoir Performance Under Uncertainty with Application to Well Location. SPE Annual Technical Conference and Exhibition, Dallas, Texas, 22-25 October. SPE-30710-MS.

Abou-Kassem, J. H., and K. Aziz. 1984. Sensitivity of Steamflood Model Results to Grid and Timestep Sizes. Society of Petroleum Engineers Journal **24** (01). SPE-11080-PA.

Afinogenov, Y. A. 1969. How the liquid permeability of rocks is affected by pressure and temperature. Soviet Mining **5** (6): 638-645.

Al-Meshari, A. A., S. L. Kokal, et al. 2007. Measurement of Gas Condensate, Near-Critical and Volatile Oil Densities and Viscosities at Reservoir Conditions. SPE Annual Technical Conference and Exhibition, Anaheim, California, 11-14 November. SPE-108434.

Al-Mohannadi, N. S., E. Ozkan, et al. 2007. Grid-System Requirements in Numerical Modeling of Pressure-Transient Tests in Horizontal Wells. SPE Reservoir Evaluation & Engineering **10** (02). SPE-92041.

Amorim, T., and D. J. Schiozer. 2012. Risk Analysis Speed-Up With Surrogate Models. SPE Latin America and Caribbean Petroleum Engineering Conference. Mexico City, Mexico, 16-18 April. SPE-153477.

Aqeel, N., and L. B. Cunha. 2006. An Investigation of Grid Design Characteristics in Numerical Modelling of Horizontal Well Pressure Transient Tests. Canadian International Petroleum Conference. Calgary, Alberta, Petroleum Society of Canada, 13-15 June. PETSOC-2006-161.

Arbabi, S., and A. Firoozabadi. 1995. Near-Critical Phase Behavior of Reservoir Fluids Using Equations of State. SPE Advanced Technology Series **3** (01).

Arps, J. J., and T. G. Roberts. 1955. The Effect of the Relative Permeability Ratio, the Oil Gravity, and the Solution Gas-Oil Ratio on the Primary Recovery From a Depletion Type Reservoir. AIME Annual Meeting, Chicago, 13-17 February. SPE-469-G

Atbi, A. M., and A. Aissaoui. 2004. Quantification of Uncertainty in Production Forecast Using Experimental Design, Case Study: Tiguentourine and Taouratine Fields.

Canadian International Petroleum Conference, Calgary, Alberta, Petroleum Society of Canada, 8-10 June. PETSOC-2006-097.

Ayala, L. F., E. d. S. Radespiel, et al. 2007. Analysis of Condensate Buildup and Flow Impairment for Near-Critical Gas Fluids in Fissured Reservoirs, Society of Petroleum Engineers. Latin American & Caribbean Petroleum Engineering Conference, 15-18 April, Buenos Aires, Argentina. SPE-107870-MS.

Biterge, M. B., and T. Ertekin. 1992. Development and Testing of a Static/Dynamic Local Grid-Refinement Technique. Journal of Petroleum Technology **44** (04). SPE-19803.

Blom, S. M. P., J. Hagoort, et al. 1997. Relative Permeability at Near-Critical Conditions. SPE Annual Technical Conference and Exhibition, 5-8 October, San Antonio, Texas. SPE-38935-MS.

Bonyadi, M., M. R. Rahimpour, et al. 2012. A new fast technique for calculation of gas condensate well productivity by using pseudopressure method. Journal of Natural Gas Science and Engineering **4**: 35-43.

Box, G. E. P., and D. W. Behnken. 1960. Some New Three Level Designs for the Study of Quantitative Variables. Technometrics **2** (4): 455-475.

Brinkman, F. H., and C. F. Weinaug. 1956. Calculated Performance Of A Dissolved Gas Drive Reservoir By A Phase Behavior Method. Fall Meeting of the Petroleum Branch of AIME, 14-17 October, Los Angeles, California. SPE-740-G.

Busahmin, B. S., and B. B. Maini. 2010. Effect of Solution-Gas-Oil-Ratio on Performance of Solution Gas Drive in Foamy Heavy Oil Systems. Canadian Unconventional Resources and International Petroleum Conference, 19-21 October, Calgary, Alberta. SPE-137866-MS

Carreras, P. E., S. E. Turner, et al. 2006. Tahiti: Development Strategy Assessment Using Design of Experiments and Response Surface Methods. SPE Western Regional/AAPG Pacific Section/GSA Cordilleran Section Joint Meeting, 8-10 May, Anchorage, Alaska. SPE-100656-MS.

Ceragioli, P., and F. Masserano. 1998. Near Critical Gas Condensate Systems: Effects of IFT on Gravity Drainage. SPE Gas Technology Symposium, 15-18 March, Calgary, Alberta. SPE-39975-MS

Chaudhary, A. S., C. A. Ehlig-Economides, et al. 2011. Shale Oil Production Performance from a Stimulated Reservoir Volume. SPE Annual Technical Conference and Exhibition, 30 October-2 November, Denver, Colorado. SPE-147596-MS

Chewaroungroaj, J., O. J. Varela, et al. 2000. An Evaluation of Procedures to Estimate Uncertainty in Hydrocarbon Recovery Predictions. SPE Asia Pacific Conference on Integrated Modelling for Asset Management, 25-26 April, Yokohama, Japan. SPE-147596-MS

Clemens, T., and K. Wit. 2001. The Effect of Fracture Spacing on Gas/Oil Gravity Drainage in Naturally Fractured Reservoirs. SPE Annual Technical Conference and Exhibition, 30 September-3 October, New Orleans. SPE-71507-MS

Cook, R. E., R. H. Jacoby, et al. 1974. A Beta-Type Reservoir Simulator for Approximating Compositional Effects During Gas Injection. Society of Petroleum Engineers Journal **14**(5): 471-481.

Corre, B., P. Thore, et al. 2000. Integrated Uncertainty Assessment For Project Evaluation and Risk Analysis. SPE European Petroleum Conference, 24-25 October, Paris, France. SPE-65205-MS.

Dahaghi, A. K., S. Esmaili, et al. 2012. Fast Track Analysis of Shale Numerical Models. SPE Canadian Unconventional Resources Conference, 30 October-1 November, Calgary, Alberta, Canada. SPE-162699-MS.

Damsleth, E., A. Hage, et al. 1992. Maximum Information at Minimum Cost: A North Sea Field Development Study With an Experimental Design. Journal of Petroleum Technology **44**(12): 1350-1356.

Davidson, L. B. 1969. The Effect of Temperature on the Permeability Ratio of Different Fluid Pairs in Two-Phase Systems. Journal of Petroleum Technology **21**(08): 1037-1046.

Dejean, J. P., and G. Blanc. 1999. Managing Uncertainties on Production Predictions Using Integrated Statistical Methods. SPE Annual Technical Conference and Exhibition, 3-6 October, Houston, Texas. SPE-56696-MS.

Descubes, E. 2012. Stochastic uncertainty analysis in compositional simulation for giant gas-condensate field reservoir performance prediction. SPE Russian Oil and Gas Exploration and Production Technical Conference and Exhibition, 16-18 October, Moscow, Russia. SPE-162045-MS.

Diamond, P. H., R. A. Pressney, et al. 1996. Probabilistic Prediction of Well Performance in a Gas Condensate Reservoir. European Petroleum Conference, 22-24 October, Milan, Italy. SPE-36894-MS.

Ding, Y., and P. A. Lemonnier. 1993. Development of Dynamic Local Grid Refinement in Reservoir Simulation. SPE Symposium on Reservoir Simulation, 28 February-3 March, New Orleans. SPE-25279-MS.

Duong, A. N. 2011. Rate-Decline Analysis for Fracture-Dominated Shale Reservoirs. SPE Reservoir Evaluation & Engineering **14** (3).

Earlougher, R. C. 1977. Advances in Well Test Analysis. SPE Monograph Series 5, Society of Petroleum Engineers.

Edmondson, T. A. 1965. Effect of Temperature on Waterflooding. Journal of Canadian Petroleum Technology **4** (04). PETSØC-65-04-09

Egeland, T., L. Holden, et al. 1992. Designing Better Decisions. European Petroleum Computer Conference, 24-27 May, Stavanger, Norway. SPE-24275-MS.

EIA. 2013. Annual Energy Outlook. U.S. Energy Information Administration

EIA. 2014. Annual Energy Outlook. U.S. Energy Information Administration

Eilerts, C. K., E. F. Sumner, et al. 1965. Integration of Partial Differential Equation for Transient Radial Flow of Gas-Condensate Fluids in Porous Structures. Society of Petroleum Engineers Journal **5** (02). SPE-716-PA

Evinger, H. H., and M. Muskat. 1942. Calculation of Theoretical Productivity Factor. Transactions of the AIME **146** (01). SPE-942126-G

Ewing, R. E., B. A. Boyett, et al. 1989. Efficient Use of Locally Refined Grids for Multiphase Reservoir Simulation. SPE Symposium on Reservoir Simulation, 6-8 February, Houston, Texas. SPE-18413-MS.

Ewing, R. E., and R. D. Lazarov. 1988. Adaptive Local Grid Refinement. SPE Rocky Mountain Regional Meeting, 11-13 May, Casper, Wyoming. SPE -17806-MS.

Fang, Y., B. Li, et al. 1998. Condensate Gas Phase Behavior and Development. SPE International Oil and Gas Conference and Exhibition in China, 2-6 November, Beijing, China. SPE-50925-MS

Fetkovich, M. D., E. T. Guerrero, et al. 1986. Oil and Gas Relative Permeabilities Determined From Rate-Time Performance Data. SPE Annual Technical Conference and Exhibition, 5-8 October, New Orleans. SPE-15431-MS.

Fevang, Ø., and C. H. Whitson. 1996. Modeling Gas-Condensate Well Deliverability. SPE Reservoir Engineering **11** (4): 221-230.

Fussell, D. D. 1973. Single-Well Performance Predictions for Gas Condensate Reservoirs. Journal of Petroleum Technology **25** (7): 860-870.

Gerami, S., A. Sadeghi, et al. 2010. New Technique for Calculation of Gas Condensate Well Deliverability. SPE Deep Gas Conference and Exhibition, 24-26 January,

Manama, Bahrain. SPE-130139-MS

Goktas, B., and T. Ertekin. 1999. Development of a Local Grid-Refinement Technique for Accurate Representation of Cavity-Completed Wells in Reservoir Simulators. Society of Petroleum Engineers Journal **4** (03). SPE-54403-PA.

Goktas, B., and T. Ertekin. 1999. Implementation of a Local Grid Refinement Technique in Modeling Slanted, Undulating Horizontal and Multi-Lateral Wells. SPE Annual Technical Conference and Exhibition, 3-6 October, Houston, Texas. SPE-56624-MS.

Gondouin, M., R. Iffly, et al. 1967. An Attempt to Predict the Time Dependence of Well Deliverability in Gas Condensate Fields. Society of Petroleum Engineers Journal **7** (02). SPE-1478-PA.

Graham, M. F., and G. T. Smart. 1980. Reservoir Simulator Employing A Fine-Grid Model Nested In A Coarse-Grid Model. SPE Annual Technical Conference and Exhibition, 21-24 September, Dallas, Texas. SPE-9372-MS.

Guehria, F. M. 2000. Inflow Performance Relationships for Gas Condensates. SPE Annual Technical Conference and Exhibition, 1-4 October, Dallas, Texas. SPE-63158-MS.

Guo, B., and D. S. Schechter. 1999. A Simple And Rigorous IPR Equation For Vertical And Horizontal Wells Intersecting Long Fractures. Journal of Canadian Petroleum Technology **38** (7).

Guyaguler, B., and R. N. Horne. 2001. Uncertainty Assessment of Well Placement Optimization. SPE Annual Technical Conference and Exhibition, 30 September-3 October, New Orleans. SPE-71625-MS.

Haajizadeh, M., and S. H. Begg. 1993. Sensitivity of Oil Recovery to Grid Size and Reservoir Description in Fluvially Dominated Deltaic Facies. SPE Western Regional Meeting, 26-28 May, Anchorage, Alaska. SPE-26080-MS.

Hall, H. N. 1953. Compressibility of Reservoir Rocks. Journal of Petroleum Technology **5** (01). SPE-953309-G

Hefley, W. E., S. M. Seydor, et al. 2011. The Economic Impact of the Value Chain of a Marcellus Shale Well. Pitt Business Working Papers, University of Pittsburgh.

Heinemann, Z. E., G. Gerken, et al. 1983. Using Local Grid Refinement in a Multiple-Application Reservoir Simulator. SPE Reservoir Simulation Symposium, 15-18 November, San Francisco, California. SPE-12255-MS.

Hernandez, J. C., V. Vesovic, et al. 2002. Sensitivity of Reservoir Simulations to Uncertainties in Viscosity. SPE/DOE Improved Oil Recovery Symposium, 13-17

April, Tulsa, Oklahoma. SPE-75227-MS.

Huang, W. W. 1985. Some Experiences With a Critical Reservoir Fluid. SPE Annual Technical Conference and Exhibition, 22-26 September, Las Vegas. SPE-14415-MS

Jones-Parra, J., and R. S. Reytor 1959. Effect of Gas-Oil Ratio on the Behavior of Fractured Limestone Reservoirs. Journal of Petroleum Technology **11** (05).

Jones, J. R., and R. Raghavan. 1988. Interpretation of Flowing Well Response in Gas-Condensate Wells. SPE Formation Evaluation **3** (3): 578-594.

Khosravi, M., S. Fatemi, et al. 2011. Assessing Structured Uncertainty in a Mature Fractured Reservoir, Using Combination of Response Surface Method and Reservoir Simulation. SPE Reservoir Characterisation and Simulation Conference and Exhibition. Abu Dhabi, UAE, Society of Petroleum Engineers. SPE 148003.

Khosravi, M., S. Fatemi, et al. 2011. Assessing Structured Uncertainty in a Mature Fractured Reservoir, Using Combination of Response Surface Method and Reservoir Simulation. SPE Reservoir Characterisation and Simulation Conference and Exhibition, 9-11 October, Abu Dhabi, UAE. SPE-148003-MS.

Khosravi, M., B. Rostami, et al. 2012. Uncertainty Analysis of a Fractured Reservoir's Performance: A Case Study. Oil & Gas Science and Technology – Rev. IFP Energies nouvelles **67** (3): 423-433.

Kilic, A., and T. Ertekin 1999. Application Of A Local Grid Refinement Protocol In Highly Faulted Reservoir Architectures. Technical Meeting / Petroleum Conference of The South Saskatchewan Section, October 18 - 21, Regina. PETSOC-99-123.

Kniazeff, V. J., and S. A. Nvaille. 1965. Two-Phase Flow of Volatile Hydrocarbons. Society of Petroleum Engineers Journal **5** (01). SPE-962-PA.

Kossack, C. A., S. Hagen, et al. 1986. Phase Behavior Calculations Near the Critical Point. SPE Annual Technical Conference and Exhibition, 5-8 October, New Orleans. SPE-15402-MS.

Kyi, K. K., N. Bt Yahaya, et al. 2009. Fluid Identification Challenges in the Near Critical Fluids: Case Studies in Malaysia. Asia Pacific Oil and Gas Conference & Exhibition, 4-6 August, Jakarta, Indonesia. SPE-123430-MS.

Landa, J. L., and B. Güyagüler. 2003. A Methodology for History Matching and the Assessment of Uncertainties Associated with Flow Prediction. SPE Annual Technical Conference and Exhibition, 5-8 October, Denver, Colorado. SPE-84465-MS

Lawal, K. A., A. O. Uwaga, et al. 2006. A Systematic Methodology for Extrapolating Gas-Oil Ratio During Declining Oil Production. Nigeria Annual International

Conference and Exhibition, 31 July-2 August, Abuja, Nigeria. SPE-105973-MS

Levine, J. S., and M. Prats. 1961. The Calculated Performance of Solution-Gas-Drive Reservoirs. Society of Petroleum Engineers Journal **1** (03)

Li, B., and F. Friedmann. 2005. A Novel Response Surface Methodology Based on "Amplitude Factor" Analysis for Modeling Nonlinear Responses Caused by Both Reservoir and Controllable Factors. SPE Annual Technical Conference and Exhibition, 9-12 October, Dallas, Texas. SPE-95283-MS.

Li, B., and F. Friedmann. 2005. Novel Multiple Resolutions Design of Experiment/Response Surface Methodology for Uncertainty Analysis of Reservoir Simulation Forecasts. SPE Reservoir Simulation Symposium, 31 January-2 February, The Woodlands, Texas. SPE-92853-MS.

Ling, K., and Z. Shen. 2011. Effects of Fluid and Rock Properties on Reserves Estimation. SPE Eastern Regional Meeting, 17-19 August, Columbus, Ohio. SPE-148717-MS.

Lo, H. Y., and N. Mungan. 1973. Effect of Temperature on Water-Oil Relative Permeabilities in Oil-Wet and Water-Wet Systems. Fall Meeting of the Society of Petroleum Engineers of AIME, 30 September-3 October, Las Vegas. SPE-4505-MS.

Maini, B. B., and J. P. Batycky. 1985. Effect of Temperature on Heavy-Oil/Water Relative Permeabilities in Horizontally and Vertically Drilled Core Plugs. Journal of Petroleum Technology **37**(8): 1500-1510.

Manceau, E., M. Mezghani, et al. 2001. Combination of Experimental Design and Joint Modeling Methods for Quantifying the Risk Associated With Deterministic and Stochastic Uncertainties - An Integrated Test Study. SPE Annual Technical Conference and Exhibition, 30 September-3 October, New Orleans. SPE-71620-MS.

Manceau, E., F. Roggero, et al. 2002. Use Of Experimental Design Methodology To Make Decisions In An Uncertain Reservoir Environment From Reservoir Uncertainties To Economic Risk Analysis. 17th World Petroleum Congress, 1-5 September, Rio de Janeiro, Brazil. WPC-32161.

Marsh, H. N., and B. H. Robinson. 1929. Means of Controlling Gas-oil Ratio. Transactions of the AIME **82** (01). SPE-929183-G

Martin, J. C. 1959. Simplified Equations of Flow in Gas Drive Reservoirs and the Theoretical Foundation of Multiphase Pressure Buildup Analyses. Petroleum Transactions, AIME 216, 321-323.

Mendoza, E. E., J. Aular, et al. 2011. Optimizing Horizontal-Well Hydraulic-Fracture Spacing in the Eagle Ford Formation, Texas. North American Unconventional Gas

Conference and Exhibition, 14-16 June, The Woodlands, Texas. SPE-143681-MS.

Miller, G. F. 1962. Theory of Unsteady State Influx of Water in Linear Reservoirs. Journal of the Institute of Petroleum **48**.

Millikan, C. V. 1926. Gas-oil Ratio as Related to the Decline of Oil Production, with Notes on the Effect of Controlled Pressure. Transactions of the AIME **G-26** (01).

Mohaghegh, S. D. 2006. Quantifying Uncertainties Associated With Reservoir Simulation Studies Using a Surrogate Reservoir Model. SPE Annual Technical Conference and Exhibition, 24-27 September, San Antonio, Texas. SPE-102492-MS.

Mohaghegh, S. D., J. S. Liu, et al. 2012. Application of Well-Base Surrogate Reservoir Models (SRMs) to Two Offshore Fields in Saudi Arabia, Case Study. SPE Western Regional Meeting, 21-23 March, Bakersfield, California,. SPE-153845-MS.

Mohaghegh, S. D., C. A. Modavi, et al. 2006. Development of Surrogate Reservoir Models (SRM) for Fast-Track Analysis of Complex Reservoirs. Intelligent Energy Conference and Exhibition, 11-13 April, Amsterdam, The Netherlands. SPE-99667-MS.

Mott, R. 2002. Engineering Calculations of Gas Condensate Well Productivity. SPE Annual Technical Conference and Exhibition, 29 September-2 October, San Antonio, Texas. SPE-77551-MS

Murtha, J. A., S. K. Peterson, et al. 2007. Risk and Decision Analysis. Petroleum Engineering Handbook by H. R. J. Warner. Richardson, Society of Petroleum Engineer. **6**: VI-446 -VI 529.

Muskat, M. 1945. The Production Histories of Oil Producing Gas-Drive Reservoirs. Journal of Applied Physics **16** (3): 147-159.

Nacul, E. C., and K. Aziz. 1991. Use of Irregular Grid in Reservoir Simulation. SPE Annual Technical Conference and Exhibition, 6-9 October, Dallas, Texas. SPE-22886-MS.

Najurieta, H. L., N. Galacho, et al. 2001. Effects of Temperature and Interfacial Tension in Different Production Mechanisms. SPE Latin American and Caribbean Petroleum Engineering Conference, 25-28 March, Buenos Aires, Argentina. SPE-69398-MS.

O'Dell, H. G., and R. N. Miller. 1967. Successfully Cycling a Low-Permeability, High-Yield Gas Condensate Reservoir, Journal of Petroleum Technology **19** (01).

Orangi, A., N. R. Nagarajan, et al. 2011. Unconventional Shale Oil and Gas-Condensate Reservoir Production, Impact of Rock, Fluid, and Hydraulic Fractures. SPE Hydraulic Fracturing Technology Conference, 24-26 January, The Woodlands, Texas. SPE-

140536-MS

Panja, P., T. Conner, et al. 2013. Grid Sensitivity Studies in Hydraulically Fractured Low Permeability Reservoirs. Journal of Petroleum Science and Engineering **112**: 78-87.

Pedrosa Jr., O. A., and K. Aziz. 1986. Use of a Hybrid Grid in Reservoir Simulation. SPE Reservoir Engineering **1** (06).

Peng, C. Y., and R. Gupta. 2003. Experimental Design in Deterministic Modelling: Assessing Significant Uncertainties. SPE Asia Pacific Oil and Gas Conference and Exhibition, 9-11 September, Jakarta, Indonesia. SPE-80537-MS.

Peng, C. Y., and R. Gupta. 2004. Experimental Design and Analysis Methods in Multiple Deterministic Modelling for Quantifying Hydrocarbon In-Place Probability Distribution Curve. SPE Asia Pacific Conference on Integrated Modelling for Asset Management, 29-30 March, Kuala Lumpur, Malaysia. SPE-87002-MS.

Peng, C. Y., and R. Gupta. 2005. Experimental Design and Analysis Methods for Assessing Volumetric Uncertainties. Society of Petroleum Engineers Journal **10** (3): 324-335.

Poston, S. W., S. Ysrael, et al. 1970. The Effect of Temperature on Irreducible Water Saturation and Relative Permeability of Unconsolidated Sands. Society of Petroleum Engineers Journal **10** (2): 324-335. SPE-1897-PA.

Prats, M., and J. S. Levine. 1963. Effect of Vertical Fractures on Reservoir Behavior-Results on Oil and Gas Flow. Journal of Petroleum Technology **15** (10).

Quandalle, P. 1983. The Use of Flexible Gridding for Improved Reservoir Modeling. SPE Reservoir Simulation Symposium, 15-18 November, San Francisco, California. SPE-12239-MS.

Quandalle, P., and P. Besset. 1985. Reduction of Grid Effects Due to Local Sub-Gridding in Simulations Using a Composite Grid. SPE Reservoir Simulation Symposium, 10-13 February, Dallas, Texas. SPE-13527-MS.

Quinones, V. A. H., and A. F. Lanchimba. 2012. A Holistic Analysis Approach for Reservoir Modeling. SPE Latin America and Caribbean Petroleum Engineering Conference, 16-18 April, Mexico City, Mexico. SPE-153387-MS

Quinones, V. A. H., A. F. Lanchimba, et al. 2010. Gas Condensate Field Development Plan by Means of Numerical Compositional Simulation. SPE Latin American and Caribbean Petroleum Engineering Conference, 1-3 December, Lima, Peru. SPE-138886-MS

Rosales, E., F. Ashford, et al. 1992. Unexpected Near-Critical Reservoir Fluid Behavior

in The North Monagas Oil Province, Venezuela. SPE Latin America Petroleum Engineering Conference, 8-11 March, Caracas, Venezuela. SPE-23712-MS

Rosenberg, D. U. v. 1982. Local Mesh Refinement for Finite Difference Methods. SPE Annual Technical Conference and Exhibition, 26-29 September, New Orleans, Louisiana. SPE- 10974-MS.

Sanyal, S. K., S. S. Marsden, Jr., et al. 1974. Effect of Temperature on Petrophysical Properties of Reservoir Rocks. SPE California Regional Meeting, 4-5 April, San Francisco, California. SPE-4898-MS.

Sanyal, S. K., H. J. Ramey, Jr., et al. 1973. The Effect of Temperature on Capillary Pressure Properties of Rocks, SPWLA 14th Annual Logging Symposium, 6-9 May, Lafayette, Louisiana. SPWLA-1973-N

Sarma, P., L. J. Durlofsky, et al. 2005. Efficient Closed-loop Production Optimization Under Uncertainty. SPE Europec/EAGE Annual Conference, 13-16 June, Madrid, Spain. SPE-94241-MS.

Schembre, J. M., G. Tang, et al. 2005. Effect of Temperature on Relative Permeability for Heavy-Oil Diatomite Reservoirs. SPE Western Regional Meeting, 30 March-1 April, Irvine, California. SPE-93831-MS.

Settari, A., and K. Aziz. 1972. Use of Irregular Grid in Reservoir Simulation. Society of Petroleum Engineers Journal **12** (02). SPE-3174-PA.

Sinnokrot, A. A., H. J. Ramey, Jr., et al. 1971. Effect of Temperature Level upon Capillary Pressure Curves. Society of Petroleum Engineers Journal **11** (01). SPE-2517-PA.

Slotte, P. A., and E. Smorgrav. 2008. Response Surface Methodology Approach for History Matching and Uncertainty Assessment of Reservoir Simulation Models. Europec/EAGE Conference and Exhibition, 9-12 June 2008, Rome, Italy. SPE-113390-MS.

Steffensen, R. J. 1987. Solution Gas Drive Reservoirs. Petroleum Engineering Handbook, Society of Petroleum; Rev. Sub edition.

Sufi, A. H., H. J. Ramey, Jr., et al. 1982. Temperature Effects on Relative Permeabilities of Oil-Water Systems. SPE Annual Technical Conference and Exhibition, 26-29 September, New Orleans, Louisiana. SPE-11071-MS

Sullivan, R. J. 1937. Gas-Oil Ratio Control in Flowing Wells. Eighteenth Annual Meeting, Chicago, American Petroleum Institute. API-37-103.

Torabzadey, S. J. 1984. The Effect of Temperature and Interfacial Tension on Water/Oil

Relative Permeabilities of Consolidated Sands. SPE Enhanced Oil Recovery Symposium, 15-18 April, Tulsa, Oklahoma. SPE-12689-MS.

Venkataraman, R. 2000. Application of the Method of Experimental Design to Quantify Uncertainty in Production Profiles. SPE Asia Pacific Conference on Integrated Modelling for Asset Management, 25-26 April, Yokohama, Japan. SPE-59422-MS.

Virine, L., and L. Rapley 2003. Decision and Risk Analysis Tools for the Oil and Gas Industry. SPE Eastern Regional Meeting, 6-10 September, Pittsburgh, Pennsylvania. SPE-84821-MS

Vogel, J. V. 1968. Inflow Performance Relationships for Solution-Gas Drive Wells. Journal of Petroleum Technology **20** (01).

Von Goten, W. D., and B. K. Choudhary. 1969. The Effect of Pressure and Temperature on Pore Volume Compressibility. Fall Meeting of the Society of Petroleum Engineers of AIME, 28 September-1 October, Denver, Colorado. SPE-2526-MS

Wan, J., V. R. Penmatcha, et al. 1998. Effects Of Grid Systems on Predicting Horizontal Well Productivity. SPE Western Regional Meeting, 10-13 May, Bakersfield, California. SPE-46228-MS.

Wasserman, M. L. 1987. Local Grid Refinement for Three-Dimensional Simulators. SPE Symposium on Reservoir Simulation, 1-4 February, San Antonio, Texas. SPE-16013-MS.

Weinbrandt, R. M., H. J. Ramey, Jr., et al. 1975. The Effect of Temperature on Relative and Absolute Permeability of Sandstones. Society of Petroleum Engineers Journal **15** (05). SPE-4142-PA

Whitson, C. H., and S. Sunjerga. 2012. PVT in Liquid-Rich Shale Reservoirs. SPE Annual Technical Conference and Exhibition, 8-10 October, San Antonio, Texas. SPE-155499-MS

Williams, J. K., and R. A. Dawe. 1989. Near Critical Condensate Fluid Behavior in Porous Media- A Modeling Approach. SPE Reservoir Engineering **4** (02). SPE-17137-PA

Xiao, J. J., and A. J. Al-Muraikhi. 2004. A New Method for the Determination of Gas Condensate Well Production Performance. SPE Annual Technical Conference and Exhibition, 26-29 September, Houston, Texas. SPE-90290-MS.

Xie, J., S. Lee, et al. 2013. Uncertainty Assessment of Production Performance for Shale Gas Reservoirs. International Petroleum Technology Conference, 26-28 March, Beijing, China. IPTC-16866.

Yang, C., L. X. Nghiem, et al. 2007. Reservoir Model Uncertainty Quantification Through Computer-Assisted History Matching. SPE Annual Technical Conference and Exhibition, 11-14 November, Anaheim, California. SPE-109825-MS.

Yeten, B., A. Castellini, et al. 2005. A Comparison Study on Experimental Design and Response Surface Methodologies. SPE Reservoir Simulation Symposium, 31 January-2 February, The Woodlands, Texas. SPE-93347-MS.